

AD-A085 767

CALIFORNIA UNIV LOS ANGELES DEPT OF PHYSICS
A STUDY OF PERSISTENT CURRENTS IN SUPERFLUID ^4He , (U)
MAR 80 R K TALAGHANY

F/6 20/13

N00014-75-C-0246

UNCLASSIFIED

TR-40

NL

1-2

AC

AD-A085 767

1-2

AC

AD-A085 767

1-2

AC

AD-A085 767

1-2

AC

AD-A085 767

1-2

AC

AD-A085 767

1-2

AC

AD-A085 767

1-2

AC

AD-A085 767

1-2

AC

AD-A085 767

1-2

AC

AD-A085 767

1-2

AC

AD-A085 767

1-2

AC

AD-A085 767

1-2

AC

AD-A085 767

1-2

AC

AD-A085 767

1-2

AC

AD-A085 767

1-2

AC

AD-A085 767

1-2

AC

AD-A085 767

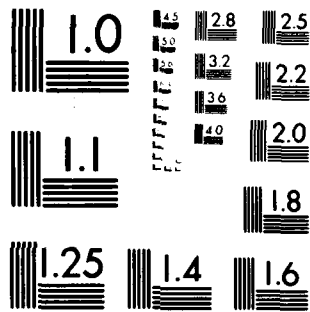
1-2

AC

AD-A085 767

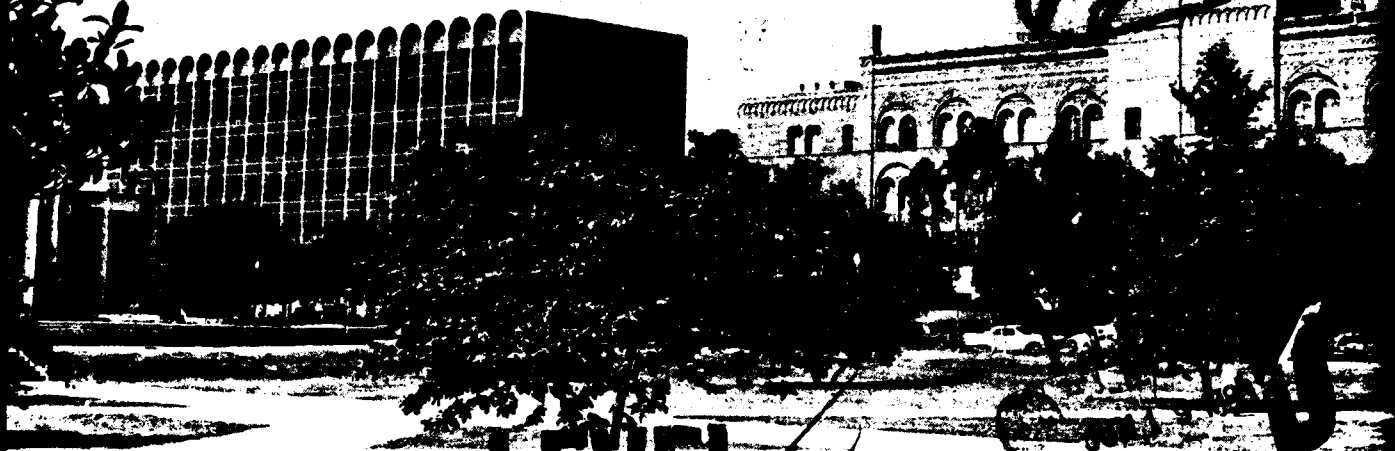
1-2

AC



MICROCOPY RESOLUTION TEST CHART
NATIONAL BUREAU OF STANDARDS 1963 A

UCLA
• Department of Physics



LEVEL II

ADA 085767

LOS ANGELES 90024
CALIFORNIA

This document has been approved
for public release and sale; its
distribution is unlimited.

FILE COPY

80 6 18 0 20

2

TECHNICAL REPORT No. 40

March 1980

Submitted by

I. Rudnick, Project Director

DTIC
ECTE
JUN 13 1980

A Study of Persistent Currents
in Superfluid ^4He

by

Roset Khosropour Talaghany

Office of Naval Research
Contract
N00014-75-C-0246
NR No. 384-302

Department of Physics
University of California
Los Angeles, Calif. 90024

APPROVED FOR PUBLIC RELEASE; DISTRIBUTION UNLIMITED

Reproduction in whole or in part is permitted
for any purpose of the United States Government

UNCLASSIFIED

SECURITY CLASSIFICATION OF THIS PAGE (When Data Entered)

REPORT DOCUMENTATION PAGE		READ INSTRUCTIONS BEFORE COMPLETING FORM
1. REPORT NUMBER 40	2. GOVT ACCESSION NO. AD-A085 767	3. RECIPIENT'S CATALOG NUMBER
4. TITLE (and Subtitle) A STUDY OF PERSISTENT CURRENTS IN SUPERFLUID LHE		5. TYPE OF REPORT & PERIOD COVERED Interim
7. AUTHOR(s) Roset Khosropour / Talaghany		6. PERFORMING ORG. REPORT NUMBER Technical Report No. 40
9. PERFORMING ORGANIZATION NAME AND ADDRESS University of California, Los Angeles Physics Department Los Angeles, California 90024		8. CONTRACT OR GRANT NUMBER(s) N00014-75-C-0246
11. CONTROLLING OFFICE NAME AND ADDRESS Office of Naval Research, Physics Program Office Arlington, Virginia 22217		10. PROGRAM ELEMENT, PROJECT, TASK AREA & WORK UNIT NUMBERS NR. No. 384-302
14. MONITORING AGENCY NAME & ADDRESS (if different from Controlling Off. ce) (1) Doctoral thesis		12. REPORT DATE (11) Mar 1980
		13. NUMBER OF PAGES 103
		15. SECURITY CLASS. (of this report) UNCLASSIFIED
		15a. DECLASSIFICATION/DOWNGRADING SCHEDULE
16. DISTRIBUTION STATEMENT (of this Report) APPROVED FOR PUBLIC RELEASE; DISTRIBUTION UNLIMITED (14) TF-40		
17. DISTRIBUTION STATEMENT (of the abstract entered in Block 20, if different from Report)		
18. SUPPLEMENTARY NOTES		
19. KEY WORDS (Continue on reverse side if necessary and identify by block number) SUPERFLUIDITY SUPERFLUID HELIUM CRYOGENIC FIRST SOUND SECOND SOUND FOURTH SOUND GRAVITY WAVES DECAY OF SUPERFLUID PERSISTENT CURRENTS SUPERLEAK HYBRID SUPERFLUID SOUND		
20. ABSTRACT (Continue on reverse side if necessary and identify by block number) See over		

DD FORM 1 JAN 73 1473

EDITION OF 1 NOV 68 IS OBSOLETE
S/N 0102 LF 014 6601UNCLASSIFIED 072367
SECURITY CLASSIFICATION OF THIS PAGE (When Data Entered)

UNCLASSIFIED

SECURITY CLASSIFICATION OF THIS PAGE(When Data Entered)

20. ABSTRACT

Decay of saturated persistent currents in superleaks in contact with bulk superfluid helium has been studied using doppler shifts of the acoustic modes of an annular resonator partially packed with superleak. The two acoustic modes are an interpolated first-fourth sound and a modified second sound. Decay of such currents have been measured at 1.35°K for annuli 10, 20, 40, 60, 80, 90, 95 and 100 percent filled with superleak. The main result which is somewhat surprising, is that the saturated persistent current and its fractional decay rate varies only slightly with superleak depth and the average decay rate is about 2.5% per decade.

Another phenomena which was also studied is the doppler shift of gravity waves in a partially packed powder. The velocity of gravity waves is about three orders of magnitude smaller than the fourth sound velocity in a similar geometry. Thus it seemed appropriate to use its doppler shift for measuring small persistent currents. A theoretical study of the problem showed that the gravity waves are not doppler shifted in the presence of a persistent current in superleak, however the waves are still doppler shifted by the persistent currents in the free region. Experiments support the theoretical prediction, and also indicate the existence of a small current of about 8 millimeters per second in the free region.

Accession For	
NTIS SW&I	<input checked="checked" type="checkbox"/>
DDC TAB	<input type="checkbox"/>
Unannounced	<input type="checkbox"/>
Justification	
By	
Distribution/	
Availability Codes	
Dist	Avail and/or special
A	

UNCLASSIFIED

SECURITY CLASSIFICATION OF THIS PAGE(When Data Entered)

TABLE OF CONTENTS

	Page
LIST OF FIGURES AND TABLES	vi
ACKNOWLEDGEMENTS	ix
VITA AND PUBLICATIONS	x
ABSTRACT	xi
CHAPTER	
I. INTRODUCTION	
A. History of Superfluid Helium and Development of the Theories	1
B. Development of the Two Fluid Theory.	5
C. Derivation of the Landau Two-Fluid Equations	7
D. Sounds in Helium	9
E. Sound Waves in Partially Packed Geometries	13
F. Quantum Mechanics - Hydrodynamics - Thermodynamics .	15
G. History of Persistent Currents, and Measurement Techniques	22
H. Decay of Persistent Currents	24
II. MEASUREMENT OF THE DECAY OF PERSISTENT CURRENTS IN PARTIALLY PACKED GEOMETRIES	
1. Introduction	27
2. Theory	28
3. Experimental Apparatus	36
A. Waveguide	38
B. Dewar, and the Rotating Probe	42

4.	Electronics, and Temperature Measurements and Control	47
5.	Measurements of Decay Rate as a Function of the Depth of the Powder	50
6.	Results and Discussions	52
III.	TEMPERATURE DEPENDANCE OF SPLITTING FACTOR $[\rho_g/\rho + G(T)]$	64
IV.	GRAVITY WAVES, AND PERSISTENT CURRENT IN HE II	
1.	Introduction	69
2.	Theory	73
3.	Experimental Apparatus and Techniques	82
4.	Electronics	89
5.	Doppler - Shift of Gravity Waves	89
6.	Results and Discussion	95
7.	Further Experiments	97
	BIBLIOGRAPHY	99

LIST OF FIGURES AND TABLES

FIGURE	PAGE
1. Temperature dependance of first, second, fourth and Fifty sound	8
2. Various sound modes in He	14
3. C_{14} versus T with various percentages of the annulus filled with powder. The solid lines are C_1 and C_4	16
4. C_{II} versus T with various percentages of the annulus filled with powder. The solid line is C_2	17
5. Schematic of vortex line configurations	29
6. Resonances in air of an annular cavity of radius $R = 5.25$ cm and height and width of 0.5 cm	34
7. Cutaway drawing of annular resonator used in decay measurements. L is .5 cm, as is the width of the annulus, $R = 5.25$ cm	37
8. Packing tool used to pack powder into the annulus	39
9. Open view of the resonator with top plate	40
10. Open view of the annulus	41
11. Schematic of rotating apparatus used in measurements of the decay of persistent currents	43
12. Block diagram of electronics used in measurements of the decay of persistent currents	45
13. Beating of fourth sound doublet in free decay	46
14. Schematic of electronic apparatus for measurement of persistent current decay	49

FIGURE	PAGE
15. C_{14} resonances with and without splitting	51
16. Decay of saturated persistent current in 100% packed annulus at 1.35°K	53
17. Decay of saturated persistent current in 95% packed annulus at 1.35°K	54
18. Decay of saturated persistent current in 90% packed annulus at 1.35°K	55
19. Decay of saturated persistent current in 80% packed annulus at 1.35°K	56
20. Decay of saturated persistent current in 60% packed annulus at 1.35°K	57
21. Decay of saturated persistent current in 40% packed annulus at 1.35°K	58
22. Decay of saturated persistent current in 20% packed annulus at 1.35°K	59
23. Decay of saturated persistent current in 10% packed annulus at 1.35°K	60
24. Fractional decay rate per decade versus percentage of the depth of the annulus filled with powder	61
25. Theoretical values of $[\rho_g/\rho + G_2(T)]$ and $[\rho_g/\rho + G(T)]$.	65
26. Experimental and theoretical values of the splitting factor $\rho_g/\rho + G(T)$	67
27. Temperature dependance of gravity wave in He in partially packed resonator	70

FIGURE	PAGE
28. Velocity of Cu against height of the liquid above the powder	71
29. Cross-section of a partially packed superfluid acoustic wave guide	74
30. A photograph of the experimental cell used in gravity wave experiments	83
31. Cross-sectional sketch of the annular resonator used in measurements of the doppler shift of the gravity wave . .	85
32. Open view of the resonator with the top plate	87
33. Closed view of resonator	88
34. A schematic drawing of the electronics used in the gravity wave experiments	90
35. A typical spectrum of the gravity wave in helium in the partially packed annulus at 1.35°K	91
36. Spectrum of gravity waves in partially packed annulus at 1.3°K	92
37. C_{14} resonances with and without a persistent current . .	93,94

TABLE	PAGE
I. Measured decay rates for various depths of powder and their associated porosity and critical velocities	62

ACKNOWLEDGEMENTS

I cannot fully express my appreciation to Professor Isadore Rudnick who has always been a source of encouragement and enlightenment, a superb advisor, and a patient and understanding teacher with great physical insight.

I am indebted to Professor Seth Putterman for many interesting and motivating discussions and also for being a very good lecturer and a friend. I am very grateful to Professor Gary Williams for his valuable counsel and efforts throughout the experiment. A very special thanks goes to Dr. Joseph Heiserman and Dr. Steve Garrett who started me in this research group.

To my colleagues and friends I owe a debt of gratitude for their discussions, suggestions, and efforts on my behalf. I would therefore like to acknowledge the contributions of Dave Scholler, Robert Keolian, Scott Adams, John Marcus, and Joe Theobald. Special thanks to Steve Baker and Mike Cabot who also helped me in editing my thesis.

I am especially grateful to Liz Muldawer for her efforts on my behalf, for her patience and skill in preparation of this thesis.

I also wish to thank the other members of the Physics Department staff who have contributed their time and expertise: James Abbott and Jackie Payne for the graphics; Albert Knox and Pete Goodman in the machine shop; Curt Hamblin in the research store room; Gail Yamamoto in the business office and Barbara Yamadera in the graduate affairs office.

ABSTRACT OF THE DISSERTATION

A Study of Persistent Currents in
Superfluid ^4He

by

Roset Khosropour Talaghany

Doctor of Philosophy in Physics

University of California, Los Angeles, 1980

Professor Isadore Rudnick, Chair

Decay of persistent currents in superleaks in contact with bulk superfluid helium has been studied using doppler shifts of the acoustic modes of an annular resonator partially packed with superleak. The two acoustic modes are an interpolated first-fourth sound and a modified second sound. They have proven to be a useful means of measuring persistent currents in both the packed and unpacked regions of the waveguide. Decay of such currents have been measured at 1.35°K for annuli 10, 20, 40, 60, 80, 90, 95 and 100 percent filled with superleak. The main result, which is somewhat surprising, is that the saturated persistent current and its fractional decay rate varies only slightly with superleak depth. This means that the stability of the current in powder is neither affected by the free exchange of mass between the two regions nor is it a strong function of the magnitude of the depth of the powder. Starting from 100%

packing the fractional decay rate is about 2% per decade and increases to about 3% per decade at 10% packing. However, there exists a local maximum in decay rate at 90% packing.

Another phenomenon which was also studied is the doppler shift of gravity waves in a partially packed annulus, in relation to its possible application in the detection of persistent currents. The velocity of the gravity wave is about three orders of magnitude smaller than the fourth sound velocity in a similar geometry. Thus it seemed appropriate to use its doppler shift for measuring small persistent currents which could not be measured by the doppler shift of first-fourth sound. Having this in mind the necessary apparatus was built and subsequently a theoretical study of the problem showed that the doppler shift of gravity waves in the presence of a persistent current in superleak is weighted down by $(C_g/C_4)^2 \sim 10^{-6}$, which is very small and negligible. However the waves are still doppler shifted by a current in the unpacked region. Experiments were performed to detect the doppler shift of these waves and at the same time to establish the existence of a persistent current in powder after the apparatus was rotated above T_λ and brought to rest at the desired temperature (1.3°K). Measurements show that in spite of the fact that a current is present in the powder, gravity waves are not doppler-shifted. Some splitting of the fundamental mode is detected which corresponds to velocities ~ 8 cm/sec.

This splitting can indicate the existence of a current in the free region. Finally a decrease of the quality factor, Q , is observed after rotation.

CHAPTER I. INTRODUCTION

The history of physics is marked by breakthroughs into new, unexpected worlds of discovery. One such event occurred just more than seven decades ago, in 1908. H. Kamerlingh Onnes of the University of Leiden succeeded in cooling helium gas down to the liquid state.⁽¹⁾ His breakthrough into this low temperature region, close to absolute zero, led to the discovery of two strange properties of matter, totally different from those familiar to us at ordinary temperatures. Both of these properties involve the phenomenon of "frictionless" flow. One of them is superconductivity, the frictionless flow of electrons. The other, not discovered until 1938, is the superfluidity of liquid helium, the frictionless flow of entire atoms.

The He^4 atom has a particularly simple, stable, and symmetrical structure. The nucleus containing two protons and two neutrons has no resultant angular momentum or magnetic moment. The two electrons fill the innermost energy levels and being so close to the nucleus, are firmly bound. The ionization potential is greater than that of any other atom. The atom has no electric or magnetic dipole moment and its electric polarizability is very small. It is the last fact which explains the weakness of the interatomic forces, for these forces are related to the electric polarizability of the atom, which in turn depends upon the separation of the energy levels of the electrons,⁽²⁾ so we can see a direct connection

between the low boiling point of the liquid helium and the high excitation energy of the helium atom. He^4 is the most difficult of all substances to liquefy.

Classically at absolute zero all motion stops, but quantum mechanically this is not so. In fact the most mobile substance known is helium at absolute zero. Helium stays liquid, as London⁽³⁾ has shown, because the inter-atomic forces are very weak. The quantum zero point motion is large because the atomic mass is small and it remains fluid even at absolute zero. Experiments have shown that it stays liquid down to zero temperature, and solidification occurs only by applying 25 atmospheres of pressure.

Liquid helium behaves like a classical fluid obeying ordinary hydrodynamics until it is cooled below the lambda temperature which, at its vapor pressure, is $T_\lambda = 2.172^\circ\text{K}$. At this temperature liquid helium goes through a transition which completely changes its character. For purposes of distinction the liquid above T_λ is referred to as He I and below T_λ it is called He II. Four very remarkable discoveries, all made between 1936 and 1938, indicated that the properties of He II are strikingly different and more complex than a classical liquid and showed that some of the customary differential equations of macroscopic physics do not apply to liquid helium below the λ -point.

1. Thermal Superconductivity

In 1936, Keesom and Miss Keesom⁽⁴⁾ noticed an enormous increase of heat exchange in liquid ^4He when it was cooled below

the λ -point.

2. Superfluidity

Keesom and Van den Ende⁽⁵⁾ observed quite accidentally that liquid ^4He passed with annoying ease through certain extremely small leaks which at a higher temperature were perfectly tight for He I. This observation seemed to indicate an enormous drop of viscosity when liquid helium passed below the λ -point. However measurements of the viscosity by Keesom and Macwood with the rotating disk method showed that the viscosity of helium below the λ -point, although it decreases with decreasing temperature for $T > 1.8^\circ\text{K}$ quite considerably, nevertheless varies continuously and certainly was not very different from the viscosity of He I.

In contrast to Keesom and Macwood's results, though in confirmation of Keesom and Van den Ende's earlier observations, Kapitza⁽⁶⁾, and independently Allen and Misener⁽⁷⁾, reported measurements based on the capillary flow method which showed the viscosity of liquid He dropping by many orders of magnitude to an immeasurably small value when the temperature is lowered through the λ -point.

3. The Fountain Effect

The third of the new discoveries, and the most interesting of all, was made in 1938 by Allen and Jones.⁽⁸⁾ They used an apparatus which consists of a reservoir and a small vessel, both filled with liquid helium and connected by a fine capillary ($< 10^{-4}$ cm in width). When heat was added to the inner vessel, they observed that the inner helium level rose above that of the reservoir. The rise

increased with heat input and, for constant input, with falling temperature. The inverse experiment is the mechanocaloric effect which was first described by Daunt and Mendelssohn in 1939.⁽⁹⁾ They observed the behavior of the temperature of two vessels initially at the same temperature, when He II was allowed to flow, say under the influence of gravity, from one vessel to the other through a superleak (packed powder). Their results indicated that the temperature of a given vessel increased as the liquid flowed out. According to the Euler equations a temperature difference can lead to a flow, or convection of liquid, but the mass flow and entropy flow are in the same direction. In the fountain effect, the mass flow may oppose the heat flow.

The landmark experiment of Kapitza in 1941⁽¹⁰⁾ provided a clear and quantitative unification of the above observation and showed that (1) the fluid which passed through the capillary had zero entropy, and (2) the fluid on either side of the capillary came to mechanical equilibrium when the chemical potentials at the same level on either side of the capillary were equal.

4. Superfluid Helium Film

In order to reach very low temperature with liquid helium, Kamerlingh Onnes worked with an arrangement that consisted of a small Dewar vessel in a large one filled with liquid He II. Some mysterious process led to a quick equalization of the levels.⁽¹¹⁾ At first it was thought that this was due to a rapid evaporation-condensation effect. Rollin⁽¹²⁾ suggested that this

effect was due to an adsorbed film of helium which forms a bridge between the vessels. Later Daunt and Mendelssohn⁽¹³⁾ showed that the equalization took place through a flow of this film. This phenomenon (the frictionless flow of liquid film) does not occur in the case of any ordinary fluid, and it is unique to liquid helium below T_λ .

Development of the Two Fluid Theory

There have been many efforts to understand the unusual macroscopic properties of liquid He II from the microscopic or first principles approach. Since the theories of gaseous and solid states are established on a firm foundation it is tempting to treat a liquid either as a very imperfect gas in which the intermolecular forces have become important or as a broken down solid in which the binding forces are too weak to localize the atom near lattice points. London advanced the hypothesis that the transition of liquid helium I into helium II might be caused by the condensation mechanism of the Bose-Einstein gas, allowing for the presence of intermolecular forces and for the circumstance that we are dealing with the liquid and not with the gaseous state.⁽¹⁴⁾ It was Tisza⁽¹⁵⁾ who first recognized the possibility of employing the qualitative properties of a weakly interacting Bose-Einstein gas to develop a consistent macroscopic theory.

Three years after Tisza published his theory, Landau in Moscow independently published another version of essentially the same two-fluid theory.⁽¹⁶⁾ Landau rejected the approach from the side of

gas statistics, arguing that a liquid is generally much more like a solid than like a gas. He attempted to put his two-fluid theory on an entirely different basis, one in which the Bose-Einstein condensation plays no role, except that condensate is "background" or "vacuum" for propagation of excitations. He tried to represent the liquid as a quasi-continuum whose excitations are quantized. Landau assumed that there are two kinds of elementary excitations in a liquid, the "phonons" and the "rotons". The phonons are the excitations of the longitudinal sound waves and are supposed to represent the potential motions of liquid, characterized by $\text{curl } \mathbf{V}_s = 0$. In an extremely crude picture rotons could be described as the elementary excitation of a vortex spectrum ($\text{curl } \mathbf{V} \neq 0$) and the roton spectrum is assumed to be separated by an energy gap from the lowest phonon state. Both phonons and rotons carry momentum and it is their net drift which is identified with the "normal fluid". The remaining mass is to correspond to superfluid, which moves with its own velocity, once the possibility of the two velocity fields is granted the development of the macroscopic hydro-thermodynamics has to proceed along the same line as in Tisza's theory. It was Landau⁽¹⁷⁾ in 1941 who first succeeded in devising a complete system of differential equations for the macroscopic two-fluid thermo-hydrodynamics. In this form the theory provided the incentive for the beautiful experiments of Peshkov⁽¹⁸⁾ and Andronikashvili,⁽¹⁹⁾ whose convincing evidence contributed decisively to the consolidation of the two-fluid concept. This theory has indeed proved to be capable of

reducing a great number of the most striking facts concerning liquid helium II to a common theoretical basis and, moreover, of predicting the properties of liquid helium. All the experimental evidence leaves little doubt that the two-fluid concept of liquid helium II is very close to the truth. However, this connection is as yet hypothetical and intuitive rather than based on a rigorous microscopic theory.

Derivation of the Landau Two-Fluid Equations

In this phenomenological theory He II is considered to consist of two interpenetrating fluid components: the superfluid component of mass density ρ_s and a normal fluid component of density ρ_n . The two components have independent velocity fields \vec{V}_s and \vec{V}_n respectively. The total mass density of the fluid is the sum of the densities of the normal and superfluid components.

$$\rho = \rho_n + \rho_s \quad (I-1)$$

and the total mass flux is

$$\rho \vec{V} = \rho_n \vec{V}_n + \rho_s \vec{V}_s \quad (I-2)$$

where \vec{V} is the velocity of the center of mass.

The equations of the two-fluid theory can be derived from macroscopic first principles if one assumes that eight independent variables (ρ, S, V_n, V_s) form a complete set. The application of mass and entropy conservation, Newton's laws, the First and Second Laws of Thermodynamics and Galilean relativity will yield a unique set

of equations which can describe the dynamics of He II. ⁽²⁰⁾

The equation of conservation of mass is identical to that of an Euler fluid

$$\frac{\partial \rho}{\partial t} + \nabla \cdot (\rho \vec{V}) = 0 \quad (I-3)$$

where
$$\rho \vec{V} = \rho_n \vec{V}_n + \rho_s \vec{V}_s \quad (I-4)$$

But the equation of conservation of entropy takes a different form than the Euler equation for ordinary fluids.

$$\frac{\partial \rho s}{\partial t} + \nabla \cdot (\rho s \vec{V}_n) = 0 \quad (I-5)$$

Just like the Euler liquid, there is a law of conservation of momentum for helium

$$\frac{\partial J_i}{\partial t} + \frac{\partial P_{ik}}{\partial r_k} = 0 \quad (I-6)$$

where
$$P_{ik} = p \delta_{ik} + \rho_n V_{ni} V_{nk} + \rho_s V_{si} V_{sk} \quad (I-7)$$

The remaining three equations determine the acceleration of the superfluid component, which is driven by gradients in the chemical potential in accordance with the results of Kapitza, mentioned in the preceeding sections in this chapter:

$$\frac{D_s \vec{V}}{Dt} = - \nabla \mu \quad (I-8)$$

where
$$\frac{D_s}{Dt} = \frac{\partial}{\partial t} + (\vec{V}_s \cdot \nabla)$$

Equations 3, 5, 6 and 8 form eight independent equations for the eight independent variables $(\rho, S, \vec{v}_n, \vec{v}_s)$ which describe the dynamics of He II. Along with equation of state for ρ_n, p, μ in terms of these variables

$$dp = \rho d\mu + \rho s dT + \frac{1}{2} \rho_m d(\vec{v}_n - \vec{v}_s)^2 \quad (I-9)$$

equations (I-1) through (I-6) form a complete closed description of the flow on the reversible level.

Sounds in Liquid Helium

According to the two-fluid equations, which were largely motivated by Kapitza's experiment, eight independent variables are needed to describe the dynamics of He II. Two interpenetrating liquids with two independent velocities are implied by the theory. Therefore there is an extra degree of freedom in liquid helium which allows a new sound mode to propagate in bulk helium.

If we linearize Landau's two-fluid equations and solve for a dispersion law we find: ⁽²⁰⁾

$$(1 - \frac{u_1^2}{u_s^2})(1 - \frac{u_2^2}{u_s^2}) = (1 - \frac{c_v}{c_p}) \quad (I-10)$$

where

$$c_v = T \left. \frac{\partial S}{\partial T} \right|_p$$

$$c_p = T \left. \frac{\partial S}{\partial T} \right|_p$$

$$u_1^2 = (\partial P / \partial \rho)_s$$

$$u_2^2 = (\rho_s / \rho_m) \left(\frac{s^2 T}{c_v} \right)$$

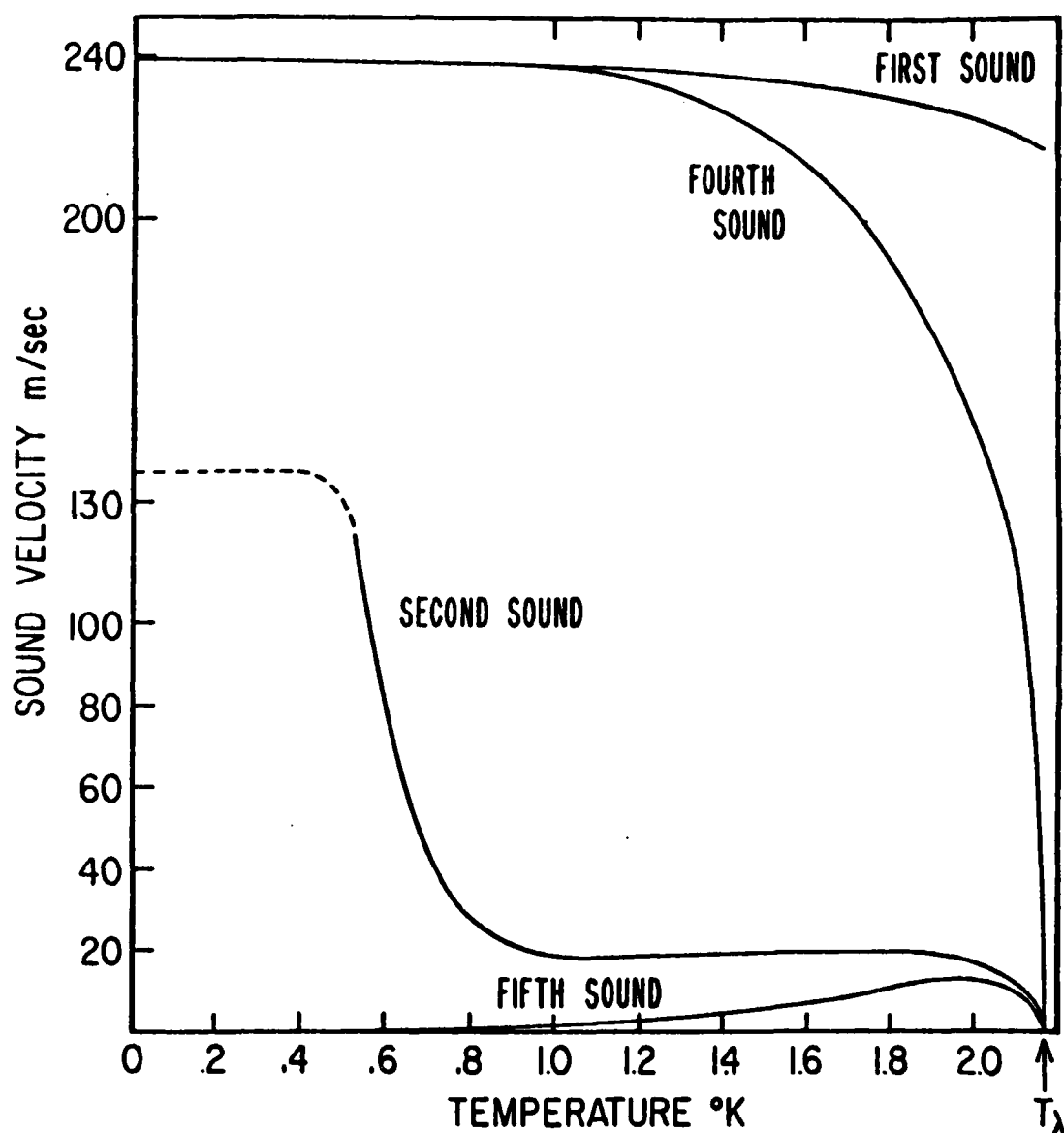


FIGURE 1. -TEMPERATURE DEPENDANCE OF FIRST, SECOND, FOURTH AND FIFTH SOUND

In He II at all accessible temperatures $1 - C_v/C_p \ll 1$. For these cases the right hand side of equation (I-10) can be neglected and the two solutions are given simply by $u^2 = u_1^2$, and $u^2 = u_2^2$. The first solution corresponds to a compression or a density wave in helium where normal and super components move together which is similar to ordinary sound in an Euler fluid. The first measurements of first sound velocity were made by Findlay⁽²¹⁾, Pitt, Grayson-Smith and Wilhelm (1938) using a standing wave technique. The second solution corresponds to a temperature wave which has no pressure variations. δp is zero, therefore, the center of mass velocity is zero, that is, $\rho_n V_n + \rho_s V_s = 0$. The superfluid and normal fluid move in the opposite directions in such a way to keep the center of mass stationary.

Historically this was the prediction of Landau⁽¹⁷⁾ and Tisza that He II could support two different propagating waves. The confirmation of their prediction came from the landmark experiment of Peshkov⁽¹⁸⁾ in 1944. He discovered second sound and measured its velocity by a resonance technique. This discovery was a striking support for the two-fluid idea, and a quantitative means of measuring the basic parameters ρ_s and ρ_n .

Fourth Sound

One of the most striking properties of He II is its ability to flow through narrow constrictions without any resistance. In these geometries the normal fluid is held at rest due to its viscous interaction with the walls, while the superfluid flows freely.

If we take a waveguide or a tube packed with small powders so that the pore size is smaller than the viscous penetration depth, $\sqrt{\frac{2\eta}{\rho\omega}}$, the normal fluid will be immobilized (this medium is called a superleak). Then $v_n = 0$, and the dynamics of the fluid now is described by five variables and only five of the eight of Landau's equation are needed. On the other hand, because there is an external force applied by the powder and container to keep the normal fluid from moving, the equation for the conservation of momentum is no longer satisfied. The remaining five equations can be linearized and solved for possible sound modes.⁽²²⁾ One finds that there is one possible sound mode (fourth sound), which is unique to He II with velocity

$$u_4^2 = \rho \frac{\partial \mu}{\partial \rho} \Big|_{ps} \\ = \rho_s / \rho u_1^2 \left[1 + \frac{2ST}{\rho C_p} \left(\frac{\partial \rho}{\partial T} \Big|_p \right) \right] + \rho_n / \rho u_2^2 \quad (I-11)$$

which can be approximated by $u_4^2 = \rho_s / \rho u_1^2$ with an error of less than 2%.

Fourth sound was experimentally observed by Rudnick and Shapiro in 1962.⁽²³⁾ The temperature dependence of its velocity is shown in Fig. 1. It is well known that observed values of fourth sound are lower than calculated values, due to temperature independent multiple acoustic scattering by the powder particles in the superleak. It has been found experimentally that the empirical index of refraction

$$(2 - p)^{1/2}$$

gives agreement with experiment to within 3% over a large range of powder sizes.⁽²⁴⁾

Equation (I-11) could be rewritten in the following form:

$$u_a^2 = u_{a,T}^2 + u_s^2 \quad (I-12)$$

where
$$u_{a,T}^2 = P/\rho u_i^2 \left[1 + \frac{2SI}{\rho C_p} \frac{\partial P}{\partial T} \Big|_P \right] \quad (I-13)$$

and
$$u_s^2 = P_m/\rho u_i^2 \quad (I-14)$$

u_s is the velocity of a pressure released thermal wave in a superleak (fifth sound) which has a strikingly different phase velocity⁽²⁵⁾ from the isothermal superleak mode. Fifth sound was experimentally observed by Williams et. al.⁽²⁶⁾ The temperature dependence of it is also shown in Fig. 1.

Useful summaries of the characteristics of sounds in He are shown in Table I.

Also included in Table I is the propagating surface wave in thin He II films known as third sound⁽²⁷⁾ which will not be considered here.

Sound Waves in Partially Packed Waveguides

In a waveguide packed to a fraction of its height with powder and filled with He II, two acoustic modes can propagate.⁽²⁸⁾ The nature of the two modes is determined by the possible propagating modes in the two different regions as well as the boundary conditions. Fourth sound can propagate in the packed region and first


SOUND	NORMAL COMPONENT VELOCITY	SUPERFLUID COMPONENT VELOCITY	TYPE OF WAVE	WAVE VELOCITY
1 st	→	→	PRESSURE DENSITY	$c_1 = \left[\left(\frac{dp}{d\rho} \right)_s \right]^{1/2}$
2 nd	→	←	TEMPERATURE ENTROPY	$c_2 = \left[\frac{\rho_s}{\rho_n} \frac{T s^2}{c_p} \right]^{1/2}$
3 rd	ZERO		SURFACE WAVE IN FILMS	$c_3 = \left[\frac{\rho_s}{\rho} f d \right]^{1/2}$
4 th	ZERO	→	PRESSURE WAVE IN SUPERLEAK	$c_4 = \left[\frac{\rho_s}{\rho} c_1^2 \right]^{1/2}$
5 th	ZERO	→	THERMAL WAVE IN SUPERLEAK	$c_5 = \left[\frac{\rho_n}{\rho} c_2^2 \right]^{1/2}$

FIGURE 2. VARIOUS SOUND MODES IN HE.

and second sound in the free region. The boundary conditions which are used at the interfacial surface of the superleak are:

- 1) The mass current is continuous across the interface, and the heat current vanishes at the interface.
- 2) The superfluid circulation around any path at the boundary vanishes. (These boundary conditions are intended to apply to the sound wave only).

Using the wave equations for first, second and fourth sound and imposing the boundary conditions, one arrives at expressions for the phase velocities of the two modes.⁽²⁸⁾

$$C_{14}^2 = C_1^2 \frac{L-d}{(L-d)+Pd} + C_4^2 \frac{Pd}{(L-d)+Pd} \quad (I-15)$$

$$C_{II}^2 = C_2^2 \frac{[L - (1-P)d]}{[L - (1-P)d - Pd(1-P/\rho)]} \quad (I-16)$$

From the above equations C_{14}^2 can be interpreted as a mean of C_1^2 and C_4^2 weighted by the fraction of the waveguide that each occupies. C_{II} can be interpreted as a second sound wave modified by the presence of the superleak. Velocities of C_{14} and C_{II} were measured by J. Heiserman and I. Rudnick⁽²⁹⁾, Figs. 3 and 4 show plots of the experimental velocities of C_{14} and C_{II} versus temperature (p is the porosity of the packed powder).

Quantization of Circulation and Critical Velocity

The form of the superfluid equation (I-8) was chosen as a

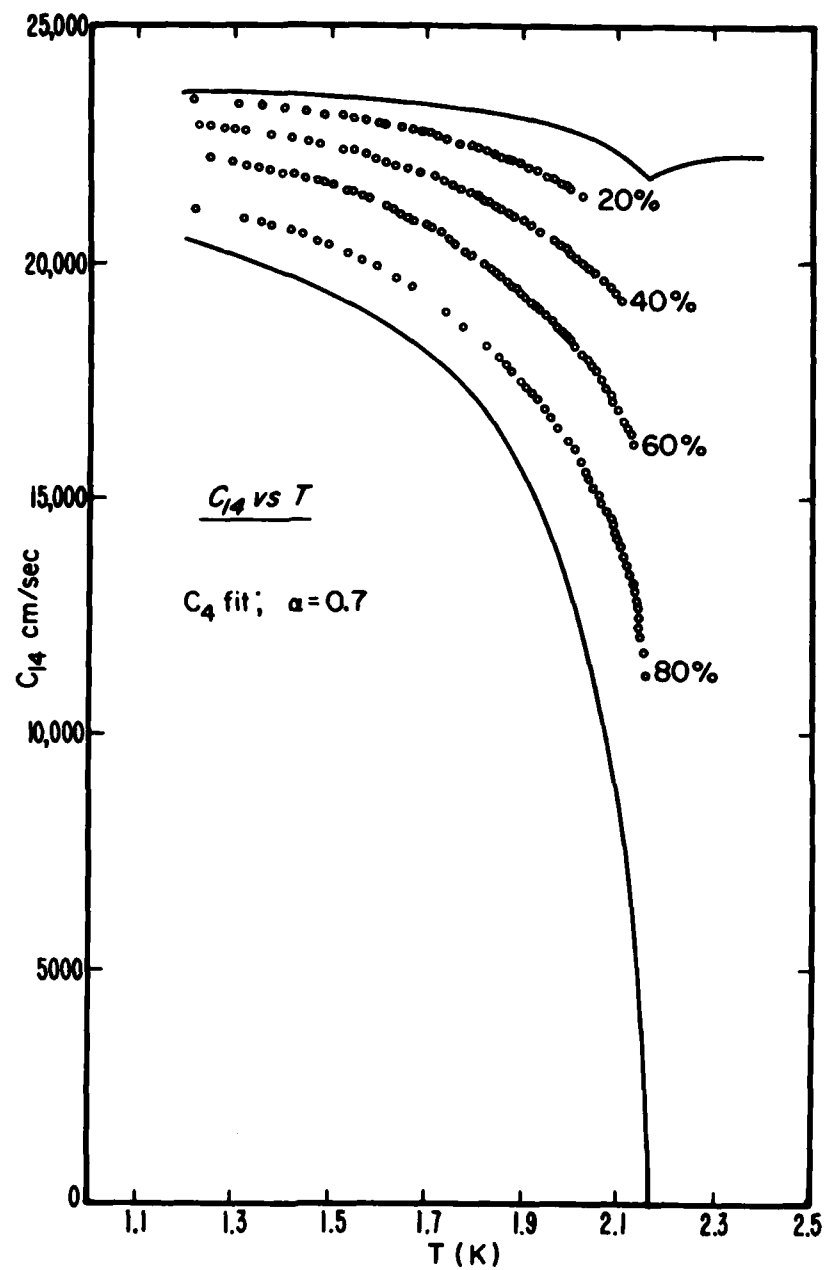


FIGURE 3. C_{14} VERSUS T WITH VARIOUS PERCENTAGES OF THE ANNULUS FILLED WITH POWDER. SOLID LINES ARE C_1 AND C_4 .

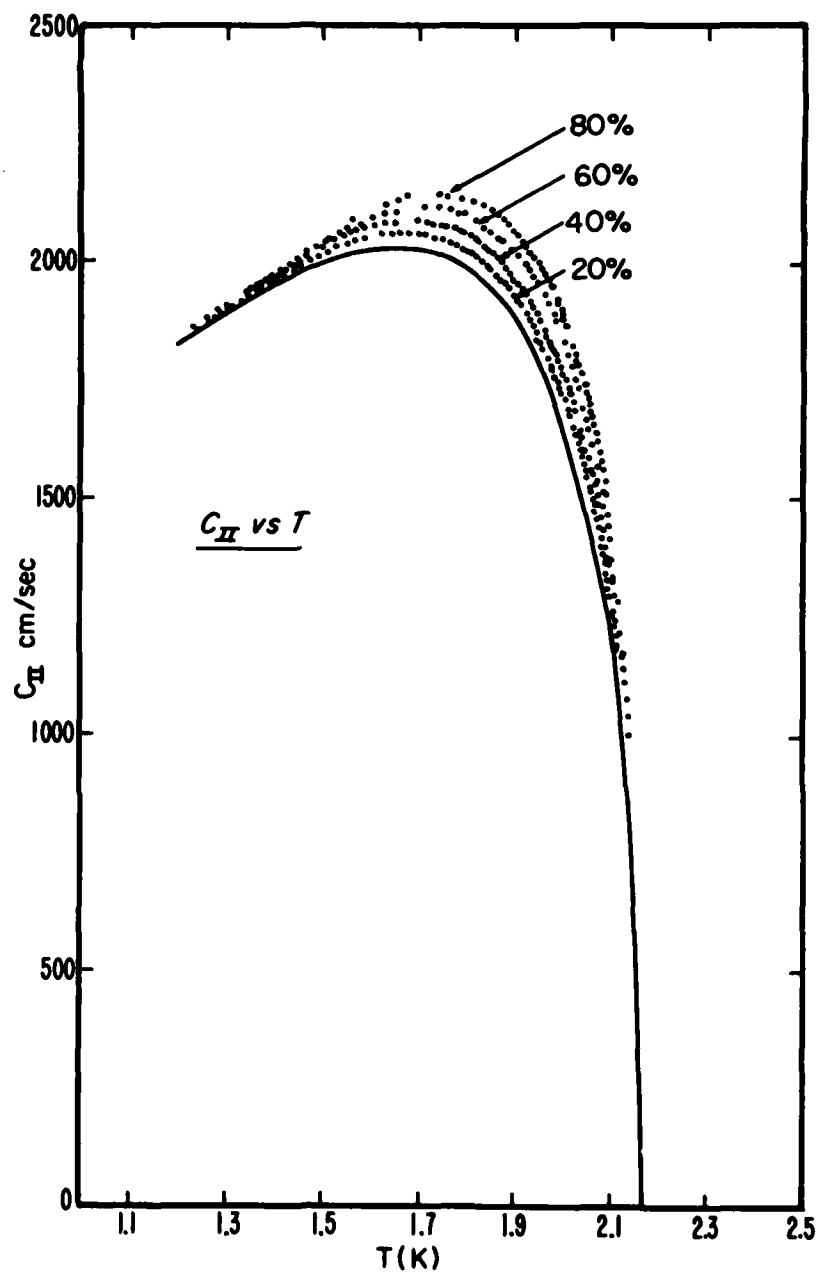


FIGURE 4. C_{II} VERSUS T WITH VARIOUS PERCENTAGES OF THE ANNULUS FILLED WITH POWDER PACKING. THE SOLID LINE IS C_2 .

basic assumption to satisfy a Kelvin circulation theorem:

$$\frac{D_c}{Dt} \left[\oint \vec{V}_s \cdot d\vec{l} \right] = 0 \quad (I-17)$$

or that the circulation is unchanged as one follows the motion of the superfluid particles. From (I-8) one can also write:

$$\begin{aligned} \frac{\partial \vec{V}_s}{\partial t} &= -\nabla(\mu + \frac{1}{2} V_s^2) + \vec{V}_s \times (\nabla \times \vec{V}_s) \\ \frac{\partial (\nabla \times \vec{V}_s)}{\partial t} &= \nabla \times [\vec{V}_s \times (\nabla \times \vec{V}_s)] \quad (I-18) \end{aligned}$$

so if $\nabla \times \vec{V}_s = 0$ everywhere at $t=0$ (I-18) tells us the time derivative is zero and hence it will stay zero. In fact, Landau always supplemented his equations with the requirement that the superfluid motion be restricted to this irrotational behavior. From the above relations it was concluded that superfluid initially at rest in a cylindrical container cannot be brought into rotation as the container is rotated. However normal fluid circulation is not conserved, and the viscous forces will drag the normal fluid to follow the motion of the container.

Osborne (1950)⁽³⁰⁾ rotated a glass vessel containing liquid He II and plotted the contour of the resulting parabolic surface. He found that liquid He II behaved like a normal liquid and the contour was classical. Andronikashvili and Kaverkin (1955)⁽³¹⁾ repeated Osborne's experiment and confirmed that the liquid has a normal parabolic surface.

Allen and Misener (1939)⁽³²⁾ had already noted from the flow rate measurements through narrow slits that "pure" superfluid flow took place only below certain maximum (critical) flow rates which depended on the width of the slit. It seemed then, that the Landau criterion, $\nabla \times \mathbf{V}_s = 0$, might hold strictly true only for velocities smaller than some critical velocity, and that the experiments of Osborne, and Allen and Misener contradicted the two-fluid theory.

This apparent contradiction could be resolved by inquiring about the limitations that thermodynamics imposes on the equilibrium of a rotating superfluid and then investigating the relation between the thermodynamic equilibrium conditions and the hydrodynamical equations of motion.

It is found that in thermal equilibrium $\mathbf{V}_n = \omega \times \mathbf{r}$ (solid body rotation for the normal component) and $\nabla \times \mathbf{V}_s = 0$ in the superfluid. While $\nabla \times \mathbf{V}_s = 0$ precludes the possibility of solid body rotation, superfluid can rotate if, for instance, one dimensional regions are excluded from the superfluid; i.e., $\rho_s = 0$ at one dimensional regions. A solution with $\nabla \times \mathbf{V}_s = 0$ except at these one dimensional regions correspond to a motion about vortex lines. If there are many vortex lines then it will appear as if the superfluid is rotating with the normal fluid. But for this solution to be a stable one at equilibrium the free energy must be a minimum., and one can show that this minimum is realized for a uniform distribution of very many and very weak vortex lines which approximate solid body rotation.⁽³³⁾ But how weak should the vortices be was a problem which was answered

from a very different approach to the problem. As was mentioned before, superfluid helium behaves quite differently from an ordinary fluid, and Landau's two-fluid equations are very different from Euler's equations for a simple classical fluid. However, Euler's equations can be demonstrated to be a consequence of the interacting molecules moving according to Newton's laws; thus two-fluid theory does not follow from Newton's laws. Therefore in order to understand helium there is one possibility left, that is, a quantum mechanical approach. But the two-fluid equations, which form the theoretical foundation of our understanding of superfluid helium do not contain Planck's constant.

The first effort to bring h into the macroscopic picture of helium was made in 1948 by the landmark work of Onsager.⁽³⁴⁾ He proposed that in order to guarantee the single valuedness of the superfluid wave function, the circulation of the superfluid ought to be quantized in units of h/m , that is:

$$\oint \mathbf{v}_s \cdot d\mathbf{l} = n(h/m) \quad (I-19)$$

where n is an integer and m is the mass of helium atom. In this way h directly enters the macroscopic theory and it also could be measured by a careful measurement of superfluid circulation. The above relation suggests the existence of quantized vortices in superfluid He, and also is consistent with the two-fluid theory. Therefore the superfluid could be set into rotation by introducing quantized vortices into the liquid.

The first experimental work to observe the macroscopic quantum

effect was done in 1961 by Vinen.⁽³⁵⁾ He showed that the superfluid circulation $\oint \mathbf{v}_s \cdot d\mathbf{l}$ is quantized. A later experiment of Rayfield and Reif⁽³⁶⁾, and also the more elaborate experiment of Whitmore and Zimmermann⁽³⁷⁾, confirmed the early observations and also the validity of Onsager's relation. The experiments proved that superfluid could take part in rotation in the form of quantized vortices.

Experiments on the flow of superfluid through narrow capillaries^(32,38) indicated that there exists a so called critical velocity ($V_{s,c}$) above which the superflow breaks down. Bijl⁽³⁹⁾ et. al. noticed that for these experiments on steady flow the critical velocity was given approximately by the following relation:

$$V_{s,c} \approx \frac{h}{md} \quad (I-20)$$

where d is the width of the channel. The magnitude of the critical velocity ($V_{s,c}$), the velocity at which vortices start entering the liquid for a particular geometry, can be worked out from free energy considerations⁽⁴⁰⁾, or from the requirement of the consistency of thermodynamics and hydrodynamics. For a rotating bucket of radius d one finds that for angular velocities ω just above ω_{cr}

$$\omega_{cr} = \frac{4h}{md^2} \ln \frac{d\sqrt{\epsilon}}{2a} \quad (I-21)$$

the first vortex will enter the liquid where a is the radius of the vortex core. Thermodynamically, below ω_{cr} the most stable state is $V_s=0$ and above ω_{cr} the state with one vortex at the center is

most stable. For higher ω another transition is reached at which two vortices become most stable and so on. In this manner one arrives at a relation between the number of vortex lines and the speed of rotation which obeys a quantum step structure. The quantum step structure of rotation was observed by Packard and Sanders⁽⁴¹⁾, and Williams and Packard.⁽⁴²⁾

Persistent Currents

The occurrence of frictionless flow, that is, persistent current, is undoubtedly the most dramatic feature of the superfluid helium. A circulation once started will continue indefinitely. Many experimentalists looked for persistent currents in bulk helium but due to the smallness of the critical velocity in the geometries they used they failed to get a positive result. Hall⁽⁴³⁾ was the first to report the observation of a persistent current. In his experiment he used a cylindrical can filled with closely spaced parallel Mica disks. The can was filled with He II and brought into steady rotation. It was then suddenly brought to rest and the torque exerted on it and the disks by the subsequent motion of the liquid was measured as a function of time. For a disk spacing of 7.7×10^{-3} cm and an initial angular velocity of 0.2 radian/sec the time integral of the torque was only about 30% of the maximum possible angular momentum, indicating the presence of residual angular momentum in the form of a persistent current. This current appeared to have suffered no detectable change after 300 sec.

Vinen's⁽⁴⁴⁾ experiment, already mentioned in connection with the quantization of circulation, showed that the superfluid circulation around a wire once created can persist in a stationary container for a time of the order of one hour.

Reppy and Depatie⁽⁴⁵⁾ used a similar geometry to the one used in Hall's experiment to study the persistent current. The current was prepared by rotating a cylindrical container, which was packed with closely spaced mica discs, at a speed far above the critical velocity for the superfluid. The apparatus was then stopped by a magnetic brake after a waiting period which was varied from five minutes to twelve hours (without any observable difference in the result). The liquid in the can was heated above the λ -point with an external light beam, thus destroying the current and the angular momentum of the current which was transferred to the can could then be measured.

Other techniques were developed later to measure the current by non-destructible means. Reppy and co-workers⁽⁴⁶⁾ and Mehl and Zimmermann⁽⁴⁷⁾ used gyroscopic effects associated with the angular momentum of the current. The apparatus in Mehl and Zimmermann's experiment consisted essentially of a torsion pendulum formed by attaching a powder filled glass sphere to the lower end of a long glass rod, the upper end of which was suspended from a sensitive torsion fiber at room temperature. After the current was created by rotating above T_λ and cooling to the desired temperature, the sphere was tilted through an angle in the vertical direction

by the application of a magnetic field. This tilting causes a time rate of change in the vertical component of the angular momentum which leads to a torque about the wire, and a deflection of the cell in the horizontal plane. This deflection can be measured to determine the angular momentum of the persistent current. In all these measurements still another independent measurement of ρ_s is needed to know the persistent current velocity. This is done by measuring the temperature dependence of the period of the free decay of the cell as a torsion pendulum.

Finally, to date the most accurate means of measuring the velocity of a persistent current is by measuring the doppler shift of the fourth sound velocity, which was developed by Rudnick and co-workers.⁽⁴⁸⁾ This is the technique used in most of the experiments throughout this thesis. By this method the velocity of a persistent current can be measured in both rotating and stationary annuli by a non-destructive method.

Decay of Persistent Currents

Any state of non-zero superflow is thermodynamically in a meta-stable state in the sense that it could always decay through some mechanism and make a transition to a state of lower velocity and thus, lower free energy. The exact mechanism responsible for the decay is not known. However, it is speculated that processes such as thermal fluctuations, Magnus force and mechanical vibrations could be causing the decay of persistent currents in superfluid helium. But there is as yet no single unified theory to

explain and predict the decay rate of any particular experiment.

Langer and Fisher⁽⁴⁹⁾, based on a theory of thermal activation of vortex excitations in superfluid helium, predicted a decay logarithmic in time. The main idea in their theory is that the persistent current could decay below $V_{s,c}$ through thermal fluctuations.⁽⁵⁰⁾ Transitions occur by the vortex ring fluctuating over the free energy barrier. The theory is based on a few fundamental assumptions:

- 1) Any thermodynamically stable or metastable state of the superfluid is uniquely characterized by the velocity of superflow, and that this velocity remains invariant when the system undergoes reversible transformations.
- 2) Any state of non-zero superflow is metastable in the sense that there is always some mechanism intrinsic to the system itself by which the system can make a transition to a state of lower velocity, and thus, lower free energy.
- 3) The ergodic hypothesis, which states that any possible configuration can be achieved with a probability which depends only on the energy of the configuration. Specifically, the probability of finding the system in a given configuration with energy E is proportional to the Boltzmann factor, $\exp(-E/K_B T)$.

Langer-Fisher theory predicts a logarithmic decay law and also a unique decay rate as a function of magnitude of the superfluid velocity. Experimental results of Kukich, et al⁽⁵¹⁾ and Kojima, et al⁽⁵²⁾ support the logarithmic decay law. But Kojima's result

show that the magnitude of the superfluid velocity alone does not determine the instantaneous decay rate, dV_s/dt . The decay rate depends on how the initial state is prepared. Furthermore, this theory is based on a persistent current flow which is vortex free.

Kojima's results indicate that the vortex flow as well as potential flow plays an important role in the decay of persistent currents. Clearly the interaction of vortex flow which results in the Magnus force⁽⁵³⁾ will push the vortices over the free energy barrier and will result in the decay of the persistent current. This mechanism is analogous to flux creep in superconductors, the theory of which was developed by Anderson.⁽⁵⁴⁾ And finally, mechanical vibration of the system also might play a crucial role in the decay of a persistent current.⁽⁵⁵⁾ For a classical fluid the coupling of vibrations to the fluid motion can take place through its viscous interaction with the wall. The superfluid has no viscosity and therefore it should couple to it in a basically quantum mechanical fashion.

CHAPTER II. MEASUREMENTS OF THE DECAY OF PERSISTENT CURRENT IN PARTIALLY PACKED ANNULI USING THE DOPPLER SHIFT OF C_{14}

1. Introduction

The acoustic modes of a partially packed waveguide have been extensively studied before. It has been observed that there exists two propagating modes. One is a first-fourth sound and the other a modified second sound mode.⁽²⁹⁾ Also, experiments have been performed to study the existence of persistent currents in such a configuration.⁽⁵⁷⁾ Consider an annulus packed with 500A powder particles to a fraction of its height and filled with superfluid helium. In spite of the free exchange of superfluid mass at the boundary, there exists two independent persistent currents in the two regions. A high velocity current in the powder of about 80 cm/sec exists in the proximity of a very low or vanishing velocity of less than 1 cm/sec above the powder. The magnitude of persistent current in the packed region in this configuration is the same as the one found in a fully packed annulus⁽⁵⁷⁾ and the vanishingly small velocity in the free region is also consistent with the results of previous efforts to observe persistent currents in bulk helium.^(58,59)

As discussed in Chapter I persistent currents decay. Decay of saturated persistent currents in a fully packed annulus has been studied.⁽⁶⁰⁾ It has been shown that the current decays logarithmically with time. The saturated current in a geometry packed with 500A powder particles decays a mere 12% in 10^{17} seconds which is approximately the age of the universe. Persistent currents in bulk helium do not enjoy the same stability as in the powder, and they decay much faster. Now

if we have a situation which is a combination of a stable high velocity region and an unstable low velocity region next to each other, how do they interact? If there is any interaction between the two velocity fields, one would expect that it would manifest itself somehow in the decay of the currents. Also the vortex configuration, in the presence of two independent currents, is another ambiguous feature of this geometry which could affect the decay rate. If there exists a small current in the free region, would some of the vortices in the powder extend through the unpacked portion to close to the top plate of the resonator, or are they going to bend and close to the side walls or onto themselves? A schematic drawing of these two possibilities are shown in Fig. 5.

The experiments which will be described and discussed in this chapter are designed to answer the above questions and also examine how the decay rate varies as a function of the depth of the powder.

The decay of persistent currents was measured by monitoring the magnitude of the currents as a function of time, using the doppler-shift of the first-fourth sound mode in the annulus.

2. Theory

When a wave propagates through a medium which is moving with some velocity, the wave is doppler-shifted. Many examples of this can be found in sound propagation, light propagation and etc. In helium we can use the fact that the sounds get doppler-shifted by the presence of the moving liquid to observe the persistent currents. Starting from Landau's two-fluid theory and allowing the normal fluid and superfluid to have steady non-zero velocity fields, we find expressions for the



**Non-zero current
in the unpacked region**



**Non-zero current
in the unpacked region**



**Zero current
in the unpacked region**

FIGURE 5. SCHEMATIC OF VORTEX LINE CONFIGURATION

doppler-shifts of the first and second sound waves. ⁽⁶¹⁾

$$C_1 = C_{10} + (\rho_s/\rho V_s + \rho_n/\rho V_n) \quad (\text{II-1})$$

$$C_2 = C_{20} + (\rho_s/\rho V_s + \rho_n/\rho V_n) + (V_n - V_s) \left[\frac{2A}{\rho} - \frac{5}{\rho_n} \frac{\partial \rho_n}{\partial T} \right]_T \times \frac{\partial I}{\partial S} \Big|_T \quad (\text{II-2})$$

where the subscript zero denotes a quantity measured in the absence of the steady flow. The doppler-shift of first sound is analogous to the classical result. But the second sound doppler-shift has an extra term that is a direct manifest of the basic two-fluid assumption, which is not classical.

We can simplify the doppler-shift relation for the second sound by using the fact that all the entropy is carried by normal fluid, that is, $\rho S = \rho_n S_n$ and the Tisza approximation ⁽⁶²⁾ that S_n is approximately a constant, independent of temperature. This is valid in the range of the temperature 1.1°K to T_λ where S_n changes only 20%. Then (II-2) becomes

$$C_2 = C_{20} + (\rho_s/\rho V_s + \rho_n/\rho V_n) + (V_n - V_s)(\rho_s/\rho - \rho_n/\rho) \quad (\text{II-3})$$

The fourth sound velocity is also doppler-shifted in the presence of a persistent current ⁽⁶³⁾,

$$C_4 = C_{40} + [\rho_s/\rho + G(T)] V_s \quad (\text{II-4})$$

where

$$G(T) = S \left[\frac{\partial(\rho_n/\rho)}{\partial T} \right]_P / \frac{\partial S}{\partial T} \Big|_P - \rho \left[\frac{\partial(\rho_n/\rho)}{\partial P} \right]_T / \frac{\partial \rho}{\partial P} \Big|_T \quad \text{II-5}$$

At low temperatures ($T < 1.4\text{K}$), $G(T)$ is small (less than about 2%)⁽⁶⁴⁾ and the dominant factor in front of V_s in Equation (II-4) is ρ_s/ρ ;

$$C_1 = C_{10} + \rho_s/\rho V_s \quad (T < 1.4\text{K}) \quad (\text{II-6})$$

The three above equations (II-1,3,4) can be simplified further if the doppler-shift is caused only by the persistent current,

$$C_1 = C_{10} + \rho_s/\rho V_s \quad (\text{II-7})$$

$$C_2 = C_{20} + \rho_s/\rho V_s \quad (\text{II-8})$$

$$C_1 = C_{10} + [\rho_s/\rho + G(T)]V_s \quad (\text{II-9})$$

In a partially packed annulus the two sound modes C_{14} and C_{11} are doppler-shifted in the presence of a persistent current both in the packed and free regions.⁽⁶⁵⁾ The easiest way to arrive at an expression for the doppler-shifted velocities is to write down the most general solution to the wave equations in both regions and apply the boundary conditions at the interface. The details are worked out in Reference 65 and the results are:

$$C_{14} = C_{140} + \frac{G/\rho(L-d)V_F + (\rho_s/\rho + G(T))P(2-P)dV_P}{(L-d) + P(2-P)d} \quad (\text{II-10})$$

$$C_{II} = C_{II0} + P_m / \rho V_F \quad (II-11)$$

where v_F and v_p are the persistent currents in the free and packed regions.

Consider an annular cavity with outer radius a , inner radius b , and depth l . The pressure distribution of normal modes in the cavity⁽⁶⁶⁾ is given, in cylindrical coordinates, by

$$\begin{aligned} \Phi &= p_0 \cos m\tau \cos \frac{\pi z \pi}{l} z F_m(k_\lambda r) \cos 2\pi f t \\ &= p_0 \cos m\tau \cos 2\pi f t H(z, r) \end{aligned} \quad (II-12)$$

$$H(z, r) = \cos \frac{\pi z \pi}{l} z F_m(k_\lambda r) \quad (II-13)$$

where $z=0$ at one of the end walls, p is the acoustic pressure and p_0 its amplitude, m and m_z are integers, f is the resonant frequency and $F_m(k_\lambda r)$ is given by

$$F_m(k_\lambda r) = J_m(k_\lambda r) - \frac{J'_m(k_\lambda b)}{N'_m(k_\lambda b)} N_m(k_\lambda r) \quad (II-14)$$

J_m and N_m are the m -th order Bessel function of the first and second kind, respectively. The values of $k_\lambda = \frac{\pi \gamma_{mn}}{a}$ are obtained from

$$\frac{J'_m(\pi \gamma_{mn})}{N'_m(\pi \gamma_{mn})} = \frac{J'_m(\pi \gamma_{mn} h/a)}{N'_m(\pi \gamma_{mn} h/a)} \quad (II-15)$$

Using a trigonometric identity, equation (II-4) can be written as

$$P = P_0/2 \left[\cos(2\pi f t + m\varphi) + \cos(2\pi f t - m\varphi) \right] H(z, \lambda) \quad (\text{II-16})$$

Equation (II-15) represents the two running modes which travel in opposite directions in the annulus and are degenerate as long as the velocity of sound in both directions is the same.

If we look at the resonant frequencies in this cavity we see that the low frequency solutions (that is, when the wave length is larger than the height and width of the annulus), $|b-a|, \lambda \ll \lambda$ are plane waves running in both directions around the cavity. In this range of frequencies one can write the following relation for the resonance frequencies:

$$F_m = \frac{nC}{2\pi R} \quad (\text{II-17})$$

where n is an integer and R is the mean radius of the cavity. More complicated resonant modes occur when one of the height or width modes get excited. A spectrum of amplitude versus frequency for the resonances in air of an annular cavity of diameter 10.5 cm and channel width and depth of .5 cm (taken from Reference 65) is shown in Fig. 6. Since the ratio of the circumference to twice the width or height of the channel is ~ 33 , there are 33 azimuthal modes before the first height or width mode which comes in at about 35 KHz.

Consider now the above cavity packed with powder. A persistent current can be generated. Then the two waves traveling in the two different directions are not degenerate anymore and one travels with velocity $C_{40} + \alpha V_p$ and the other with velocity $C_{40} - \alpha V_p$ where $\alpha = \rho_s / \rho + G(T)$.

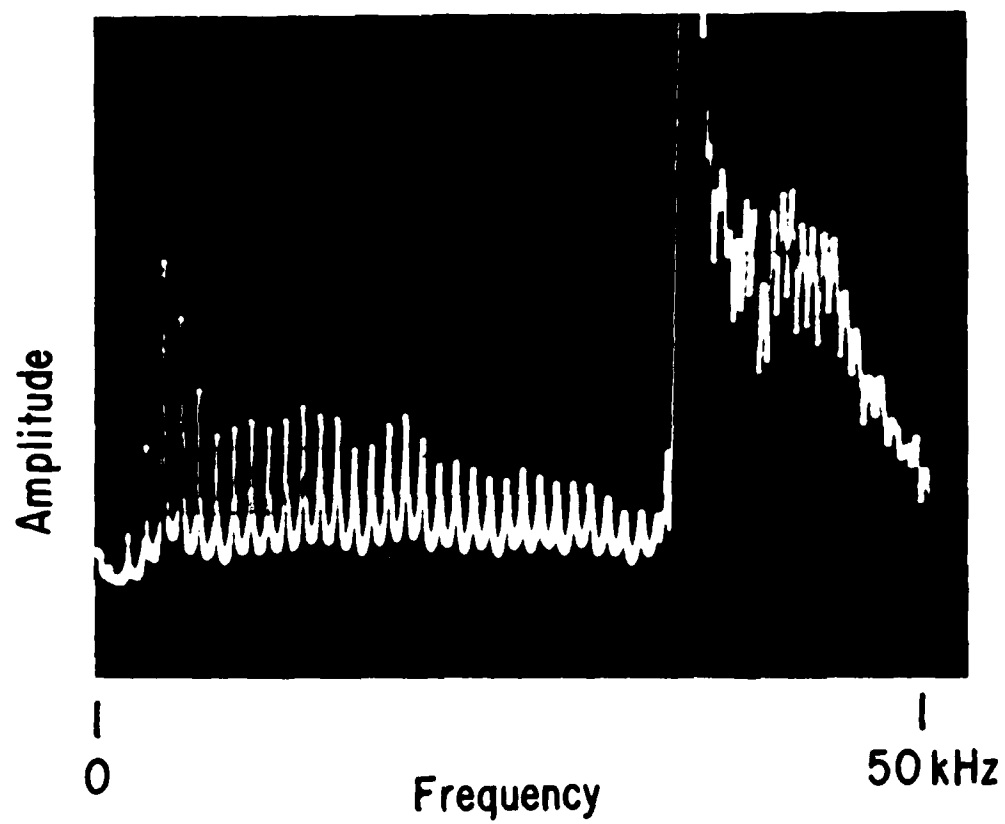


FIGURE 6. -RESONANCES IN AIR OF AN ANNULAR CAVITY OF RADIUS $R=5.25\text{cm}$ AND HEIGHT AND WIDTH OF 0.5cm

Therefore, the two resonant frequencies will be:

$$F_1^+ = n_1 (C_{10} + \alpha V_p) / 2\pi R \quad (\text{II-18})$$

$$F_1^- = n_1 (C_{10} - \alpha V_p) / 2\pi R \quad (\text{II-19})$$

$$V_p = \frac{\Delta F_1 (\pi R)}{n_1 \alpha} \quad (\text{II-20})$$

Applying the same method to derive the persistent current in case of a partially packed annulus and in the case where $V_F \ll V_p$ we have:

$$F_{1,q}^+ = n_{1,q} (C_{10} + \alpha' V_p) \quad n_{1,q} = 1, 2, 3 \dots \quad (\text{II-21})$$

$$F_{1,q}^- = n_{1,q} (C_{10} - \alpha' V_p) \quad (\text{II-22})$$

$$\alpha' = \left[\frac{P(2-P)d}{(L-d) + P(2-P)d} \right] P/p \quad (\text{II-23})$$

subtracting the two equations and substituting for α we get:

$$V_p = \frac{\pi R}{n_{1,q}} (P/p) \left[\frac{(L-d) + (2-P)Pd}{P(2-P)d} \right] \Delta F_{1,q} \quad (\text{II-24})$$

and $V_F = \frac{\pi R}{n_{II}} (P/p_m) \Delta F_{II}$ where $n_{II} = 1, 2, 3 \dots$
(II-25)

Therefore the observed splitting of C_{14} mode could be directly related to the persistent current velocity in the powder. These results have been rigorously derived by J. Rudnick.⁽⁶⁷⁾

3. Experimental Apparatus

Measurements of the decay of a persistent current were made by observing the resonances of a closed cavity as shown in Fig. 7. It is an annular cavity with a square cross section which is packed with powder to a height "d". The superleak was prepared to lock the normal component. To do so the pore sizes have to be much smaller than the viscous wavelength. The powder used was 500Å diameter Al_2O_3 powder.⁽⁶⁸⁾ The grains are roughly spherical, and an electron microscope photograph shows that 500Å is the upper limit of the size distribution, and the average size is in the range of $\sim 325\text{Å}$. Taking the average grain size $\sim 300\text{Å}$, $\eta \sim 10^{-5}$ poise, and $\rho_n \approx 8.7 \times 10^{-3} \text{ g/cm}^3$. At $T = 1.35^\circ\text{K}$, and using the equation for viscous wavelength λ_n ;

$$\lambda_n = \sqrt{\frac{2\eta_n}{\rho_n \omega}} \quad (\text{II-26})$$

and solving for ω , we find $\omega \sim 10^{10} \text{ sec}^{-1}$. This requires that the angular frequency ω be much less than 10^{10} sec^{-1} . Angular frequencies used in the experiments were at most $5 \times 10^5 \text{ sec}^{-1}$. It is clear that the normal fluid is well locked.

The packing procedure is as follows. An appropriate amount of powder is poured into the cavity and it is pressed into the cavity by a plunger with an hydraulic press. This was done in many stages. In every stage less than 1 millimeter of powder was packed, leveled, and then the porosity for that layer was calculated, before the next layer was packed. Also, the pressure applied to each layer was increased relative to the previous layer to achieve constant porosity throughout the depth of the powder. Finally, the annulus was put in a milling

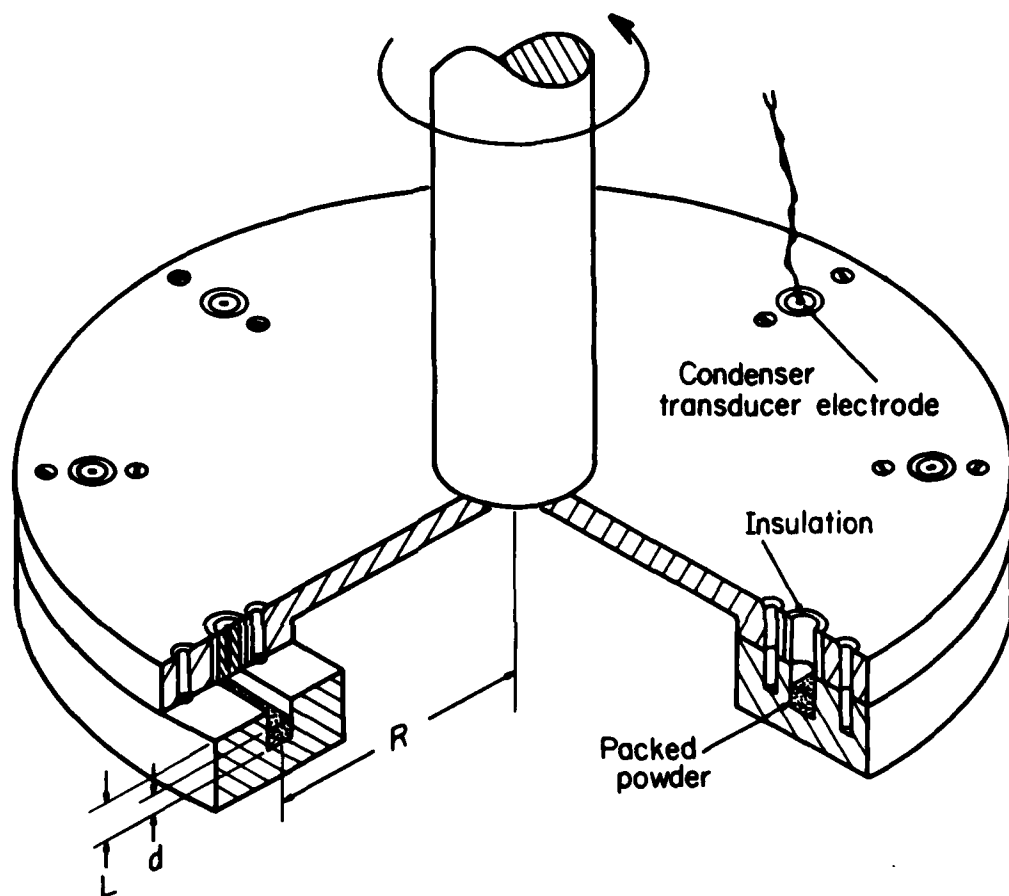


FIGURE 7. CUTAWAY DRAWING OF ANNULAR RESONATOR USED IN DECAY MEASUREMENTS

L IS 5mm, AS IS THE WIDTH OF THE ANNULUS. $R=5.25\text{cm}$

machine and the powder was machined to the desired depth. Eight identical annuli were prepared in this fashion with different powder depths for the decay measurements. The packing tool is shown in Fig. 8.

The porosity was determined by weighing the amount of powder, W , measuring the packed volume of the cavity, V_p , and knowing the specific gravity of the powder, ρ_p . The porosity is given by:

$$P = 1 - \frac{W}{\rho_p V_p} \quad (X-27)$$

For detecting and generating the modes in the annulus pressure transducers are used. Eight circular metal buttons are mounted on the top plate as shown in Fig. 9, and the transducer, which consists of 13 μ m thick teflon sheet⁽⁶⁹⁾ aluminized on one side, is laid against the top plate of the annulus. The assembled resonator is shown in Fig. 10. The aluminized teflon and the button form a capacitor which acts as a drive or a pickup. Teflon is used for this purpose due to its ability to permanently trap electric charges. Materials with this quality are known as electrets.⁽⁷⁰⁾ The aluminized teflon used in this experiment first is placed on a glass plate which is then sandwiched between two metallic plates, and then a large D.C. voltage (~ 8 kV) is applied to the plates for about 20 minutes. By doing this we permanently polarize the teflon and eliminate the need for an external biasing supply.

Figs. 11 and 12 are the schematic drawing and a photograph of the rotating probe. The cell is suspended from a 1.5" diameter stainless steel tubing which runs through three self-aligning ball bearings, two at the top at room temperature and one, degreased and placed near the

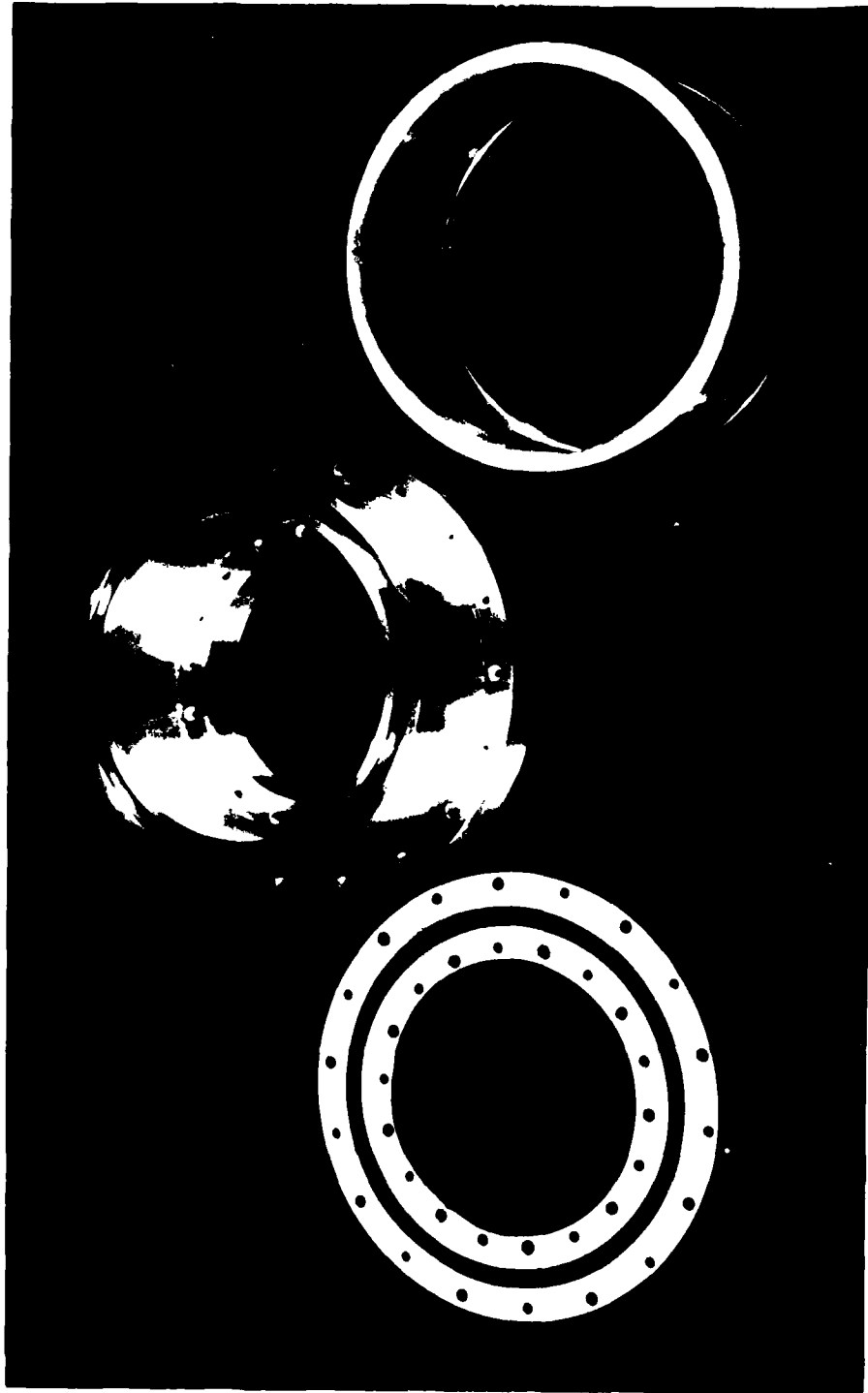


FIGURE 8. PACKING TOOL USED TO PACK POWDER INTO THE ANNULUS.



FIGURE 9. OPEN VIEW OF THE RESONATOR WITH TOP PLATE



FIGURE 10. CLOSED VIEW OF THE RESONATOR

bottom which provide the necessary alignment and keep the probe from wobbling. The probe is also centered by three adjustable teflon pads which press against the inner wall of the helium dewar. There is also a rubber O ring pressed on the main rotating tube on the top which provides the vacuum seal. The probe is provided with a large fly wheel to make the rotation smooth. The assembly is rotated by a D.C. motor which is connected to the stainless steel shaft through belts and gears, and the speed could be varied by adjusting the voltage applied to the motor. The angular frequency of rotation is measured with the help of an optical switch (HEI Inc., OS-5915) and a timing wheel composed of an aluminum disk with 100 holes equally spaced around the circumference.

The temperature is lowered by pumping away the vapor by a Stokes vacuum pump (Model 212) and temperatures as low as 1.2K could be reached. A 50 mm Wallace and Tiernan pressure gauge (Model FA 160) calibrated with a 1958 helium temperature scale was used to measure temperature. A co-axial capacitive He level indicator is used to monitor the helium level in the bath.⁽⁷¹⁾

All electrical signals are carried through stainless steel coaxial cables which run inside the main stainless steel shaft. At the top the pick up cables enter a rotating amplifier box. All the cables are carefully shielded.

Rotating slip rings (Fabricast, Inc., South El Monte, CA) are assembled at the top of the probe in order to be able to make measurements while rotating. A standard 6" stainless steel double dewar was used throughout the experiments.

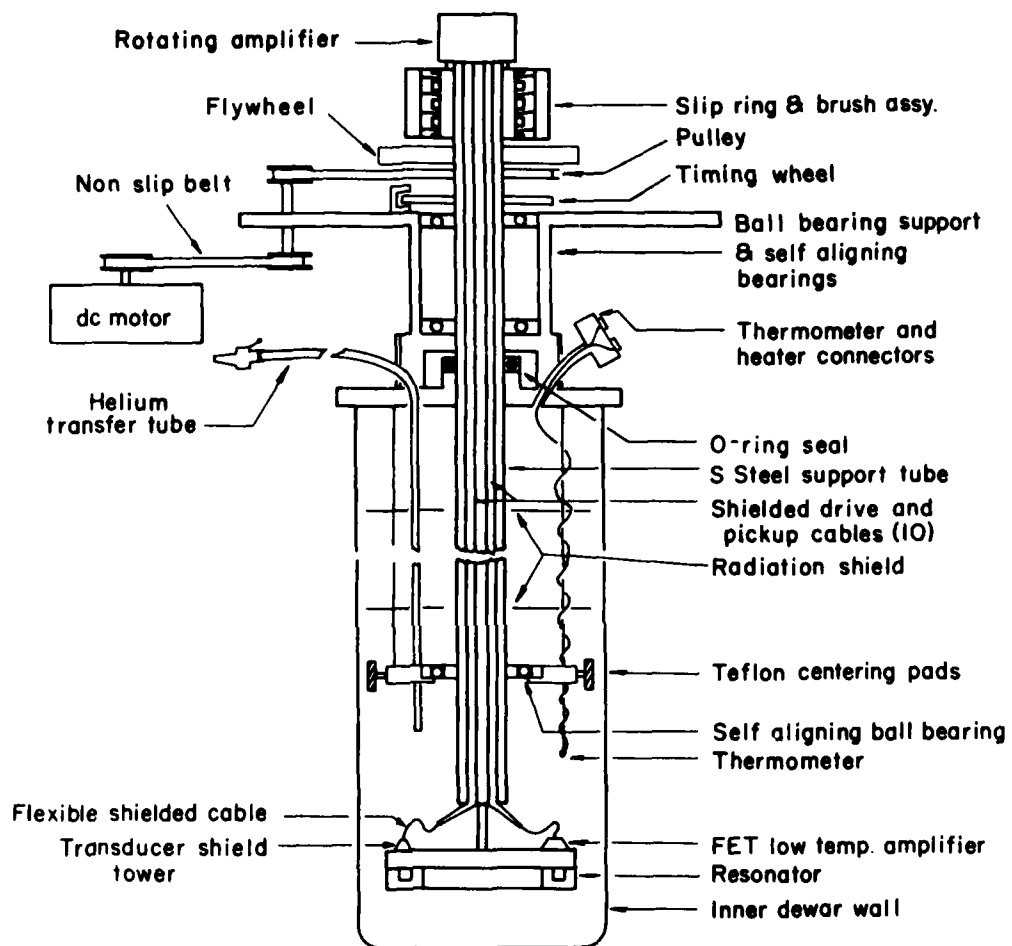


FIGURE 11. SCHEMATIC OF ROTATING APPARATUS USED IN MEASUREMENTS OF THE DECAY OF PERSISTENT CURRENT.

4. Electronics and Temperature Measurements

In order to measure the decay of persistent current, its velocity must be measured as a function of time. As discussed in Chapter I, if the persistent current in a partially packed annulus decays at all, one will expect the decay rate to be logarithmic with time. Consequently, the amount of decay per unit time is found to be greatest just after it has been created. In this time region measurements have to be made rather quickly and the usual technique for observing persistent current velocity (sweeping the resonance curve through the splitting) is not suitable. Since it requires at least 20-30 seconds to complete one measurement, and the current will be decaying during this time interval, two different methods were used for time regions below 500 sec and above 500 up to 10,000 sec which are discussed here.

A. Free Decay Technique

This method allows us to make 2 measurements in 1 second. This technique is commonly used in acoustical measurements of the reverberation time of a room. If we apply a narrow band of frequencies to a resonator, all the frequencies are excited. Now if we turn the source off only the resonance frequencies within that band will be present and they decay exponentially with time. Now if the narrow band of frequencies includes the split C_{14} doublet, it will excite both modes. Then after the source is turned off they will free decay and also beat against each other. The beat frequency equals ΔF_{14} in Equation (II-23) and thus gives V_p .

In most experimental measurements of first-fourth sound resonances, for resonance frequencies of about 15000 Hz, a typical quality factor,

Q , is about 2000. Therefore the free decay time $\tau = \frac{2Q}{\omega_0} \sim \frac{1}{4}$ sec which makes it possible to make the aforementioned 2 measurements per second. Fig. 13 shows a block diagram of the complete electronic apparatus used in this part of the experiment. A modulated beat frequency oscillator (B&K, type 1013) is the narrow band signal generator. The amplifier output is turned on and off electronically by the tone burst generator (G.R. 1396A). Due to the asymmetry of the experimental cell, that is, irregularities of the annulus, packing, the transducer and etc., most of the time the two peaks in a doublet were not equally excited. To correct for that, two drive transducers were used and the drive signal on the second transducer was phase shifted to compensate for the irregularities. The output of the receiver transducer was fed into an FET amplifier⁽⁶⁵⁾ which was designed to operate at these low temperatures and to compensate for cable losses and eliminate pick up. The pre-amplifier is connected at the top of the probe to a low noise operational amplifier (Analog Devices 606)⁽⁶⁵⁾ which rotates with the assembly. The output of the signal at this stage is passed through a band pass filter (B&K, type 1612) and then fed into the audio frequency spectrometer (B&K, type 2112). The output of the audio spectrometer is continuously fed into a tape recorder (Sony Corp., TC 800) which stores the data for a later analysis. For the data analysis the tape recorder is played back at a reduced speed (1/4 of the actual recording speed). Its output is fed into a wave analyzer (G.R. 1900A) operated in its normal mode, as a narrow band filter and amplifier. Finally, the output of the wave analyzer is recorded on a high writing speed level recorder (B&K, type 2305). From the recorded signal one can calculate the

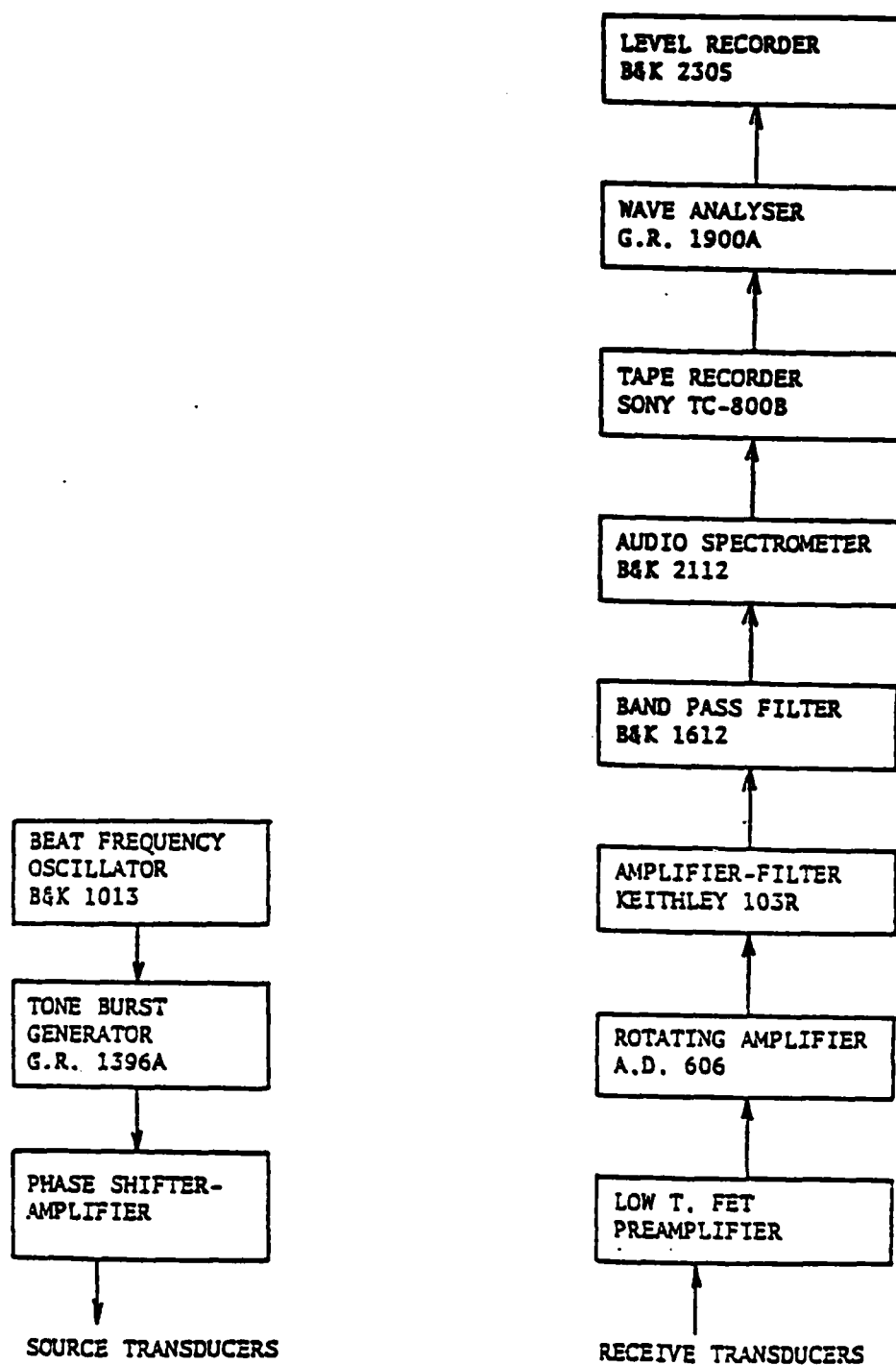


FIGURE 12. BLOCK DIAGRAM OF ELECTRONICS USED IN MEASUREMENTS OF THE DECAY OF PERSISTENT CURRENTS

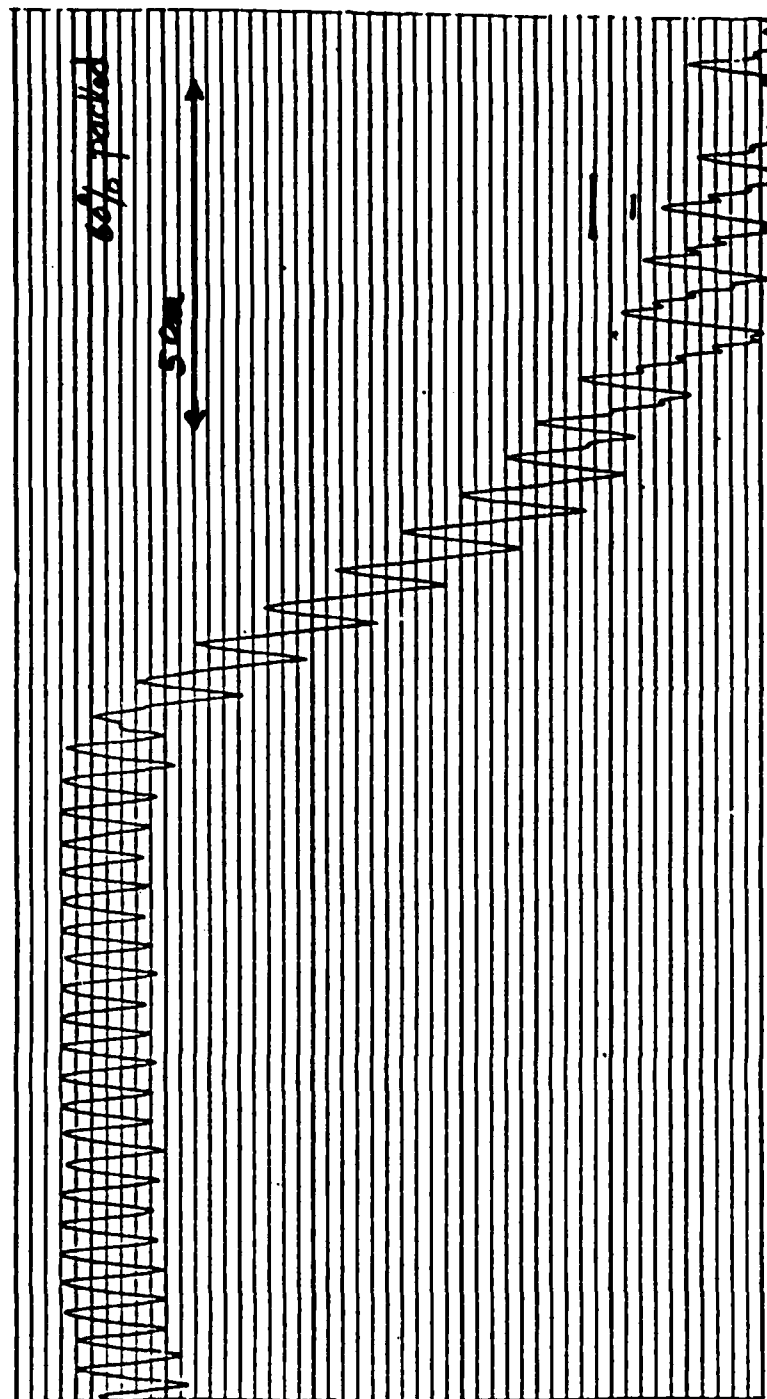


FIGURE 13. BEATING OF FOURTH SOUND DOUBLET IN FREE DECAY

the frequency of the doublet.

A photograph of free decay recording is shown in Fig. 14. The scale used for amplitude is logarithmic and each division in the recording corresponds to 1 db. The splitting is determined by measuring the distance between two peaks over several of the beatings. Knowing the paper speed and the tape recorder speed one can calculate the frequency.

B. Sweeping through Resonance

This technique is used to $t > 500$ seconds. The decay during the time interval taken for a complete sweep (20-30 sec) is unobservable. A block diagram of the complete electronics used in this part is shown in Fig. 15.

A Hewlett-Packard 3580A spectrum analyzer in its tracking oscillator mode was used to drive and detect the signals. Its output level can be adjusted from zero to 2V rms. The oscillator output of the analyzer is amplified and run through a phase shifter network. As was mentioned in part A, two drive transducers were used to equalize the peaks of the doublet. In the case when ΔF (splitting of the doublet) is much larger than δF (the band width of the unsplit mode) the inequality of the heights does not introduce a problem. Only when δF and ΔF become comparable is equal excitation advisable. The signal from the receiver transducer is passed through the two amplifiers mentioned in part A (the FET in liquid helium and the Analog Devices 606 operational amplifier, rotating with the probe).

Then the signal is passed through the sliprings to the input of the wave analyzer. In this manner, most of the amplification takes

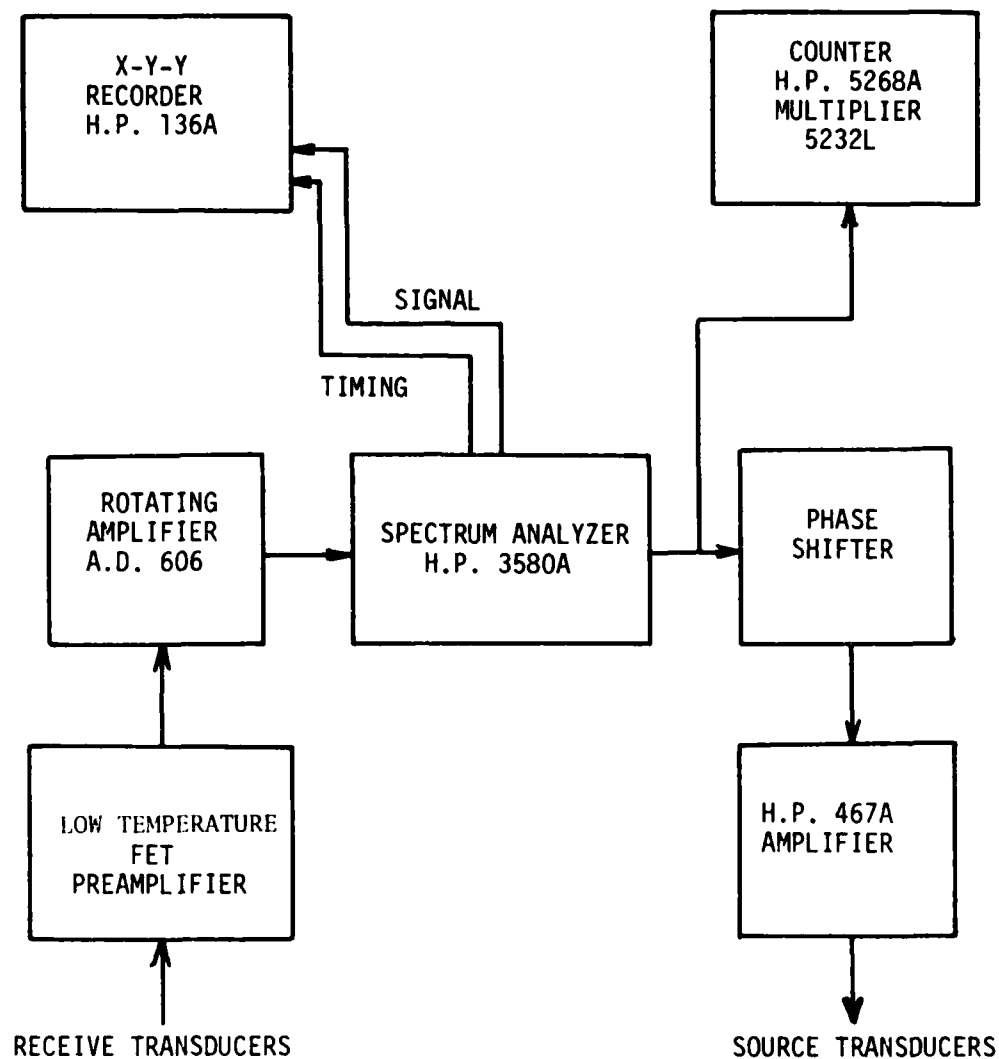


FIGURE 14. BLOCK DIAGRAM OF ELECTRONICS USED IN MEASUREMENTS OF THE DECAY OF PERSISTENT CURRENTS.

place in the probe and minimizes the noise caused by the sliprings during rotation. The analyzed output of the spectrum analyzer is fed into a chart recorder which permanently records the data on graph paper. Fig. 16 shows the two graphs obtained in this manner before and after creation of a persistent current. The graph is a plot of amplitude versus frequency for (27th) mode in a fully packed annulus. The frequency information could also be recorded on the same paper simultaneously by another pen.

In all measurements temperature was stabilized by a temperature controller modeled after a low noise bridge circuit suggested by Anderson⁽⁷²⁾ that used a ratio transformer (Gertsch, model 216) and a phase sensitive detection circuit. The off-balance signal from the detector was amplified and sent into a heater in the bath (350 Ω wire wound resistor) to form a negative feed back circuit which maintained the bath temperature constant to within ~ 1 mK.

5. Measurements of Decay Rate as a Function of the Depth of Powder

The rotating probe and electronics described in the previous sections were used to measure the persistent current velocity by observing the splitting of C_{14} and using the relation (II-24). All measurements were made at 1.35°K, therefore $G(T)$ could be ignored. Before generating a persistent current all the plane wave resonances of C_{14} were examined for quality factor, Q , amplitude, and splitting in the absence of a current. In all of the experimental runs an effort was made to choose a high Q and a non-split mode. After examining the spectrum of the desired resonances, the system was warmed above

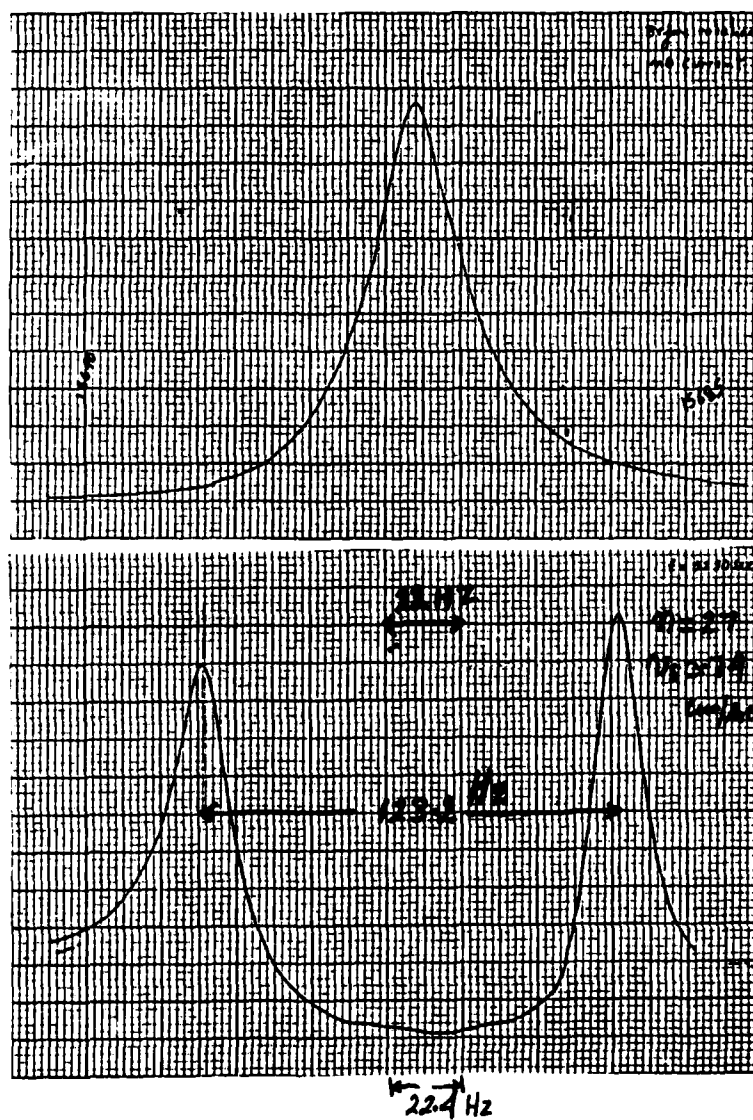


FIGURE 15. C_{14} RESONANCES WITH AND WITHOUT SPLITTING.

T_{λ} . While rotating at constant speed, (about 9 c.p.s.), always above the saturation critical velocity in the powder, the system was cooled to 1.35°K. Then the speed of rotation was reduced to 1.5 c.p.s. and the temperature was regulated within ± 0.05 mk. When the necessary electronic adjustments were made the rotation was suddenly stopped. The results of the measurements of the saturated persistent current velocities against time for various depths of powder are plotted on a semi-log paper and are shown in Figs. 17 through 24. All the graphs show a logarithmic decay, but the decay rate varies for different resonators. A summary of relevant information including the fractional decay rate per decade for all the resonators is shown in Table I. Also Fig. 25 shows a plot of the fractional decay rate per decade versus depth of the powder. Different points for the same powder depth refer to different runs. Many of the runs were repeated to check the consistency of the data.

6. Results and Discussions

The main result obtained from measurements of the fractional decay rate as a function of the depth of the powder, is the fact that the fractional decay rate for all depths stays more or less constant with an average decay rate of 2.5% per decade. This means that the stability of the persistent current is affected neither by the free exchange of mass between the two regions, nor by the variation in the depth of the powder. Other features of Fig. 25 are that there is a local maximum at 90% packed annulus, and also there exists a slight increase in the decay rate as the powder depth is decreased.

These remarkable results could only be understood by considering

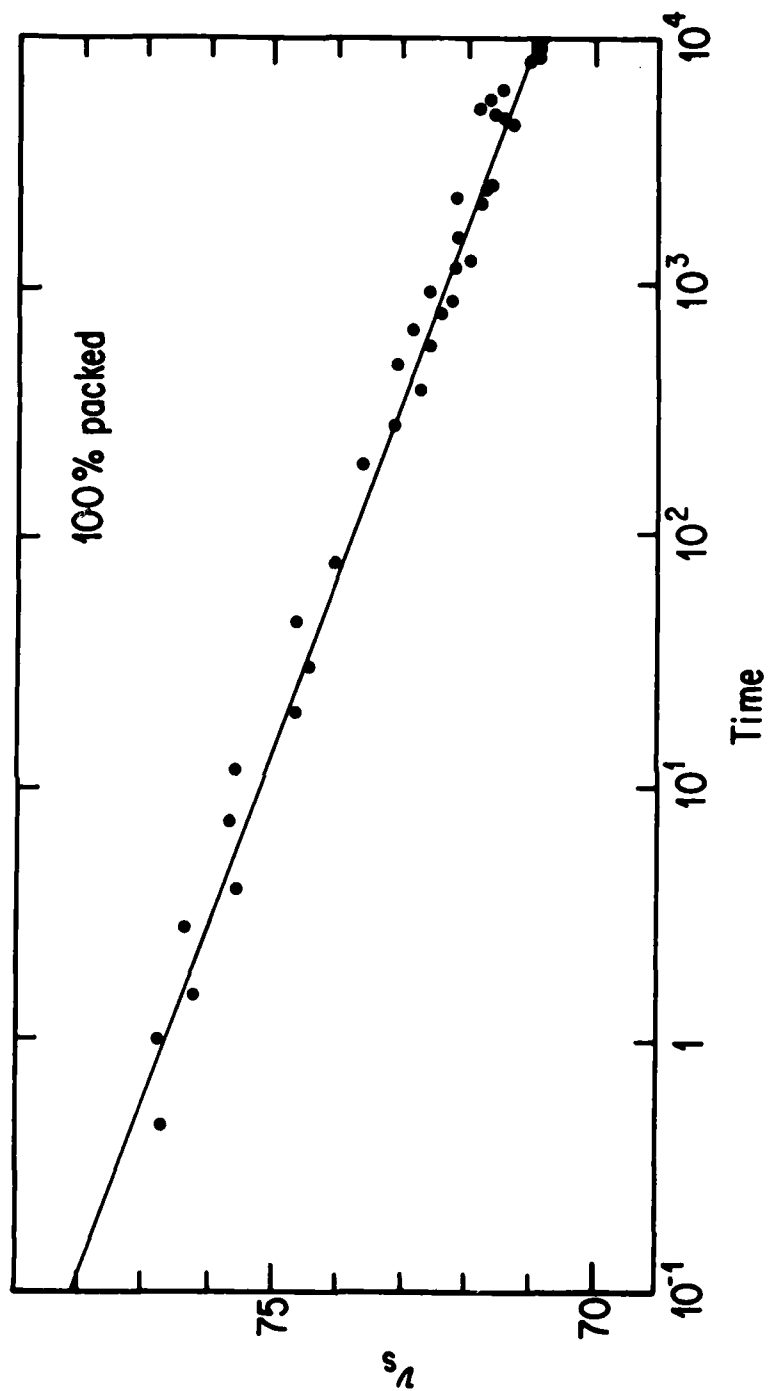


FIGURE 16. DECAY OF SATURATED PERSISTENT CURRENT IN 100% PACKED ANNULUS AT 1.35°K.

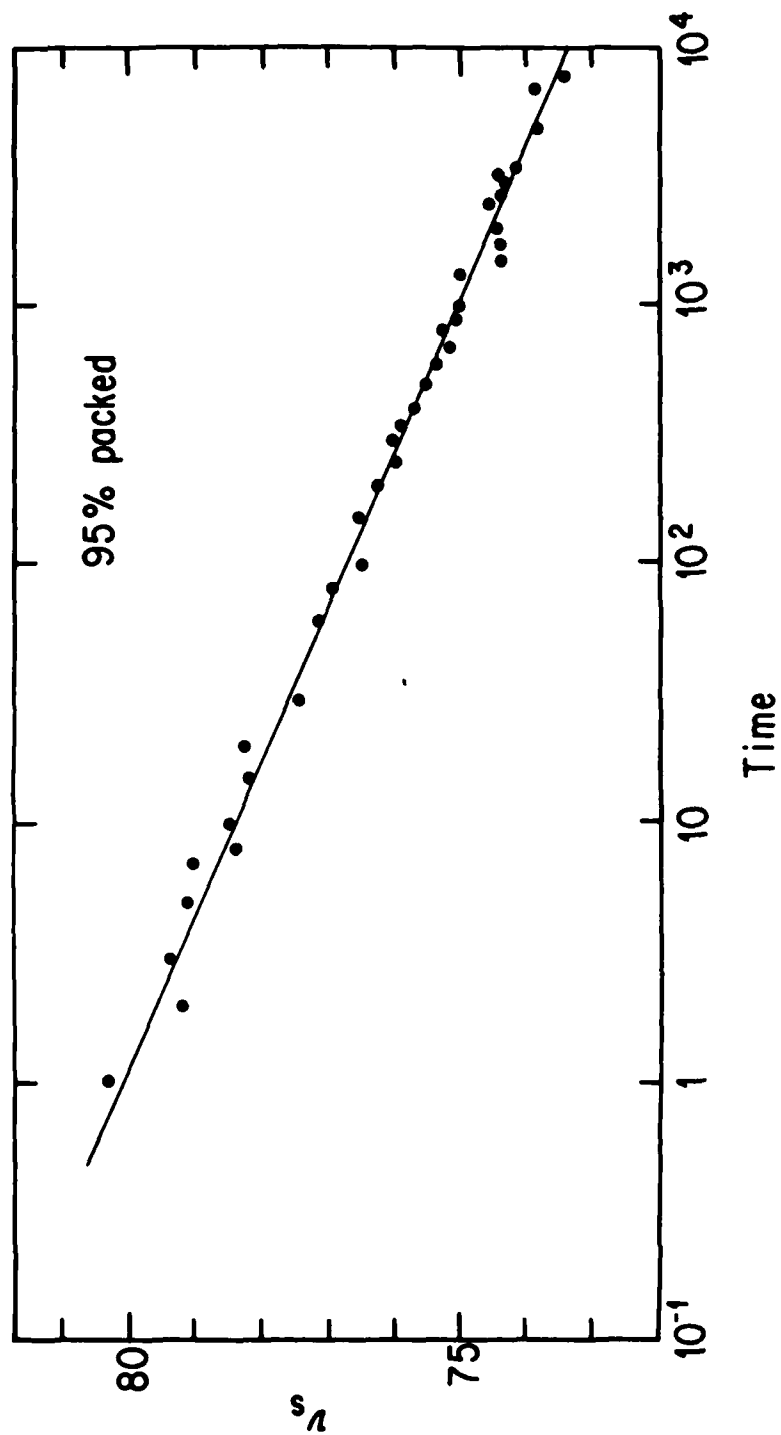


FIGURE 17. DECAY OF SATURATED PERSISTENT CURRENT IN 95% PACKED ANNULUS AT 1.35°K.

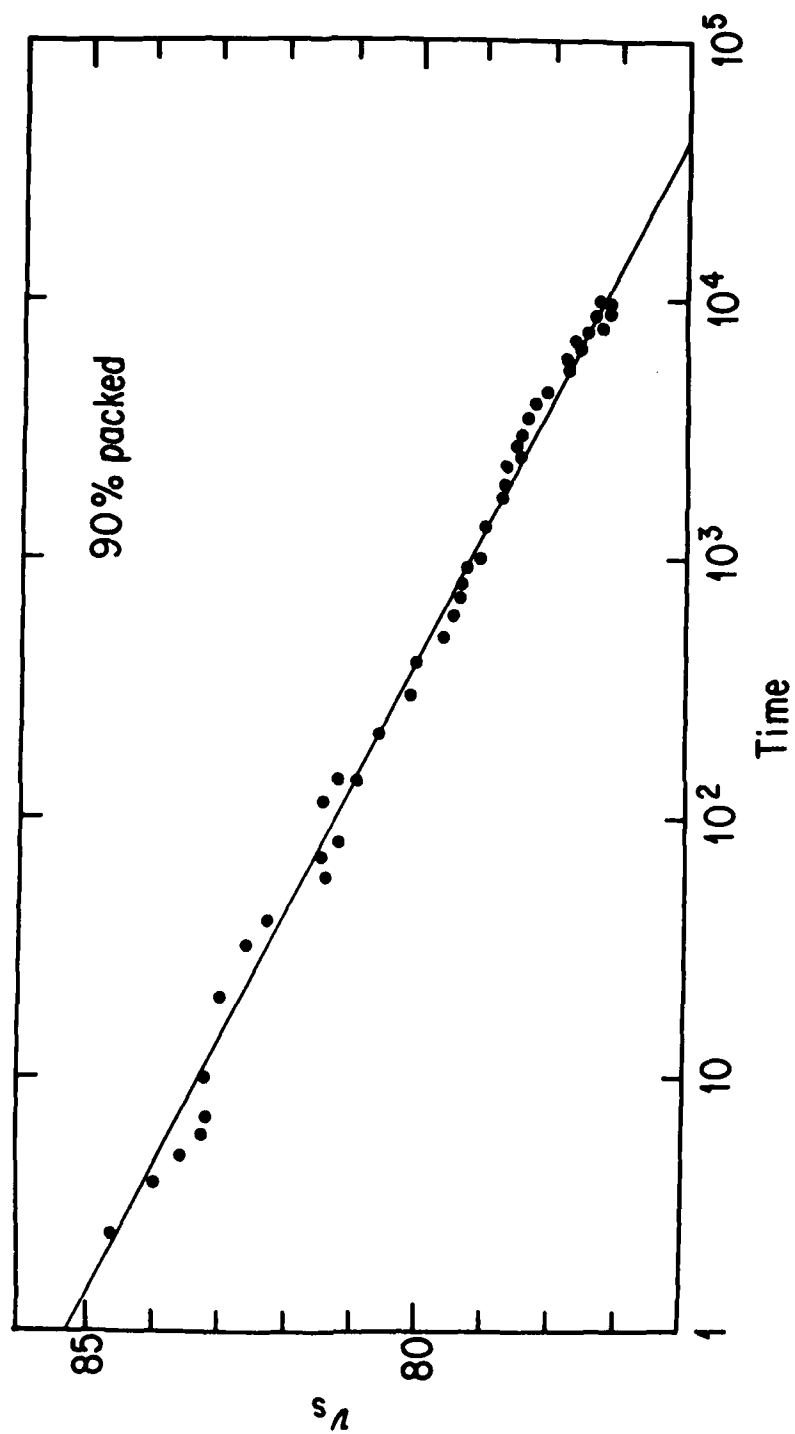


FIGURE 18. DECAY OF SATURATED PERSISTENT CURRENT IN 90% PACKED ANNULUS AT 1.35° K.

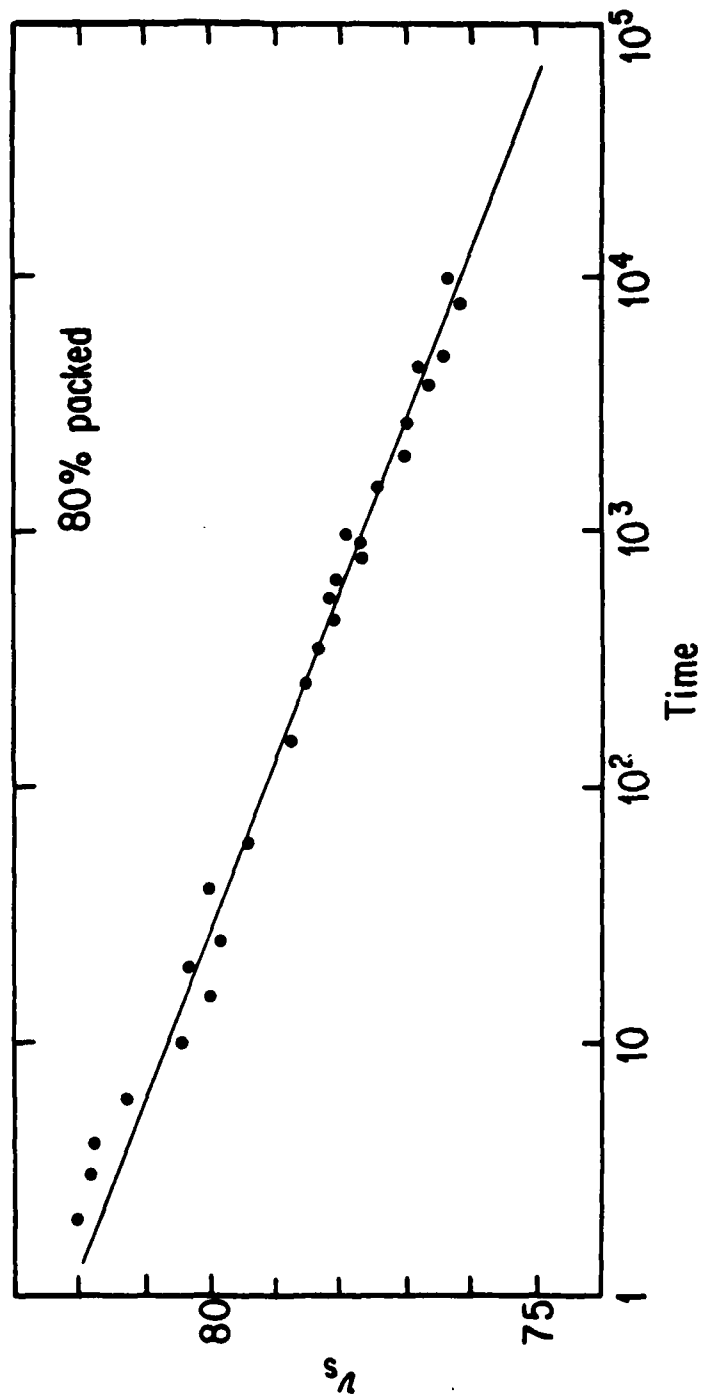


FIGURE 19. DECAY OF SATURATED PERSISTENT CURRENT IN 80% PACKED ANNULUS AT 1.35°K.

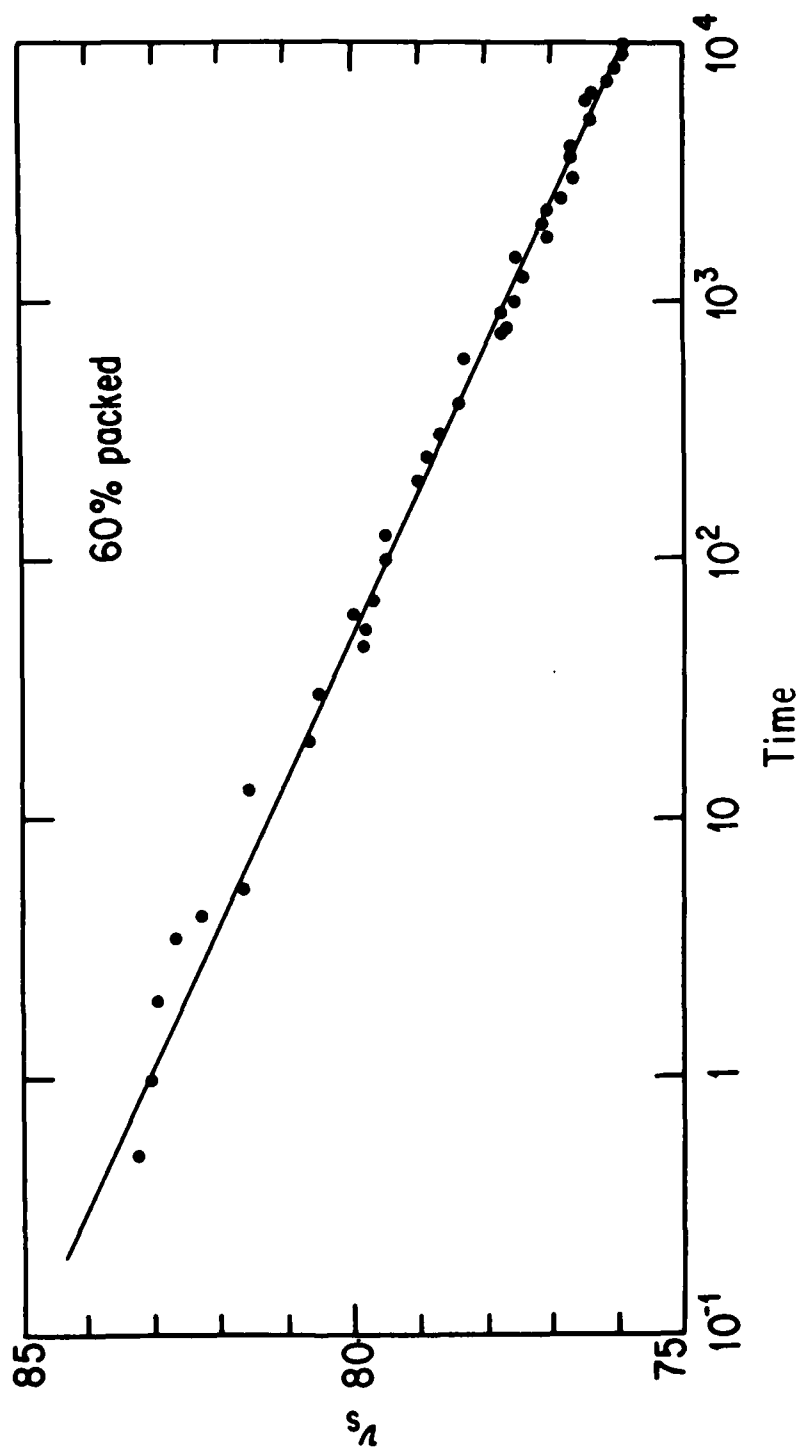


FIGURE 20. DECAY OF SATURATED PERSISTENT CURRENT IN 60% PACKED ANNULUS AT 1.35°K.

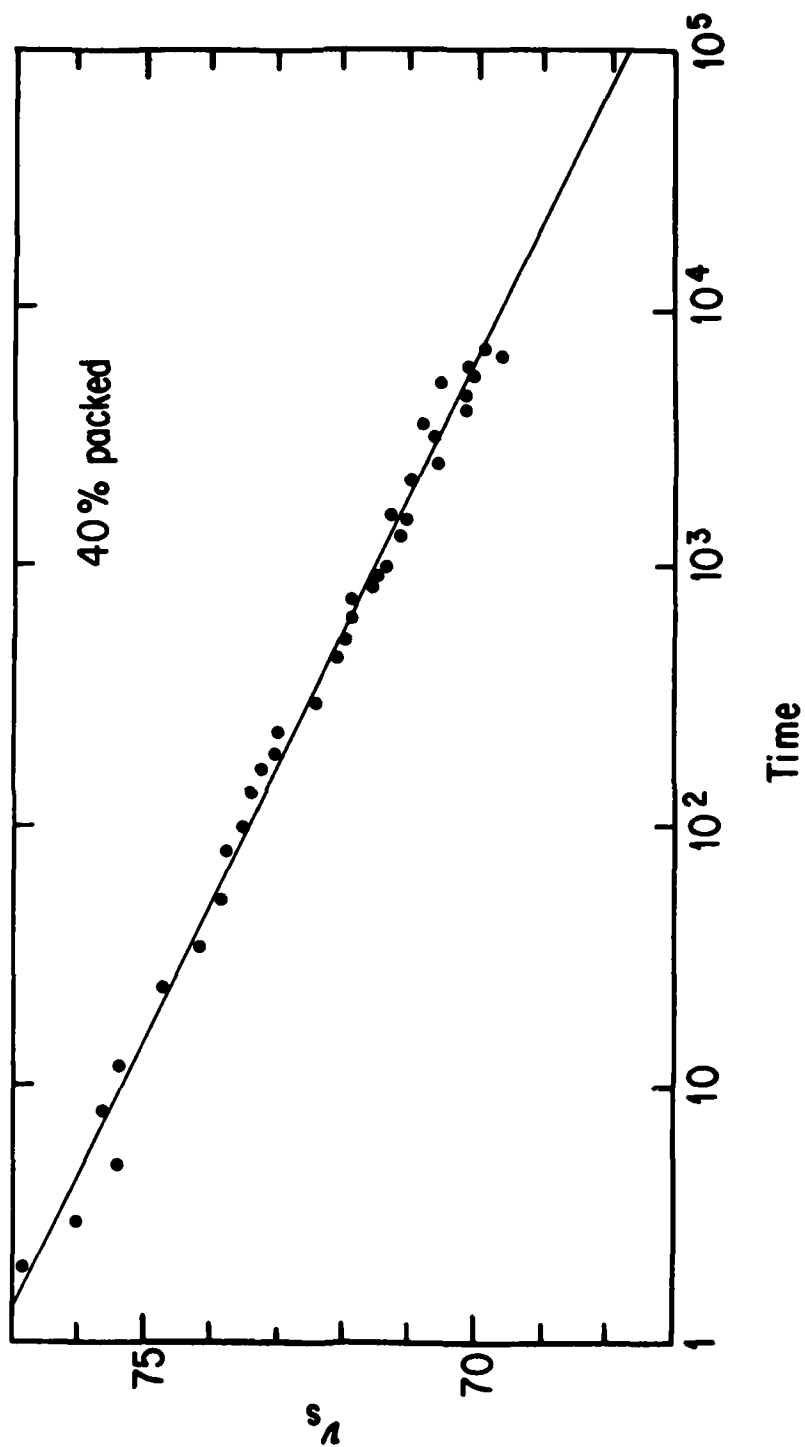


FIGURE 21. DECAY OF SATURATED PERSISTENT CURRENT IN 40% PACKED ANNULUS AT 1.35°K.

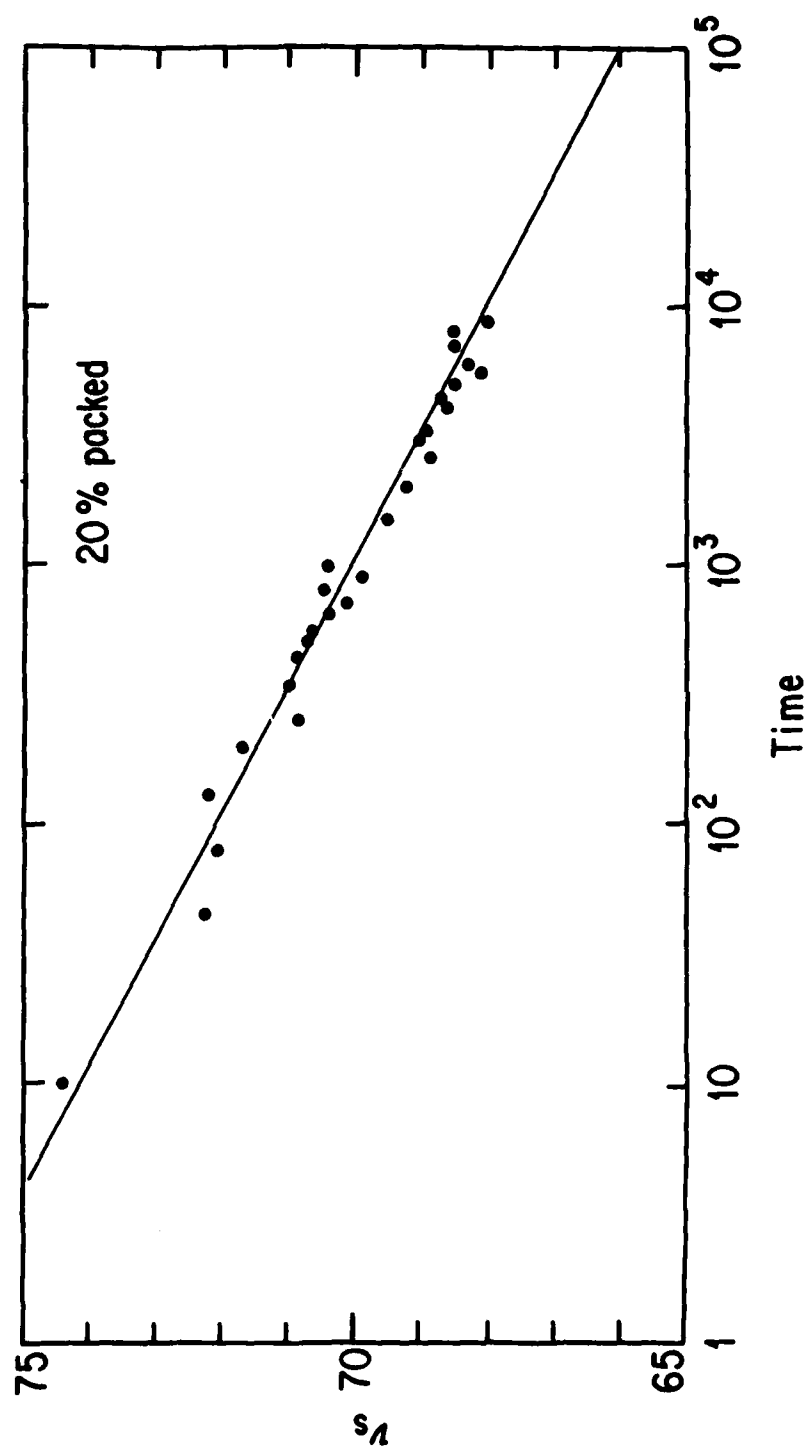


FIGURE 22. DECAY OF SATURATED PERSISTENT CURRENT IN 20% PACKED ANNULUS AT 1.35°K.

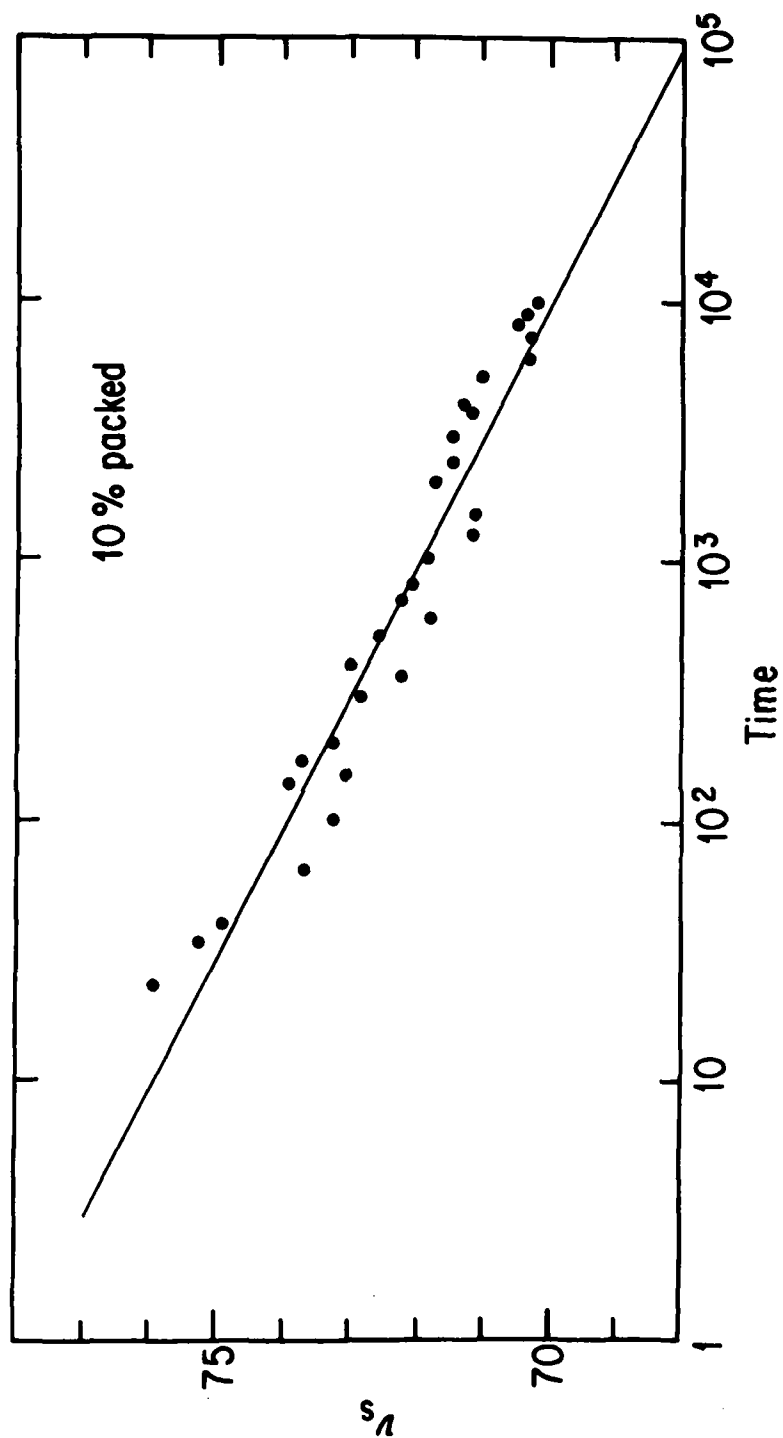


FIGURE 23. DECAY OF SATURATED PERSISTENT CURRENT IN 10% PACKED ANNULUS AT 1.35°K.

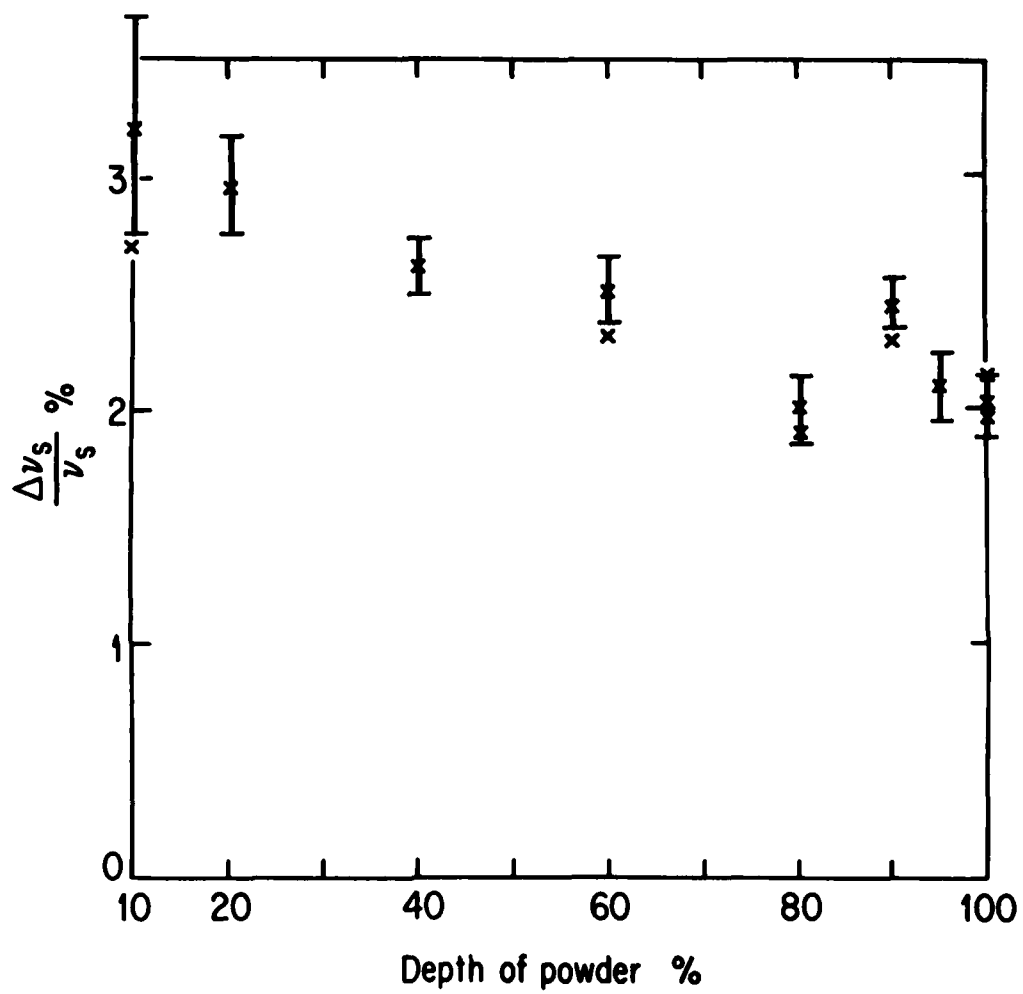


FIGURE 24. FRACTIONAL DECAY RATE PER DECADE VERSUS PERCENTAGE OF THE DEPTH OF THE ANNULUS FILLED WITH POWDER.

% Packing	100	95	90	80	60	40	20	10
P	.70	.71	.70	.71	.71	72	71	.71
$\frac{\Delta V_s}{V_s}$ % Per 100	2.14 1.97	2.1	2.28 2.43 2.44	1.9	2.3 2.75 2.49	2.601	2.954	2.664
$V_{s,c}$	77	80	85	82	83	77.2	76	78

TABLE I. MEASURED DECAY RATES FOR VARIOUS DEPTH OF POWDER AND
THEIR ASSOCIATED POROSITY AND CRITICAL VELOCITIES.

the possible vortex configurations in this geometry. If we assume zero current in the free region then the vortices in the powder will not extend through the free region; also they cannot terminate on the powder particles on the interface, for by Kelvin circulation theorem Equation (I-14), which hold throughout the fluid, the vortex must terminate on the container or itself. Thus there is a vortex sheath at the interface which seems to confine the current to the superleak and is also necessary or responsible for the stability of the persistent current in the powder. (See Fig. 5). If a large persistent current ($\sim 100\text{cm/sec}$) in the superleak co-exists with a very small current ($< 1\text{cm/sec}$) in the free region (see Ref. 65), there might exist a combination of vortex sheath and a small number of vortex lines which extend through the free region and terminate on the top of the annulus, as shown in Fig. 5. Then higher fluctuations and instability in the free region might enhance the decay rate of the persistent current in the powder. This approach could explain the local maximum observed at 90% packed annulus if one assumes a small current in the free region for this geometry, which is logically expected to have the largest persistent current in the free region compared to the other packings. Finally as the depth of the powder is decreased the observed splitting of C_{14} resonances decreases and the percentage of the error in the measurements will increase. The error bars in Fig. 25 indicate this fact. Therefore, the increase in the error could account for a part of the increase in the fractional decay rate as the powder's depth decreases.

CHAPTER III. TEMPERATURE DEPENDENCE OF SPLITTING FACTOR $[\rho_s/\rho + G(T)]$

We have shown before that fourth sound velocity will be doppler-shifted in the presence of a persistent current in a fully packed annulus and the velocity of the waves are given by the following relation:

$$C_4 = C_{40} + [\rho_s/\rho + G(T)] V_s \quad (\text{III-1})$$

where $G(T)$ consists of two parts

$$G_1(T) = -\beta \left[\frac{\partial \rho_s/\rho}{\partial T} - s \cdot \rho \frac{\partial \rho_s/\rho}{\partial P} \right] \frac{T C_p^2}{C_p} \quad (\text{III-2})$$

$$G_2(T) = s \cdot \frac{\partial \rho_s/\rho}{\partial T} \frac{T}{C_p} - \rho C_p^2 \frac{\partial \rho_s/\rho}{\partial P} \quad (\text{III-3})$$

$$G(T) = G_1(T) + G_2(T) \quad (\text{III-4})$$

The values of $G_1(T)$ and $G_2(T)$ may be derived from published thermodynamic data for superfluid helium II. In the absence of such data for our superleak, bulk data were used. This could be a source of discrepancy between the calculated and experimental values. Fig. 26 shows plots of calculated values for $[\rho_s/\rho + G_2(T)]$ and $[\rho_s/\rho + G(T)]$ against temperature. These functions were evaluated using ρ_s/ρ in a superleak from Kriss and Rudnick⁽²⁴⁾ (and also from References 64 and 65), evaluating $\frac{d}{dT} (\rho_s/\rho)$ for superleak, by taking the derivative of the known data for ρ_s/ρ , and for the rest of the thermodynamic variables the data for bulk helium II from Maynard⁽⁷³⁾ were used. From Fig. 26 one can

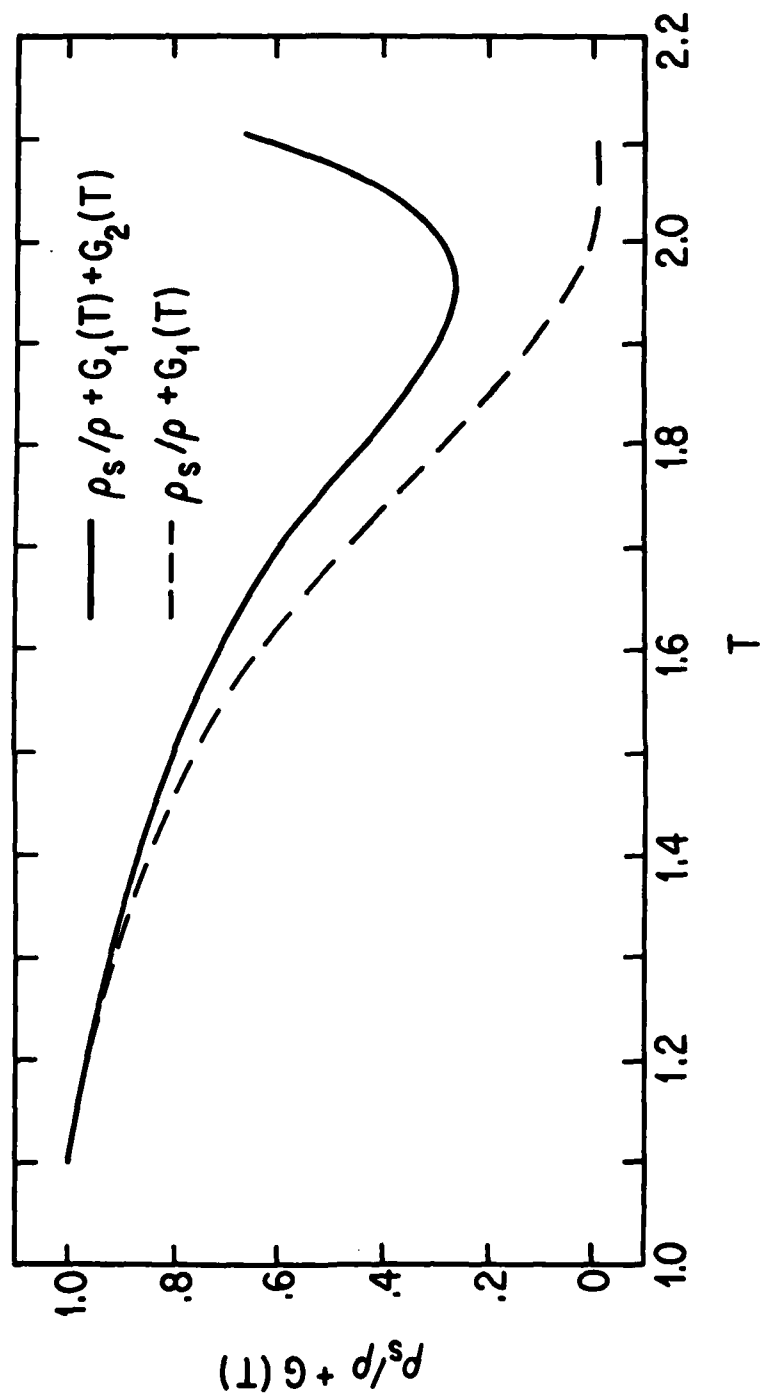


FIGURE 25. -THEORETICAL VALUES OF $[\rho_s/\rho + G_2(T)]$ AND $[\rho_s/\rho + G_1(T)]$

see that there exists a considerable contribution due to $G_1(T)$ especially near T_λ , therefore this part should be included in the calculation of $G(T)$. However in the previous calculations, due to unavailability of precise and complete thermodynamic tables, $G_1(T)$ was considered small and negligible compared to $G_2(T)$.⁽⁶⁴⁾

In order to make the experimental measurements of $G(T)$ versus temperature, splitting of the 22th and 18th modes as a function of temperature were measured while keeping V_s constant (two different resonances were used for consistency purposes) and from the following relation:

$$\Delta F_4 = \frac{m}{\pi R} (\rho_s/\rho + G(T)) V_s \quad (\text{III}-5)$$

the value of $G(T)$ could be determined.

To make the measurements the system was set into rotation above T_λ and while rotating cooled to a desired temperature T_i , and ΔF_i was measured and then cooled back down to the reference temperature ($T=1.35^\circ\text{K}$) and again $\Delta F_{1.35}$ was measured. Using the following relations, one can measure $[\rho_s/\rho + G(T)]$ as a function of temperature,

$$\Delta F_i = \frac{m}{\pi R} [(\rho_s/\rho)_i + G(T)_i] V_{si} \quad (\text{III}-6)$$

$$\Delta F_{1.35} = \frac{m}{\pi R} [(\rho_s/\rho)_{1.35} + G(T)_{1.35}] V_s \quad (\text{III}-7)$$

$$[\rho_s/\rho + G(T)]_i = [\rho_s/\rho + G(T)]_{1.35} \frac{\Delta F_i}{\Delta F_{1.35}} \quad (\text{III}-8)$$

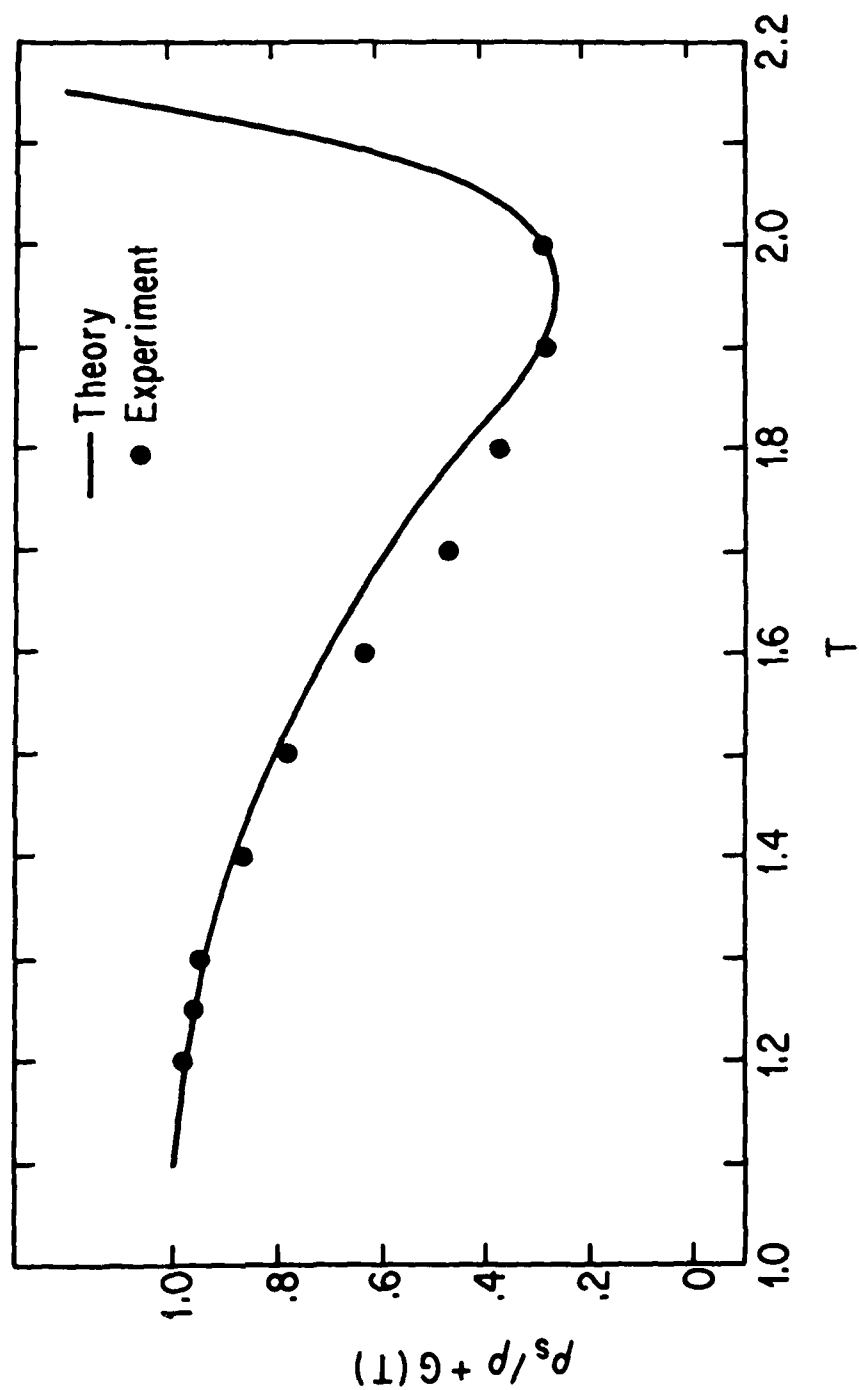


FIGURE 26. --EXPERIMENTAL AND THEORETICAL VALUES OF THE SPLITTING FACTOR $\rho_s / \rho + G(T)$

Fig. 27 shows a plot of experimental results taken in the above manner. As the temperature increases, the critical velocity decreases and consequently the splitting gets smaller and smaller. Also close to T_λ , Q decreases which makes it almost impossible to see the rise of $G(T)$ near T_λ .

CHAPTER IV. GRAVITY WAVES AND PERSISTENT CURRENTS IN ^4He

1. Introduction

As shown in the preceeding chapters measurements of the acoustic modes of a waveguide, fully or partially packed with powder and filled with superfluid helium, is a useful means of studying the flow properties of superfluid helium.⁽⁷⁴⁾ In principle one can simultaneously determine V_p and V_F (persistent current velocities in the powder and in the unpacked region) in a partially packed geometry by measuring the doppler-shifts of C_{14} and C_{II} resonances. Experimentally it is found that in a typical waveguide used in Chapter II, which is packed with 500Å powder particles, the smallest value of a persistent current which can be detected by observing the doppler-shift of fourth sound is about a few centimeters per second. This introduces a limit in studying small persistent currents. Hence it would be desirable to obtain a new low velocity mode which would enable us to detect small persistent currents. For this reason it was suggested⁽⁷⁵⁾ that gravity waves could be used for this purpose since their velocity is about three orders of magnitude smaller than the fourth sound velocity in a similar geometry.

Consider a partially packed annulus packed to a height d , filled with liquid helium to a height L , so that the free surface of the liquid stays below the top boundary of a waveguide. Then two acoustic modes will propagate. One is a temperature wave, and the other a gravity wave, modified by the presence of the superleak. However, due to the presence of vapor the temperature wave is coupled strongly to the sound in vapor and the result is a combined temperature and pressure wave.⁽⁷⁶⁾

Both of these modes have been experimentally observed.⁽⁷⁷⁾ Fig. 27 shows graphs of the gravity wave velocity (C_g) against temperature for different heights of liquid above the powder. Fig. 28 is a graph of velocity of the temperature wave (C_u) against height of the liquid above the powder, where C_v is the velocity of the sound in helium vapor.

The gravity wave is a very slow mode, and considering a typical value of its quality factor, Q , which is ~ 40 in the geometry used, it seems that one should be able to utilize the doppler-shift of these waves to resolve persistent current velocities ~ 1 millimeter per second, which is at least an order of magnitude improvement over the fourth sound technique.

Since it had been shown before that in similar geometries the first-fourth sound was doppler-shifted in the presence of a persistent current in the powder, the same was also assumed for gravity waves. With this in mind the necessary apparatus for performing the experiment was built. In the meantime the theory was also worked out⁽³²⁾ and the results of the derivation were very unexpected. It showed that the doppler-shift of gravity waves is weighted down by $(C_g/C_4)^2 \sim 10^{-6}$ which is negligible and could be considered zero. However, the waves are still doppler-shifted by a persistent current in the unpacked region. The theoretical result, which is not very intuitive, will be discussed in the next section. If this curious prediction is true, then experimentally one will find no change in the resonance frequency of a gravity wave in the presence of a current in the powder. However, the non-existence of doppler-shift would only be convincing if one could show that when a persistent current is demonstrably present that there is

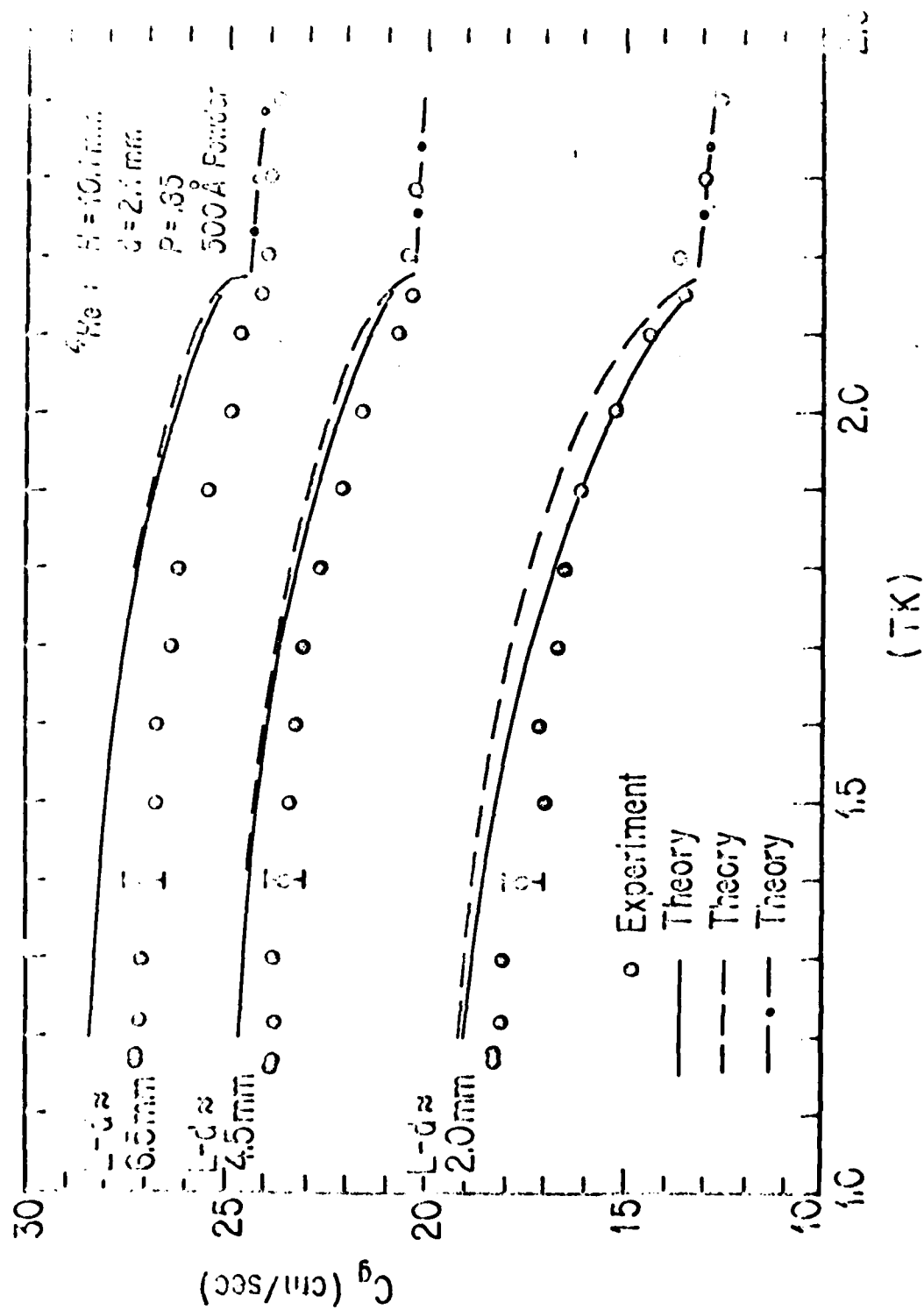


FIGURE 27. GRAVITY WAVE VELOCITY AGAINST TEMPERATURE FOR DIFFERENT HEIGHTS OF LIQUID ABOVE THE POWDER. (TAKEN FROM REF. 77.)

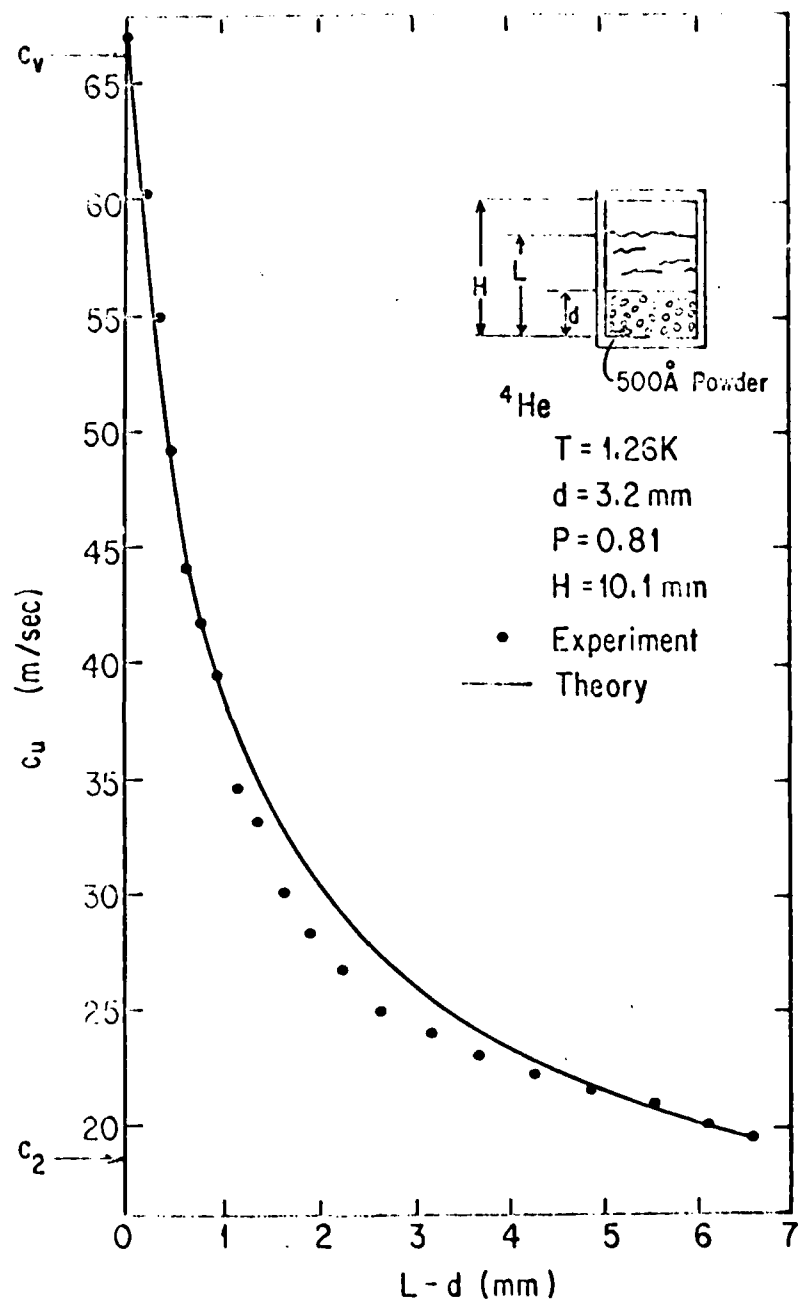


FIGURE 28. VELOCITY OF c_u AGAINST HEIGHT OF THE LIQUID ABOVE THE POWDER (TAKEN FROM REF. 77.)

no doppler-shift.

To do this gravity waves should be detected before and after rotation. No observable change in the spectrum before and after rotation could be accounted for by one of two different reasons. First, it is possible that persistent currents in this geometry are not stable and decay before being detected. Second, gravity waves are not doppler-shifted even though there exists a persistent current in the powder. To clarify the status of the current the experimental cell should be slowly filled up with helium, while keeping the temperature constant. When the cell is filled the gravity waves disappear and the first-fourth sound modes will be observed. The splitting of a C_{14} mode will give a measure of the magnitude of the current in the powder. Experiments were performed in this manner and the results seem to agree with the theoretical prediction. In the next section expressions for the doppler-shifts of C_u and C_g will be obtained. In the following sections experimental measurements will be presented and discussed.

2. Theory

A waveguide packed to a height $X=d$ with superleak and filled up with helium to a level $X=L$ is shown end on in Fig. 29. The propagation direction is into the page, and is taken to be the z axis. Now if a persistent current is generated in this waveguide there will exist two independent currents in the two regions. In the region packed with superleak, only fourth sound can propagate, and the superfluid and normal fluid velocities due to the sound waves are respectively given by:

$$\phi_a = F \cos K_x z e^{i(Kz - \omega t)} \quad (\text{IV-1})$$

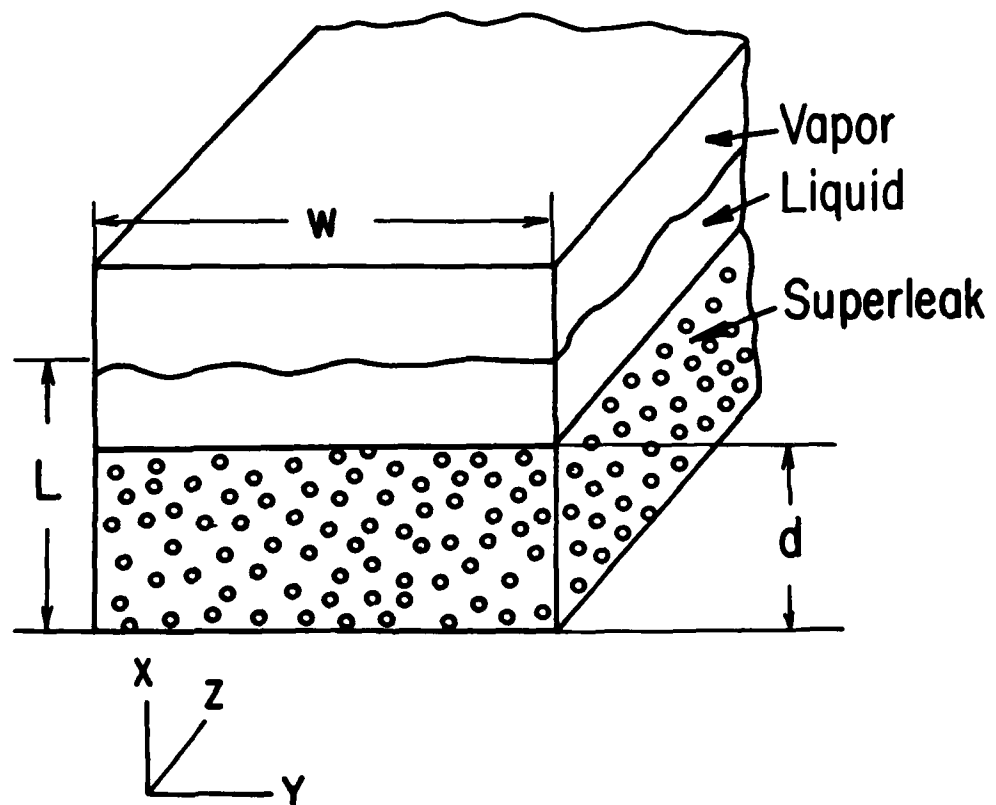


FIGURE 29. CROSS-SECTION OF A PARTIALLY PACKED SUPERFLUID
ACOUSTIC WAVE GUIDE.

$$\vec{V}_s \text{ is found by the relation } \vec{V}_s = \vec{\nabla} \phi \quad (\text{II-2})$$

$$\text{and } \vec{V}_n = 0 \quad (\text{II-3})$$

$$K_x^2 + K^2 = \frac{\omega^2 \alpha^2}{C_A^2} \quad (\text{II-4})$$

$$\text{where } \alpha = (1 \pm \rho_s/\rho V_T/C_A) \quad (\text{II-5})$$

α can be found just by substituting $Z \pm \rho_s/\rho V_p t$ for z in the expression for the fourth sound velocity potential (IV-1) where V_p is the persistent current velocity in the superleak.

In the region above the packed powder, both components (super and normal) can move, and there will exist two propagating modes: first and second sound. For the first sound mode the velocities of the two components will be:

$$V_n' = V_s' \quad \text{II-6}$$

$$\phi_i = [A \cos K_x'(L-x) + B \sin K_x'(L-x)] e^{i(K'z - \omega't)} \quad (\text{II-7})$$

$$V_s' \text{ is given by } V_s' = \nabla \phi_i \quad (\text{II-8})$$

$$K_x'^2 + K'^2 = \frac{\omega'^2 \beta^2}{C_1^2} \quad (\text{IV-9})$$

where

$$\beta = (1 \pm \rho_s/\rho V_F/c_1) \quad (\text{IV-10})$$

V_F is the persistent current velocity in the free region. β can be found by substituting $Z \pm \rho_s/\rho V_F t$ for Z in the expression for the first sound velocity potential (IV-7).

In the second sound mode the center of mass is stationary and the superfluid and normal fluid velocities are given by:

$$\phi_2 = D \cos K_x'' (L - x) e^{i(K_z'' - \omega'' t)} \quad (\text{IV-11})$$

$$V_s'' = \nabla \phi_2 \quad (\text{IV-12})$$

$$V_n'' = -\rho_s/\rho_n V_s'' \quad (\text{IV-13})$$

$$K_x''^2 + K''^2 = \frac{\omega''^2 \gamma^2}{C_2^2} \quad (\text{IV-14})$$

where

$$\gamma = 1 \pm \rho_n/\rho V_F/c_2 \quad (\text{IV-15})$$

and γ is found by substituting $Z \pm \rho_s/\rho V_F t$ for Z in the expression for

the sound velocity potential (IV-11).

The boundary conditions at the walls which are in contact with helium are that the perpendicular component of both super and normal fluid velocity are zero, and that the super and normal components move together at the free surface. These two conditions have already been introduced in the form chosen for the velocity potentials (IV-1, IV-7, IV-11). In order to solve for the doppler-shifted modes in such a waveguide one must apply the boundary conditions at the interface between the packed and free region, as well as the boundary condition at the free surface of the liquid. The first boundary condition at the interface is that the velocity of the traces of the waves along the interface are equal at all times. This requires that $k=k'=k''$ and $\omega=\omega'=\omega''$.

The second and the third boundary conditions at the interface are that the component of mass and heat currents perpendicular to the interface be continuous across the boundary, which would give the following two relations:

$$P \rho_s V_{sx} = \rho_s V'_{sx} + \rho_n V'_{nx} + \rho_s V''_{sx} + \rho_n V''_{nx} \quad (\text{IX-16})$$

where P is the porosity of the packed region and

$$V'_{nx} + V''_{nx} = 0 \quad (\text{IX-17})$$

at the interface. Equation 17 assumes that all of the heat current is carried by the normal component of the superfluid, neglecting the heat conduction by the superleak. Therefore, the normal fluid is stationary at the boundary.

The last boundary condition at the interface is that the

superfluid component's velocity (due to the sound field) be curl free across the interface. This condition requires that:

$$\phi_1 + \phi_2 = \phi_4 \quad (\text{IV-18})$$

At the free surface, neglecting the surface tension, pressure has to be continuous. Starting from Euler's equation⁽⁷⁸⁾, we obtain

$$p = -\rho g x - \rho \frac{\partial \phi}{\partial t} - \frac{1}{2} \vec{V} \cdot \vec{V} \quad (\text{IV-19})$$

where g is the acceleration of gravity. At the free surface, $p=p_0$, and we have at the surface

$$p_0 = -\rho g \xi - \rho \frac{\partial \phi}{\partial t} - \frac{1}{2} \vec{V} \cdot \vec{V} \quad (\text{IV-20})$$

where ξ is the x co-ordinate of a point on the surface. ξ is a function of x , z , and t . In equilibrium $\xi=0$, so that ξ gives the vertical displacement of the surface in its oscillations. If we substitute $\phi' = \phi + \rho_0/\rho t$ instead of the potential ϕ in Equation (IV-20), then the term p_0 is removed from the equation and we will have:

$$g\xi + \left. \frac{\partial \phi}{\partial t} \right|_{z=\xi} + \frac{1}{2} \vec{V} \cdot \vec{V} = 0 \quad (\text{IV-21})$$

At the surface we can also write:

$$V_x = \frac{d\xi}{dt} = \frac{\partial \xi}{\partial t} + (\vec{V} \cdot \nabla) \xi \quad (\text{IV-22})$$

Taking the time derivative of equation (IV-21) and neglecting the second order terms in velocity we will obtain:

$$g \frac{\partial \xi}{\partial t} + \frac{\partial^2 \phi}{\partial t^2} + \frac{1}{2} \rho_0/\rho V_F \frac{\partial V_{12}}{\partial t} = 0 \quad (\text{IV-23})$$

$$V_x = \frac{\partial \xi}{\partial t} + \rho/\rho V_F \frac{\partial \xi}{\partial z} \quad (\text{IV-24})$$

Equations (IV-23) and (IV-24) will yield the final form of the boundary condition at the free surface:

$$\frac{\partial^2 \phi}{\partial t^2} \pm \rho/\rho V_F \frac{\partial V_x}{\partial t} = \frac{-g}{1 \pm \rho/\rho V_F/c} \frac{\partial \phi}{\partial z} \quad (\text{IV-25})$$

Substituting the solutions for the velocity potentials (IV-1, IV-7, IV-11), into the four boundary conditions (IV-16, IV-17, IV-18, IV-25), yields a set of four linear homogeneous equations in the four unknowns.

$$A [\rho K_x'^2 (L-d)] - B [\rho K_x'] + F [\rho \tau K_x'^2 d] = 0 \quad (\text{IV-26})$$

$$A [K_x'^2 (L-d)] - B [K_x'] - D [\rho/\rho_m K_x'^2 (L-d)] = 0 \quad (\text{IV-27})$$

$$A + B [K_x' (L-d)] + D - F = 0 \quad (\text{IV-28})$$

$$A [\omega^2 (\rho/\rho V_F/c \pm 1)] + B [g K_x' / (1 \pm \rho/\rho V_F/c)] = 0 \quad (\text{IV-29})$$

In order for there to be a solution, the determinant of the coefficients must vanish. From this condition we obtain the following equation:

$$(K/\omega)^4 [A' + B' + D'] - \left(\frac{K}{\omega}\right)^2 [(\rho^2/c_1^2 + \rho^2/c_4^2) D']$$

$$\begin{aligned}
& + \left(\frac{\gamma^2}{C_1^2} + \frac{\alpha^2}{C_4^2} \right) A' + \left(\frac{\beta^2}{C_1^2} + \frac{\gamma^2}{C_2^2} \right) B' + \beta^2 (C' + E') \Big] \\
& + \left[B' \left(\frac{\beta^2 \gamma^2}{C_1^2 C_2^2} \right) + D' \left(\frac{\alpha^2 \beta^2}{C_1^2 C_4^2} \right) + A' \left(\frac{\gamma^2 \alpha^2}{C_2^2 C_4^2} \right) + C' \left(\frac{\gamma^2 \beta^2}{C_2^2} \right) \right. \\
& \left. + E' \left(\frac{\alpha^2 \beta^2}{C_4^2} \right) \right] = 0 \quad (\text{IV-30})
\end{aligned}$$

Where A' , B' , C' , D' , and E' are given by the following five relations:

$$A' = \rho_s / \rho_m \rho g d (L-d) - \rho_s / \rho_m \rho d (L-d)^2 \omega^2 \quad (\text{IV-31})$$

$$B' = \rho / \rho_m g (L-d)^2 \quad (\text{IV-32})$$

$$C' = \rho / \rho_m (L-d) \quad (\text{IV-33})$$

$$D' = g \rho d (L-d) \quad (\text{IV-34})$$

$$E' = \rho d \quad (\text{IV-35})$$

Equation (IV-30) can be simplified, noticing that the gravity wave's velocity is much smaller than any of the first, second and fourth sound velocities. Hence in the second square bracket we can ignore all the terms but $\beta^2 (C' + E')$ and in the third bracket the first three terms could be ignored compared to the last two.

Consequently a much simpler equation is obtained:

$$(K\omega)^4 (A' + B' + D') - (K/\omega)^2 \beta^2 (C' + E') + \left[\frac{\gamma^2 \beta^2}{C_1^2} C' + \frac{\alpha^2 \beta^2}{C_4^2} E' \right] = 0 \quad (\text{IV-36})$$

Solving the above equation to first order for (ω/κ) we find the two following equations for the doppler-shifted phase velocities of the two modes:

$$C_g = C_{g0} \pm \beta_s/\rho V_p \left[L/d \cdot C_{g0}^2/C_4^2 \right] \pm \beta_s/\rho V_F \quad (\text{IV-37})$$

$$C_u = C_{u0} \pm \beta_m/\rho V_p \left[\frac{Pd}{\rho_m/\rho (L-d)} \right] \left(\frac{C_2^2}{C_4^2} \right) \pm \beta_m/\rho V_F \quad (\text{IV-38})$$

where

$$C_{g0}^2 = g(L-d) \frac{L - (1-P)d}{\rho_m/\rho Pd + (L-d)} \quad (\text{IV-39})$$

$$C_{u0}^2 = \rho_m/\rho C_2^2 \frac{Pd}{L-d} + C_2^2 \quad \text{IV-40}$$

C_g is the doppler-shifted velocity of the gravity wave due to the persistent currents in the packed and the free regions. Taking the corresponding values for C_{g0} , C_4 and V_p , and assuming $d/L \approx 1/2$, we will get $V_p (d/L) (C_{g0}^2/C_4^2) \approx 3 \times 10^{-4}$ cm/sec which is far beyond our experimental limit. Therefore this term can be neglected in the equation (IV-37). The second contribution to the doppler-shift comes from the persistent current in the free region. If there exists any current in this region, then gravity waves will be a preferable method of detecting it over the second sound technique discussed briefly in the introduction.

The relation for the velocity of the doppler-shifted C_u mode is basically the same as the one derived before for the C_{II} mode which propagates in a partially packed geometry when filled with superfluid helium. It should be pointed out that all the equations were derived neglecting the mixing with the vapor. The gravity waves barely interact with the vapor mode, however, as it was mentioned earlier in this chapter the C_u mode strongly mixes with the vapor and the doppler-shift relation as derived here cannot be applied to real experimental situations. (76)

3. Experimental Apparatus and Techniques

The doppler-shift of the gravity waves and the first-fourth sound mode were studied experimentally by observing the splitting of the resonance frequencies of a closed cavity. Fig. 30 shows a view of the experimental cell used. All the parts are shown in the schematic drawing in Fig. 31. It consists of three parts:

1. An annular waveguide with an inner diameter of 7.62cm, an outer diameter of 8.25 cm and a depth of 0.4 cm.
2. A plate which covers the waveguide channel and also acts as a fourth sound plate.
3. An overall cover which connects the experimental cell to outside.

The annular channel is of rectangular cross-section and is packed to $3/10$ of its height with 500\AA aluminum oxide powder particles. (68) The packing technique is identical to the one discussed in Chapter II of this thesis. Also the packing tools are basically the same as before. The annulus is provided with two pairs of capacitor plates, which are

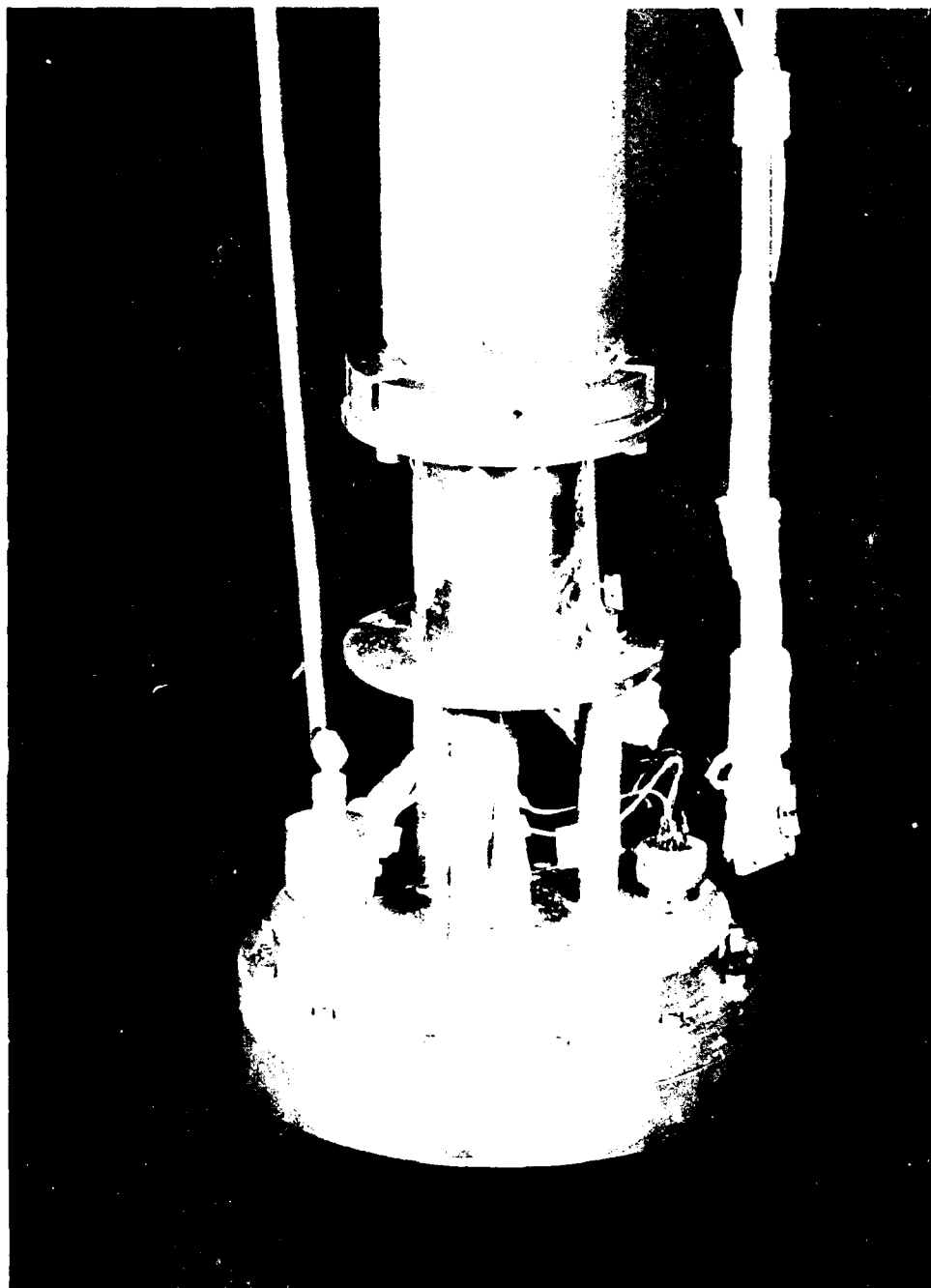


FIGURE 30. A PHOTOGRAPH OF THE EXPERIMENTAL CELL
USED IN GRAVITY WAVE EXPERIMENTS

AD-A085 767

CALIFORNIA UNIV LOS ANGELES DEPT OF PHYSICS
A STUDY OF PERSISTENT CURRENTS IN SUPERFLUID ^4He . (U)
MAR 80 R K TALAGHANY
TR-40

F/6 20/13

N00014-75-C-0246

NL

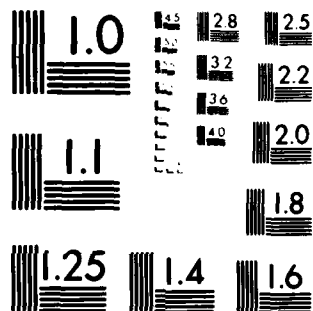
UNCLASSIFIED

2 + 2

30 Jan 77



END
DATE
FILMED
7 80
DTIC



MICROCOPY RESOLUTION TEST CHART
NATIONAL BUREAU OF STANDARDS-1963-A

epoxied on the opposite walls of the resonator body, such that they are electrically isolated from the rest of the apparatus. These plates are used for detection of gravity waves. When the gravity waves are propagated, the height of the surface of the liquid oscillates, and so does capacitance of the plates.

The gravity waves in the experiment can be generated in two different ways. One technique is based on the idea of the superfluid fountain. A side branch of 20×10^{-3} in. (5×10^{-2} cm) diameter opens in the inside wall into the lower end of the channel, such that it stays below the surface of the powder, and on the other side widens into a 2.4 millimeter hole. The hole is then connected to the fill tube as it is shown in the schematic drawing in Fig. 31. To drive the gravity wave, a heater is placed either in the side branch or in the annulus above the powder in the liquid, and heat at the desired frequency is applied. By applying the heat, liquid moves in and out of the annulus with twice the frequency of the source and gravity waves are excited. The heaters are made of about 15 cm of .00175" diameter ($43 \mu\text{m}$) nickel-chromium resistance wire⁽⁷⁹⁾, which is wound around thin pieces of a non-conductive material. The second method of exciting the gravity wave is simply to shake the dewar. This method is only efficient for exciting the fundamental mode, and also not very feasible with the heavy experimental assembly used.

It is very important that the diameter of the side branch be kept very small for the following two reasons. First, the C_{14} resonances will have geometric splittings even in the absence of any persistent currents due to the presence of the side branch. Also, possible

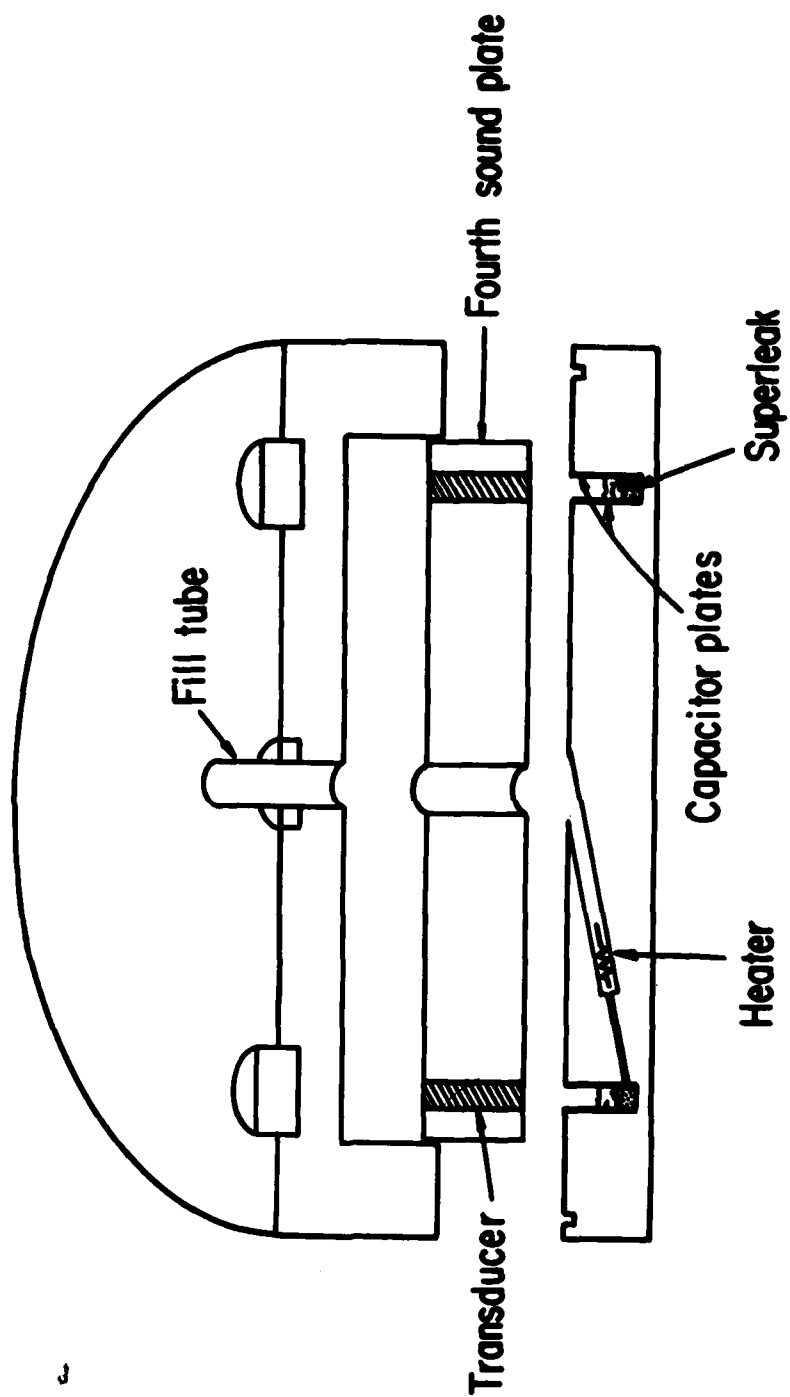


FIGURE 31. CROSS-SECTIONAL SKETCH OF THE ANNULAR RESONATOR USED
IN MEASUREMENTS OF THE DOPPLER SHIFT OF GRAVITY WAVE

overlapping of the C_{II} resonances with the split modes will complicate the measurements even further. Second, the presence of a large opening will pressure release the fourth sound and result in loss of acoustic energy, which will in turn deteriorate the quality factor, Q , and make the persistent current measurements inaccurate and at times impossible. To minimize these problems the diameter of the side branch should be very much smaller than a fourth sound wavelength used in the measurements. The wave length of the typical fourth sound resonances used in this experiment is ~ 1 cm, which is very much larger than the diameter of the side branch.

For generating and detecting the first-fourth sound resonances, the channel is covered with a 2 cm thick top plate. The top plate is provided with a few sandblasted transducer buttons that are epoxied into the top plate. A piece of aluminized teflon sheet processed to make it an electret is laid against the top plate to act as a pressure transducer. The details of the pressure transducers are discussed in Chapter II. Fig. 32 and 33 show open and closed views of the resonator with the top plate.

Finally there is another plate which covers the annulus and the fourth sound plate. In order to make the cell helium tight an indium O ring is used and all the wires are connected to the outside of the cell by using hermetically sealed feed-throughs.⁽⁸⁰⁾ A 1/4" stainless steel tube is soldered to the top cover. The tube extends all the way to the top of the probe and is attached to a high vacuum valve. The valve is connected to a gas handling system by a quick-connect fitting. Helium gas purified by a zeolite cold trap is condensed into the



FIGURE 32. OPEN VIEW OF THE RESONATOR WITH THE TOP PLATE

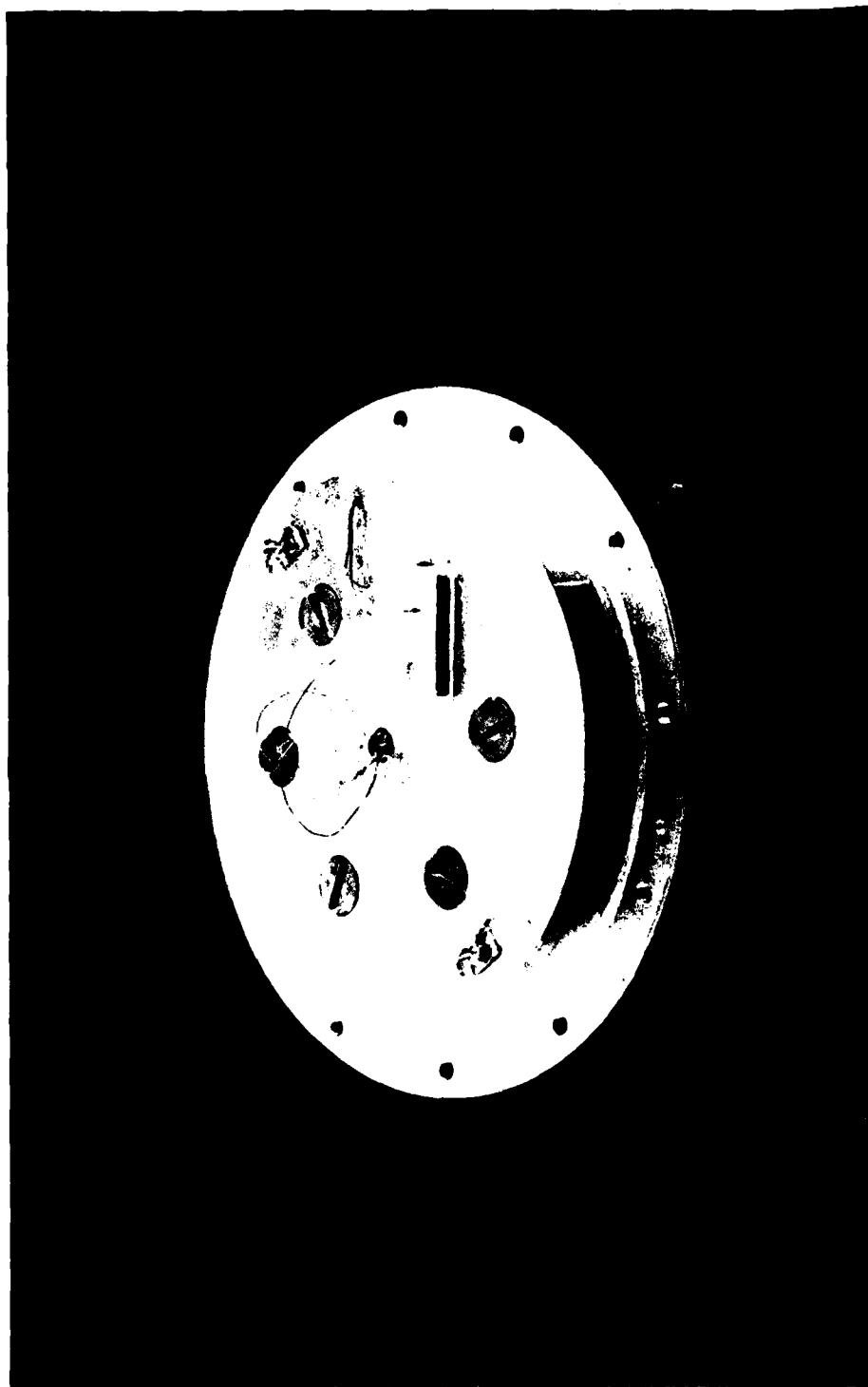


FIGURE 33. CLOSED VIEW OF THE RESONATOR

resonator. The liquid level is monitored by observing the change in capacitance as the level rises. When the desired level is attained the valve at the top of the probe is closed and the gas fill line is disconnected prior to rotation.

4. Electronics

A block diagram of the electronics used in the experiment is shown in Fig. 34. A Hewlett-Packard 3325A frequency synthesizer was used to slowly sweep over the range of .3-5 Hz at a constant voltage. The amplitude of the drive voltage was varied to get the desired output signal, not exceeding the power dissipation limit of the heater (about a few milliwatts). The gravity waves were picked up by detecting the off-null signal from a General-Radio 1615A capacitance bridge. The bridge is operated with a 2 KHz 5V peak to peak oscillator that also serves as the reference for a lock-in amplifier (P.A.R. Model 129A). The output voltage of the lock-in (which oscillates at the resonance frequencies of the gravity waves) is fed into a FFT real time spectrum analyzer (Unigon, Model 4513). The analyzed signal is then plotted versus frequency on a X-Y recorder (H-P 7044A X-Y recorder). A typical frequency sweep is shown in Fig. 35. A typical quality factor is about 40.

The electronics used for detection of the doppler-shift of C_{14} is similar to that described in Chapter II. (See Fig. 15).

5. Doppler-Shift of Gravity Waves

Measurements of the doppler-shifts of the gravity waves were made using the probe and electronics described in previous sections. Measurement procedures are as follows: At a constant temperature gravity

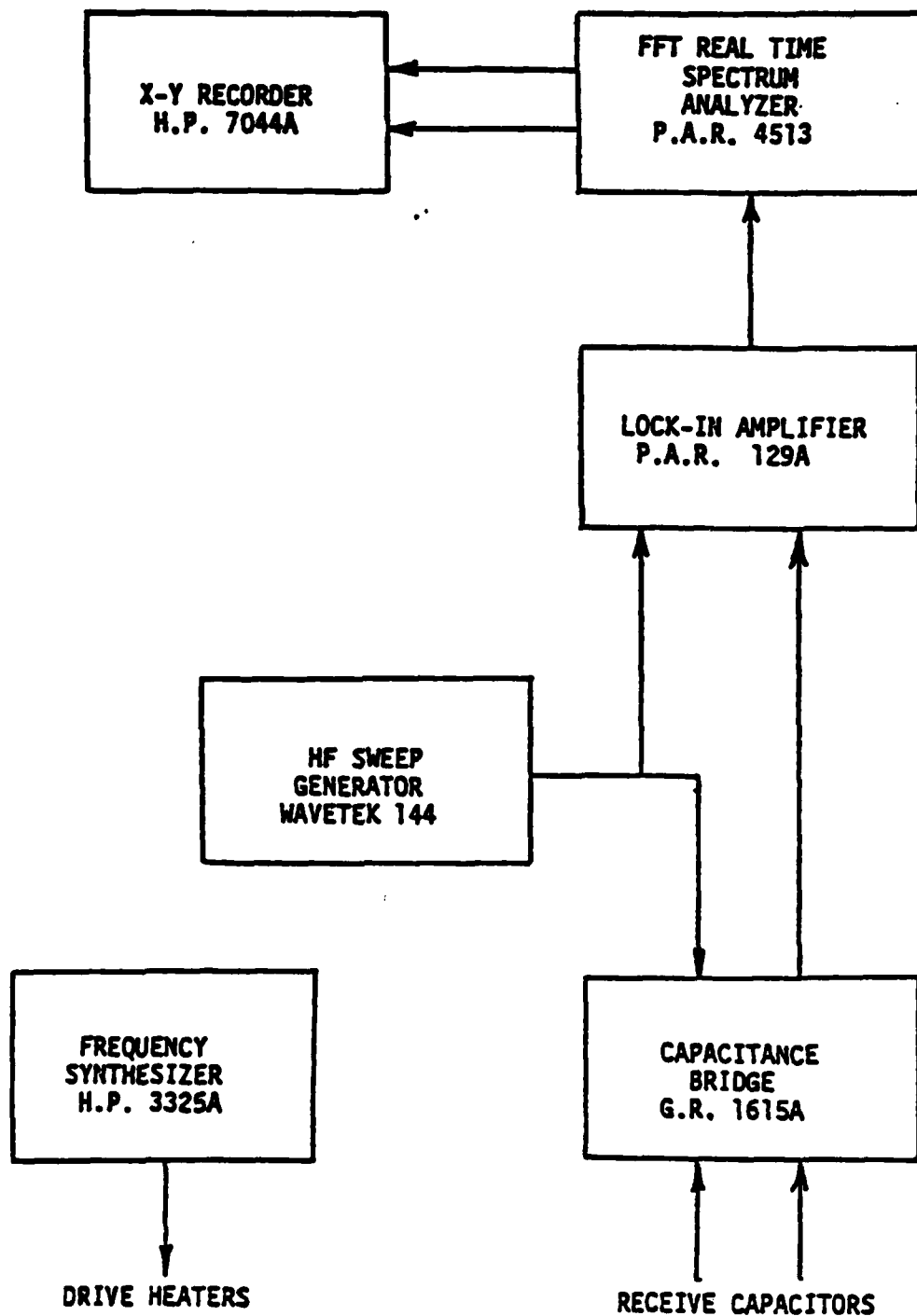


FIGURE 34. BLOCK DIAGRAM OF ELECTRONICS USED IN GRAVITY WAVE EXPERIMENTS

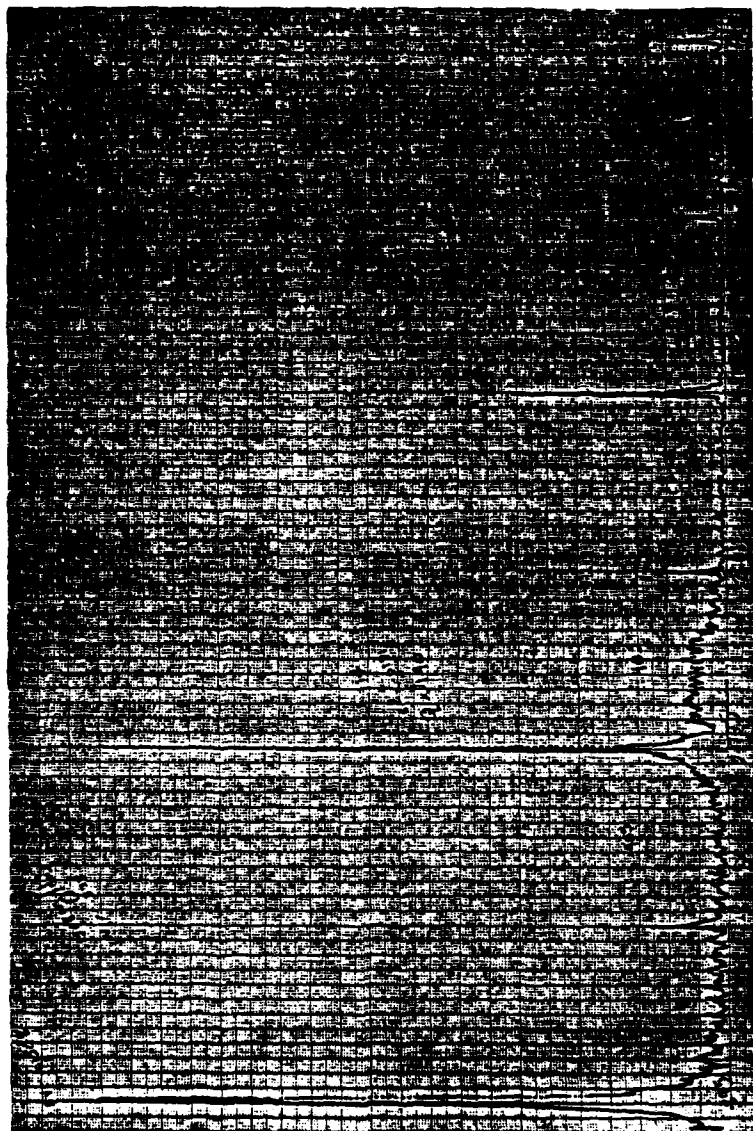


FIGURE 35. A TYPICAL SPECTRUM OF GRAVITY WAVE IN HELIUM IN THE
PARTIALLY PACKED ANNULUS AT 1.3 K

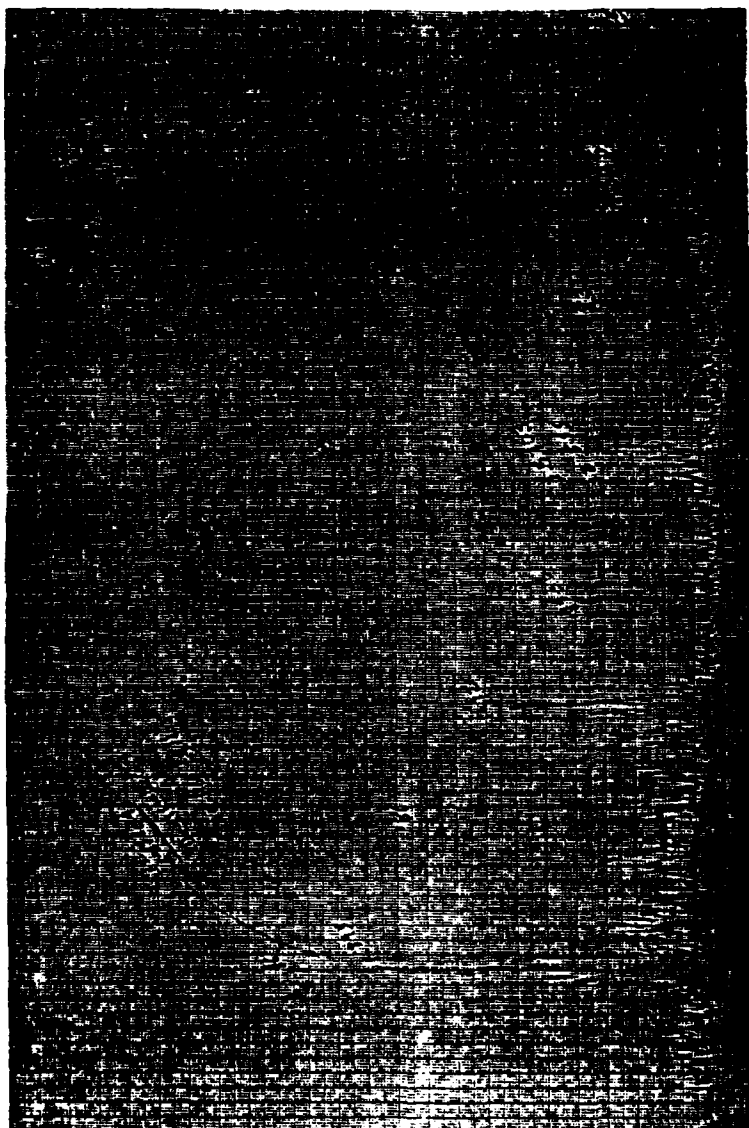


FIGURE 36. SPECTRUM OF GRAVITY WAVE IN HELIUM IN PARTIALLY
PACKED ANNULUS AFTER ROTATION AT 1.3 K

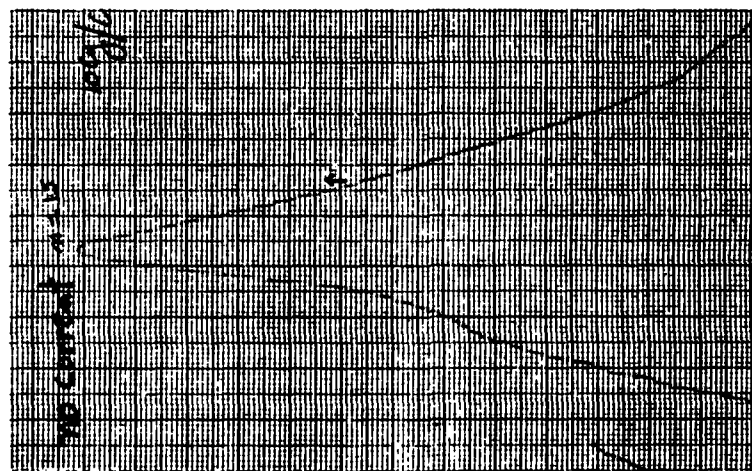
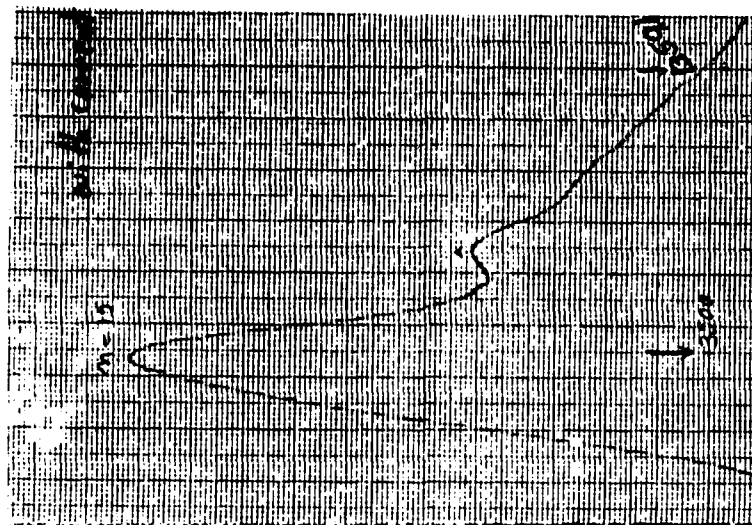


FIGURE 37 C_{14} RESONANCES WITH AND WITHOUT PERSISTENT CURRENT.

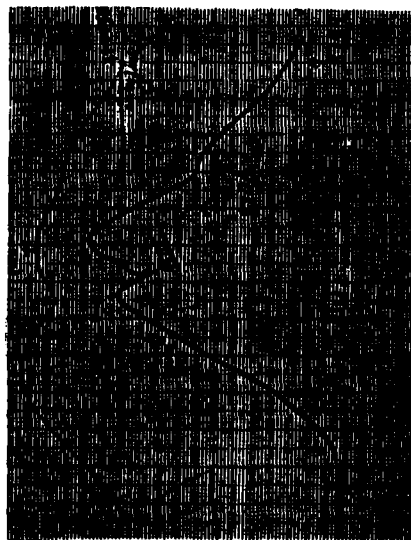
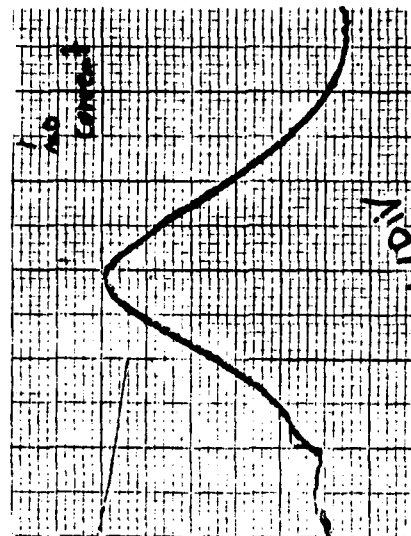


FIGURE 37. C_{14} RESONANCES WITH AND WITHOUT PERSISTENT CURRENT.

waves were excited and a graph of the spectrum of the first few harmonics were obtained. Then the system was warmed up to above T_λ and while rotating at constant speed, the system was cooled down to the desired temperature. At that time rotation was suddenly stopped. After a few minutes, when the system was settled, a new spectrum of the gravity waves was taken. Figs. 35 and 36 show the spectrum before and after rotation. To prove the existence of the current in the powder, and also its magnitude, the cell was slowly filled up until the annulus was completely filled and afterwards a graph of a doppler-shifted C_{14} resonance was recorded. To eliminate the persistent current the system was warmed up above T_λ and cooled back down to the previous temperature. A new graph of the same C_{14} resonance was taken. Fig. 37 shows a typical C_{14} resonance with and without current. Comparison of the two graphs of C_{14} proves the existence of the current and also one can find the magnitude of the current which exists in the powder.

Experiments were repeated at different rotation speeds. At low rotation speeds, the magnitude of the persistent current was small and the amount of the splitting of a C_{14} mode was unobservable. To provide a proof of the existence of the current, the velocity of rotation was increased until there was an observable splitting of a C_{14} mode which in our configuration was about 7 c.p.s. However experiments were also done at lower angular velocities (as small as 1 c.p.s.) with no observable change in the spectrum of gravity waves.

6. Results and Discussion

From the comparison of the two C_{14} resonance curves (with and without current) one can observe the existence of the current and also

calculate its magnitude. Most of the C_{14} modes were split even in the absence of any persistent current. This is mainly due to the fountain side branch and a small opening on the top plate to pass the wires. Also the irregularities of the resonator, as well as the packing contributed to this geometric splitting. The two peaks in the split C_{14} mode are not usually equally excited, and since the fourth sound top plate was only provided with two transducers, it was not possible to equalize the two peaks. This problem at times makes the measurements inaccurate. To correct for this efforts were made to look for an unsplit mode or one in which the peaks are almost equally excited. By checking many of the C_{14} resonances and comparing them one can get a reliable value for the magnitude of the persistent current. For a rotation speed of $\omega_r \sim 7$ c.p.s. in the mentioned experimental set up we get $V_s \sim 60$ cm/sec, therefore the existence and magnitude of the current is established.

Fig. 35 shows a spectrum of gravity waves in the annulus partially packed where $d = .3764$ cm and $L - d = .3762$ cm. Since the size of the capacitive pick up was chosen to be $1/8$ of the circumference then only the first seven resonances can be detected, as shown in Fig. 35. The relative height and the quality factors depend on the relative position of the fountain to the pick up capacitors and the drive heater in the liquid. The highest quality factor is found to be ~ 140 , however a typical one for the mentioned set up was ~ 40 . Now the question is what would happen to gravity waves in the presence of a persistent current?

Fig. 36 shows the spectrum after rotation. One can basically see

the same pattern as before. However, some of the resonances are not excited as well, and there is more noise present after rotation. Vibration of the wires, which make the electrical contact between inside and outside the cell, can be a possible source of noise. Since the wires were held down by tape, some of them may have become loose during rotation. The quality factor, Q , of the resonances was also significantly diminished. The decrease could be due to the attenuation of the gravity waves through the interaction of the waves and vortices.

As seen in Fig. 35 the fundamental mode is split when there is no persistent current present because of the factors previously mentioned. However, the splitting gets larger after rotation. The increase in splitting could be explained by a persistent current of ~ 8 cm/sec in the free region. The splitting in the higher harmonics is hard to detect due to the presence of noise and low quality factor.

7. Further Experiments

A. From the preceding discussion it seems that there is a possibility of utilizing gravity waves to detect a persistent current in the free region and further investigation seems to be warranted.

B. All the measurements in this thesis were done while the resonator was stationary. However it would be very interesting to look at the gravity waves while rotating. A theoretical solution for a rotating bucket of water has been worked out⁽⁸¹⁾, however the problem for a torus in helium has not yet been solved.

C. The last part of the equation (IV-37) which states that the doppler shift of gravity waves due to the persistent current in the free region is independent of the height of the liquid in the free

region has not been experimentally verified. This interesting result simply states that the doppler-shift of the gravity waves depends only on the velocity of the free surface no matter what the height of the liquid above the powder is. This result is also consistent with the absence of the doppler-shift due to the persistent current in the powder.

D. It seems that the gravity waves are being attenuated in the presence of vortices. This could be studied in a more precise fashion by measuring the quality factor, Q , as a function of rotation speed or the magnitude of the persistent current.

REFERENCES

1. H. Kamerlingh Onnes, Sci. Amst. II, 168 (1908).
2. L.D. Landau and E.M. Lifshitz, Electrodynamics of Continuous Media, Pergamon, London (1960) Ch. 8.
3. F. London, Nature, 141, 643 (1938).
4. W.H. Keesom and A.P. Keesom, Physica 3, 359 (1936).
5. W.H. Keesom and J.N. Van den Ende, Proc. Roy. Acad., Amsterdam 33, 243 (1930).
6. P. Kapitza, Nature 141, 74 (1938).
7. F. Allen and A.D. Misener, Nature 141, 75 (1938); Proc. Roy. Soc., London, A172, 467 (1939).
8. J.F. Allen and J. Jones, Nature 141, 243 (1938).
9. J.G. Daunt and K. Mendelssohn, Nature 143, 719 (1939).
10. P. Kapitza, J. Phys. USSR 5, 59 (1941); Phys. Rev. 60, 354 (1941).
11. H. Kamerlingh Onnes, Trans. Faraday Soc. 18 (1922), No. 53, B.V. Rollin and F. Simon, Physica 6, 269 (1939).
12. B.V. Rollin, Actes du ^{7me} Congr. Intern. du Froid, Amsterdam-La Hage 7, 187 (1936); B.V. Rollin and F. Simon, Physica 6, 269 (1939).
13. J.G. Daunt and K. Mendelssohn, Nature 141, 911 (1938); 142, 475 (1938); Proc. Roy. Soc. A170, 423, 439 (1939).
14. F. London, Nature 141, 643 (1938); Phys. Rev. 154, 947 (1938).
15. L. Tisza, Nature 141, 913 (1938); Compt. Rend., 207, 1035, 1186 (1938); J. Phys. Radium 7, 164, 350 (1940).
16. L. Landau, J. Phys. USSR 5, 71 (1941); 8, 1 (1944); Phys. Rev. 60, 356 (1941).

17. L.D. Landau, Zh. Eksp. Teor. Fiz. 11 (1941); J. Phys. USSR 5, 71, (1941); L.D. Landau and E.M. Lifshitz, Fluid Mechanics (Pergamon, London, 1959) Ch. 16.
18. V.P. Peshkov, J. Phys., Moscow 8, 381 (1944); 10, 389 (1946).
19. E.L. Andronikashvili, Zh. Eksp. Teor. Fiz. 16, 780 (1946); 18, 424 (1948); J. Phys. USSR 10, 201 (1946).
20. S.J. Putterman, Superfluid Hydrodynamics, North Holland/American Elsevier, New York (1974) Ch. I.
21. J.C. Findlay, A. Pitt, H. Grayson-Smith and J.G. Wilhelm, Phys. Rev. 54, 506 (1938).
22. Ref. 20, pg. 204.
23. I. Rudnick and K.A. Shapiro, Phys. Rev. Lett. 9, 191 (1962).
24. M. Kriss and I. Rudnick, J. Low Temp. Phys. 3, 339 (1970).
25. I. Rudnick, J. Maynard, G. Williams and S. Putterman, Phys. Rev. B-20, 1934 (1979).
26. G.A. Williams, R. Rosenbaum, and I. Rudnick, Phys. Rev. Lett. 42, 1282 (1979).
27. K.R. Atkins and I. Rudnick, Progress in Low Temperature Physics, Vol. 6, North Holland, Amsterdam (1970) Ch. 2.
28. J. Rudnick, I. Rudnick and R. Rosenbaum, J. Low Temp. Phys. 16, 417, (1974).
29. J. Heiserman and I. Rudnick, J. Low Temp. Phys. 22, 481 (1976).
30. D.V. Osborne, Proc. Roy. Soc. (London) A63, 909 (1950).
31. E.L. Andronikashvili and I.P. Kaverkin, J. Exp. Theor. Phys. USSR (Russian) 28, 126 (1955).

32. J.F. Allen and A.D. Misener, Proc. Roy. Soc. (London) A172, 467 (1939).
33. Ref. 20, pg. 96.
34. L. Onsager, remark at a Low Temperature Physics Conference at Shelter Island, 1948. (See also L. Onsager, Nuovo Cimento, Suppl. No. 2, 6, 249 (1949).
35. W.F. Vinen, Proc. Roy. Soc. A260, 218 (1961).
36. G.W. Rayfield and F. Reif, Phys. Rev. Lett. 11, 305 (1963); Phys. Rev. 136, A1194 (1964).
37. S.C. Whitmore and W. Zimmermann, Jr., Phys. Rev. 166, 181 (1968).
38. J.G. Daunt and K. Mendelssohn, Proc. Roy. Soc. A170, 423 (1939).
39. A. Bijl, J. de Boer and A. Michels, Physica 8, 655 (1941).
40. Ref. 20, pg. 109.
41. R.E. Packard and T.M. Sanders, Jr., Phys. Rev. Lett. 22, 823 (1969).
42. G.A. Williams and R.E. Packard, Phys. Rev. Lett. 33, 280 (1974).
43. H.E. Hall, Phil. Trans. Roy. Soc. (London) A250, 359 (1957).
44. W.F. Vinen, Proc. Roy. Soc. (London) A260, 218 (1961).
45. J.D. Reppy and D. Depatie, Phys. Rev. Lett. 12, 187 (1964).
46. J.D. Reppy, Phys. Rev. Lett. 14, 733 (1965); J.R. Clow and J.D. Reppy, Phys. Rev. Lett. 16, 887 (1966); G. Kukich, R.P. Henkel and J.D. Reppy, Phys. Rev. Lett. 21, 197 (1968).
47. J.B. Mehl and W. Zimmermann, Jr., Phys. Rev. Lett. 14, 815 (1965); Phys. Rev. 167, 214 (1968).
48. I. Rudnick, H. Kojima, W. Veith and R.S. Kagiwada, Phys. Rev. Lett. 23, 1220 (1969).
49. J.S. Langer and M.E. Fisher, Phys. Rev. Lett. 19, 560 (1967);

- J.S. Langer and J.D. Reppy, Prog. Low Temp. Phys., Vol. 6, (C.J. Gorter, ed.), North Holland, Amsterdam (1970).
50. S.V. Iordanskii, Zh. Eksp. Teor. Fiz. 48, 708 (1965); [Sov. Phys. JETP 21, 467 (1965)].
51. G. Kukich, R.P. Henkel and J.D. Reppy, Phys. Rev. Lett. 21, 197 (1968).
52. H. Kojima, W. Veith, E. Guyon, and I. Rudnick, 13th International Conference on Low Temperature Physics, (K.D. Timmerhaus, W.J. O'Sullivan and E.F. Hammel, ed.), Plenum Publishing Corp.
53. H. Kojima, Ph.D. thesis, UCLA (1972) unpublished.
54. P.W. Anderson, Phys. Rev. Lett. 9, 30 (1962).
55. Ref. 20, pg. 262.
56. Ref. 29.
57. J. Heiserman and I. Rudnick, Phys. Rev. B12, 1739 (1975).
58. W.E. Keller, Helium-3 and Helium-4, Plenum Press, New York (1969).
59. J.C. Weaver, Phys. Rev. A6, No. 1, 378 (1972).
60. Ref. 52.
61. I.M. Khalatnikov, Zh. Eksp. Teor. Fiz. 30, 617 (1956); [Sov. Phys. JETP 2, 73 (1956)].
62. F. London, Superfluids Vol. II, Macroscopic Theory of Superfluid Helium, Dover, New York (1964).
63. Ref. 48 and Ref. 20, pg. 204.
64. Ref. 53.
65. J. Heiserman, Ph.D. thesis, UCLA (1975) unpublished.
66. P.M. Morse and K.U. Ingard, Theoretical Acoustics, MacGraw-Hill, New York (1968) pg. 603.

67. J. Rudnick, unpublished work, and Ref. 65.
68. Linde B 0.05 micron Alumina polishing powder, Union Carbide Corp.
69. Teflon FEP 50A Fluorcarbon Film, E.I. Dupont de Nemours & Co.
70. G.M. Sessler and J.E. West, J. Acoust. Soc. Amer. 53, 1589 (1973).
71. H.J. Seguin and R.W. Leonard, Rev. Sci. Instrum. 37, 1743 (1966).
72. A.C. Anderson, Rev. Sci. Instrum. 44, 1475 (1973).
73. J. Maynard, Phys. Rev. B14, 3868 (1976).
74. Ref. 53 and Ref. 65
75. G. Williams, private communication.
76. S. Putterman, D. Heckerman, R. Rosenbaum and G.A. Williams, Phys. Rev. Lett. 42, 580 (1979).
77. D. Heckerman, R. Rosenbaum, S. Putterman, and G.A. Williams,
to be published in J. Low Temp. Phys. 38, No's. 5 and 6 (1980).
78. L.D. Landau and E.M. Lifshitz, Fluid Mechanics, Pergamon, London,
(1959) Ch. 1.
79. Cinema Engineering Co., Burbank, CA.
80. Inconel-X 8-pin Electrical Feed Through X27176-8 PPI. Hermetic
Seal Corp.
81. H. Lamb, Hydrodynamics, 6th Ed., Dover, New York (1932) pg. 319.
82. S. Putterman, private communication.

June 1978

REPORTS DISTRIBUTION LIST FOR ONR PHYSICS PROGRAM OFFICE
UNCLASSIFIED CONTRACTS

Director Defense Advanced Research Projects Agency Attn: Technical Library 1400 Wilson Blvd. Arlington, Virginia 22209	3 copies
Office of Naval Research Physics Program Office (Code 421) 800 North Quincy Street Arlington, Virginia 22217	3 copies
Office of Naval Research Assistant Chief for Technology (Code 200) 800 North Quincy Street Arlington, Virginia 22217	1 copy
Naval Research Laboratory Department of the Navy Attn: Technical Library Washington, D. C. 20375	3 copies
Office of the Director of Defense Research and Engineering Information Office Library Branch The Pentagon Washington, D. C. 20301	3 copies
U. S. Army Research Office Box 12211 Research Triangle Park North Carolina 27709	2 copies
Defense Documentation Center Cameron Station (TC) Alexandria, Virginia 22314	12 copies
Director, National Bureau of Standards Attn: Technical Library Washington, DC 20234	1 copy
Commanding Officer Office of Naval Research Branch Office 536 South Clark Street Chicago, Illinois 60605	3 copies

June 1978

REPORTS DISTRIBUTION LIST FOR ONR PHYSICS PROGRAM OFFICE
UNCLASSIFIED CONTRACTS

Director Defense Advanced Research Projects Agency Attn: Technical Library 1400 Wilson Blvd. Arlington, Virginia 22209	3 copies
Office of Naval Research Physics Program Office (Code 421) 800 North Quincy Street Arlington, Virginia 22217	3 copies
Office of Naval Research Assistant Chief for Technology (Code 200) 800 North Quincy Street Arlington, Virginia 22217	1 copy
Naval Research Laboratory Department of the Navy Attn: Technical Library Washington, D. C. 20375	3 copies
Office of the Director of Defense Research and Engineering Information Office Library Branch The Pentagon Washington, D. C. 20301	3 copies
U. S. Army Research Office Box 12211 Research Triangle Park North Carolina 27709	2 copies
Defense Documentation Center Cameron Station (TC) Alexandria, Virginia 22314	12 copies
Director, National Bureau of Standards Attn: Technical Library Washington, DC 20234	1 copy
Commanding Officer Office of Naval Research Branch Office 536 South Clark Street Chicago, Illinois 60605	3 copies

Commanding Officer Office of Naval Research Branch Office 1030 East Green Street Pasadena, California 91101	3 copies
San Francisco Area Office Office of Naval Research One Hallidie Plaza Suite 601 San Francisco, California 94102	3 copies
Commanding Officer Office of Naval Research Branch Office 666 Summer Street Boston, Massachusetts 02210	3 copies
New York Area Office Office of Naval Research 715 Broadway, 5th Floor New York, New York 10003	1 copy
Director U. S. Army Engineering Research and Development Laboratories Attn: Technical Documents Center Fort Belvoir, Virginia 22060	1 copy
ODDR&E Advisory Group on Electron Devices 201 Varick Street New York, New York 10014	3 copies
Air Force Office of Scientific Research Department of the Air Force Bolling AFB, D. C. 22209	1 copy
Air Force Weapons Laboratory Technical Library Kirtland Air Force Base Albuquerque, New Mexico 87117	1 copy
Air Force Avionics Laboratory Air Force Systems Command Technical Library Wright-Patterson Air Force Base Dayton, Ohio 45433	1 copy
Lawrence Livermore Laboratory Attn: Dr. W. F. Krupke University of California P. O. Box 808 Livermore, California 94550	1 copy

Harry Diamond Laboratories Technical Library 2800 Powder Mill Road Adelphi, Maryland 20783	1 copy
Naval Air Development Center Attn: Technical Library Johnsville Warminster, Pennsylvania 18974	1 copy
Naval Weapons Center Technical Library (Code 753) China Lake, California 93555	1 copy
Naval Training Equipment Center Technical Library Orlando, Florida 32813	1 copy
Naval Underwater Systems Center Technical Library New London, Connecticut 06320	1 copy
Commandant of the Marine Corps Scientific Advisor (Code RD-1) Washington, DC 20380	1 copy
Naval Ordnance Station Technical Library Indian Head, Maryland 20640	1 copy
Naval Postgraduate School Technical Library (Code 0212) Monterey, California 93940	1 copy
Naval Missile Center Technical Library (Code 5632.2) Point Mugu, California 93010	1 copy
Naval Ordnance Station Technical Library Louisville, Kentucky 40214	1 copy
Commanding Officer Naval Ocean Research & Development Activity Technical Library NSTL Station, Mississippi 39529	1 copy
Naval Explosive Ordnance Disposal Facility Technical Library Indian Head, Maryland 20640	1 copy

Naval Ocean Systems Center
Technical Library
San Diego, California 92152
1 copy

Naval Surface Weapons Center
Technical Library
Dahlgren, Virginia 22448
1 copy

Naval Surface Weapons Center (White Oak)
Technical Library
Silver Spring, Maryland 20910
1 copy

Naval Ship Research and Development Center
Central Library (Code L42 and L43)
Bethesda, Maryland 20084
1 copy

Naval Avionics Facility
Technical Library
Indianapolis, Indiana 46218
1 copy

DATE
FILMED
7-8